AWARD NUMBER: W81XWH-14-1-0268

TITLE: The Contribution of Prohibitin 1 to Prostate Cancer Chemoresistance

PRINCIPAL INVESTIGATOR: Yingjie Xu

CONTRACTING ORGANIZATION: Children's Hospital Corporation
Boston MA 02115-5724

REPORT DATE: October 2015

TYPE OF REPORT: Annual report

PREPARED FOR: U.S. Army Medical Research and Materiel Command
Fort Detrick, Maryland 21702-5012

REPORT DOCUMENTATION PAGE

Form Approved
OMB No. 0704-0188

1. REPORT DATE	2. REPORT TYPE	3. DATES COVERED
October 2015	Annual	29 Sep 2014 - 28 Sep 2015

4. TITLE AND SUBTITLE

The Contribution of Prohibitin 1 to Prostate Cancer Chemoresistance

5a. CONTRACT NUMBER

5b. GRANT NUMBER
W81XWH-14-1-0268

5c. PROGRAM ELEMENT NUMBER

6. AUTHOR(S)
Yingjie Xu

E-Mail: yingjie.xu@childrens.harvard.edu

5d. PROJECT NUMBER

5e. TASK NUMBER

5f. WORK UNIT NUMBER

7. PERFORMING ORGANIZATION NAME(S) AND ADDRESS(ES)
Children's Hospital Corporation

300 Longwood avenue,
Boston, Massachusetts 02115-
5724

8. PERFORMING ORGANIZATION REPORT NUMBER

9. SPONSORING / MONITORING AGENCY NAME(S) AND ADDRESS(ES)

U.S. Army Medical Research and Materiel Command
Fort Detrick, Maryland 21702-5012

10. SPONSOR/MONITOR'S ACRONYM(S)

11. SPONSOR/MONITOR'S REPORT NUMBER(S)

12. DISTRIBUTION / AVAILABILITY STATEMENT

Approved for Public Release; Distribution Unlimited

13. SUPPLEMENTARY NOTES

14. ABSTRACT

Prohibitin 1 (PHB1) is a member of a highly conserved eukaryotic protein family containing the stomatin/prohibitin/flotillin/HflK/C (SPFH) domain. PHB1 has been functionally linked to diverse cellular processes, including cell-cycle progression, apoptosis, mitochondrial biogenesis and tumor chemoresistance. To better understand the role of PHB1, we performed proteomic experiments to identify the PHB1 interactome and identified the X-linked inhibitor of apoptosis protein (XIAP) as a novel PHB1-interacting protein. The interaction was confirmed by GST pull-down assay, showing a direct interaction between the two proteins. The interaction is functionally significant, as silencing PHB1 decreases XIAP stability, resulting in consequent activation of apoptotic pathway members and restoration of paclitaxel sensitivity. Using deletion constructs of XIAP, we showed that PHB1 binds principally to the BIR3 domain of XIAP. These results suggest that the natural interaction of PHB1 and XIAP represents a novel mechanism for suppression of apoptosis that modulates tumor expansion and the response to chemotherapeutic agents.

15. SUBJECT TERMS
prohibitin 1, prostate cancer, chemoresistance, apoptosis

16. SECURITY CLASSIFICATION OF: Unclassified			17. LIMITATION OF ABSTRACT	18. NUMBER OF PAGES	19a. NAME OF RESPONSIBLE PERSON
a. REPORT	b. ABSTRACT	c. THIS PAGE			19b. TELEPHONE NUMBER *(include area code)*
Unclassified	Unclassified	Unclassified	Unclassified	76	USAMRMC

Table of Contents

Page

INTRODUCTION

Prostate cancer is the most common malignancy and second leading cause of cancer-related deaths in American men. Most patients with prostate cancer initially respond to androgen ablation therapy but ultimately progress to androgen resistance. Although patients with hormone-refractory prostate cancer are usually treated with taxane anti-cancer drugs such as docetaxel and paclitaxel, which have been shown to improve the survival of patients, most patients eventually develop drug resistance. Understanding the mechanisms by which tumors become resistant to taxane is key to identifying new drugs or combination regimens. Prohibitin 1 (PHB1) was recently identified as a protein that is both upregulated and relocalizes to the plasma membrane in taxane-resistant non-small cell lung cancer cells. Importantly, PHB1 silencing resensitized taxane-resistant cells to paclitaxel treatment both *in vitro* and *in vivo*. I propose that the amount and localization of this protein in human prostate cancer may be used as a tool for the identification of taxane-resistant prostate cancers. In this study, my goals are to develop the use of PHB1 as a biomarker for taxane resistance in prostate cancer and to reveal the complexity of prohibitin-induced cellular response, including the role of prohibitin in the regulation of taxane-resistant prostate cancer.

KEY WORDS: *Provide a brief list of keywords (limit to 20 words).*
Prohibitin 1, prostate cancer, chemoresistance, apoptosis, X-linked inhibitor of apoptosis protein (XIAP), interactome

ACCOMPLISHMENTS:

- **What were the major goals of the project?**

The major project goals of the previous year were: to investigate whether the expression and localization of Prohibitin 1 (PHB1) correlates with taxane resistance in prostate cancer cells, to identify and characterize the PHB1 interactome, and to investigate the role of PHB1 in the apoptosis pathway and chemoresistance.

- **What was accomplished under these goals?**

I believe that I have been successful in completing both the training-specific and research-specific tasks and in addressing each of the previous aims. My progress is summarized below:

1) Major activities

In the past year, I have completed the following tasks related to training and educational development in prostate cancer research:

a) Attended the Massachusetts General Hospital/Steele Lab's 29th Annual Tumor Course, September 29 - October 2, 2014; Cambridge, MA;
b) Presented research at departmental, bi-weekly cancer research group meetings;
c) Participated in research seminars, basic science journal club meetings, job talk practices and scientific writing lessons organized by the Office of Fellowship Training (OFT) at Boston Children's Hospital;
d) Attended and presented my work at the American Association of Cancer Research (AACR) Annual Meeting, April 18-22, 2015, Philadelphia, PA;
e) Attended and presented my work at Boston Children's Hospital's Dr. Judah Folkman Research Day, May 13, 2015, Boston, MA.

In the past year, I have identified the PHB1 interactome, both in the mitochondria and the plasma membrane. My work has further demonstrated that PHB1 binds to XIAP and that this interaction modulates the apoptosis pathway. The results support the following conclusions:

a) Unbiased proteomics reveal that XIAP binds to PHB1;
b) IP-western and *in vitro* pull-down assay analysis confirm a direct interaction;
c) Mapping results show that PHB1 preferentially binds to the XIAP-BIR3 domain;
d) siRNA-mediated knockdown of PHB1 increases cleavage of XIAP following chemotherapeutic reagent treatment, resulting in increased apoptosis;
e) Silencing XIAP phenocopies PHB1 silencing with respect to sensitizing cells to chemotherapeutic reagent-mediated cell death.

2) Specific objectives

Specific objectives include: a) To investigate whether the expression and localization of PHB1 correlates with taxane resistance in prostate cancer cells; b) To identify the PHB1 interactome and to validate specific interactions between PHB and XIAP.

3) Significant results

Specific Aim 1: To investigate the role of prohibitin in taxane-resistant prostate cancer

1A: To investigate PHB1 expression and cell surface targeting in our *in vitro* and *in vivo* selected spontaneous taxane-resistant prostate cancer cell lines

To see whether the amount and localization of PHB1 correlates with taxane-resistance in prostate cancer, I performed subcellular fractionation followed by western blot analysis, to compare the subcellular expression of PHB1 in between taxane-resistant and taxane-sensitive cells. I also did immunofluorescence staining followed by confocal microscopy analysis to compare PHB1 expression and localization in pairs of both permeabilized and non-permeabilized taxane-sensitive and taxane-resistant cells. These include the prostate cancer cells, PC-3 and PC-3-TR (taxane-resistant), and DU145 and DU145-TR. I found that PHB1 is overexpressed in the plasma membrane in prostate cancer cells PC-3-TR (Figure 1).

Figure 1

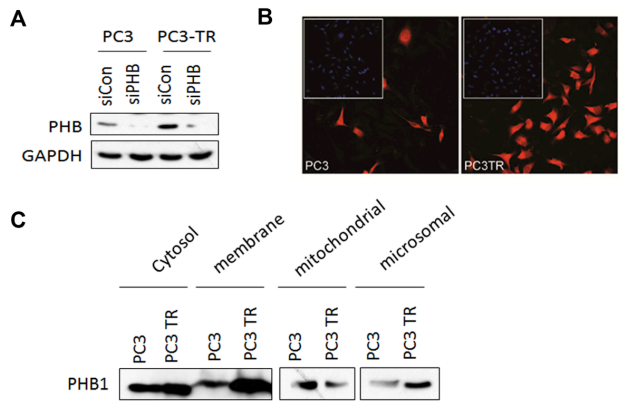

Figure 1: A) Western blot of PHB1 levels after siPHB1 treatment in PC3 and PC3-TR cells. B) membrane PHB1 expression in PC3 and PC3-TR cells. C) Subcellular fractionation followed by western blot analysis the level of PHB1.

1B: To modify the expression and localization of PHB1 and investigate its effect on taxane-resistance

In this study, I used siRNA specific to PHB1 to knock down PHB1 levels in prostate cancer cell lines (PC-3-TR, DU145-TR) to see whether prohibitin silencing would restore taxane sensitivity or not. I found that silencing of PHB1 sensitized PC-3-TR cells to paclitaxel treatment, which is similar to the effect of Bcl-2 silencing (Figure 2). More importantly, I found that PHB1 silencing promotes the activation of the cell apoptosis pathway in both PC-3 and PC-3-TR cells (Figure 3), including activation of PARP and increasing release of cytochrome C to cytosol.

Figure 2

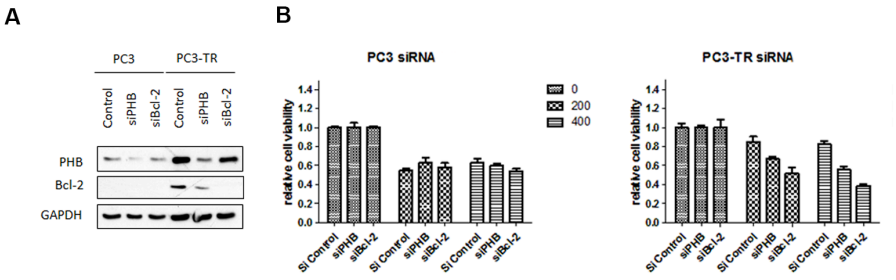

Figure 2: A) Western blot of PHB1 and Bcl-2 levels after siPHB1 treatment in PC3 and PC3-TR cells. B) Silencing PHB1 or Bcl-2 reduced cell viability analyzed with CyQUANT assay.

Figure 3

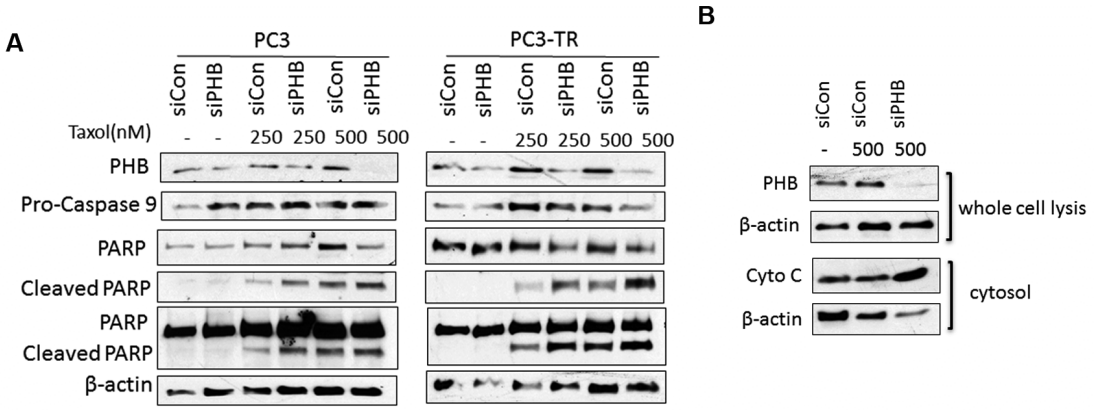

Figure 3: A) Western blot analysis of apoptosis pathway after PHB1 silencing in PC3 and PC3-TR cells. B) Increasing release of cytochrome C after PHB1 silencing followed by Taxol treatment.

In our previous study, I found that PHB1 is upregulated and also relocalizes to the plasma membrane in taxane-resistant lung cancer cells. I hypothesize that PHB1 may confer resistance to paclitaxel by increased accumulation on the cell surface. To test this hypothesis, I subcloned PHB1 into HA tagged-pDisplay plasmid (pDisplay-PHB-HA) to specifically express PHB1 on the plasma membrane of taxane-sensitive cancer cells. Then, I tested whether overexpression of PHB on the cell surface confers chemoresistance. My preliminary results showed that transient transfection of pDisplay-PHB1-HA does drive the expression of PHB1 on the plasma membrane; however, it does not confer resistance towards paclitaxel (data not shown). Stable expression of PHB1 in the plasma membrane may be needed for further examination. Another possibility of how PHB1 may confer taxane-resistance may be the ratio of PHB1 in different subcellular localizations, such as mitochondria/cytosol vs. plasma membrane.

Specific Aim 2: To identify and validate the Prohibitin 1 interactome

2A: To validate the interaction of PHB1 and XIAP and map the relevant binding domains

To gain a greater understanding of the mechanism of PHB1 action in cellular processes, I sought to identify members of the PHB1 interactome. The identity of potential PHB1-interacting proteins was determined by immunoprecipitation of PHB1 followed by mass spectrometry-based proteomic analysis. HEK293 (Human Embryonic Kidney 293) cells were transiently transfected with pHAGE vector specifying PHB1 tagged with HA (hemagglutinin) at the C-terminus. I found that PHB1-HA was predominantly, but not solely, expressed in mitochondria, consistent with previous findings (Figure 4A). The PHB1 interaction network determined by our experiments (Figure 4B) includes several known PHB1-binding proteins, such as PHB2 and RAF1, providing internal validation of the approach. The screen further identified several novel PHB1-interacting proteins, including the serine beta-lactamase-like protein LACTB, the mitochondrial carbamoyl phosphate synthase 1 (CPS1), the mitochondrial ras family GTPases Rho T1 and T2, as well as the apoptosis inhibitor XIAP. IP-MS results in experiments with HCT116 human colon cancer cells also revealed strong interaction of PHB1 with XIAP and PHB2. Many of the PHB1-interacting proteins participate in cellular functions consistent with previously known roles of PHB1, including apoptosis, mitochondrial homeostasis, the unfolded protein response and signal transduction. Identification of XIAP, a well-characterized anti-

apoptosis factor, as a PHB1 interactor suggests that this interaction may mediate the known but heretofore unexplained effects of PHB1 on apoptosis and chemoresistance.

To validate the interaction between PHB1 and XIAP, HEK293 cells were transfected with PHB1-HA and lysates were subjected to IP with anti-HA agarose and subsequently analyzed by western blotting using antibodies to PHB1 or to XIAP. Figure 4C reveals the presence of XIAP in the PHB1 immunoprecipitate; the presence of PHB2 served as positive control. Experiments with His-V5-PHB1 did not demonstrate significant interactions between PHB1 and other IAP family members, including c-IAP1, C-IAP2 and survivin (Figure 4D). More importantly, my experiments showed that XIAP interacts with *endogenous* PHB1 in both PC3 cells and Mes-Sa uterine sarcoma cells (Figure 4E). To investigate whether the binding between PHB1 and XIAP is direct or indirect, I performed an *in vitro* binding assay using recombinant 6XHis-XIAP and GST-PHB1. GST pull-down assays revealed that these two proteins were able to bind directly *in vitro* (Figure 4F). Together, these results indicate that PHB1 binds directly to XIAP, both *in vivo* and *in vitro*.

Figure 4

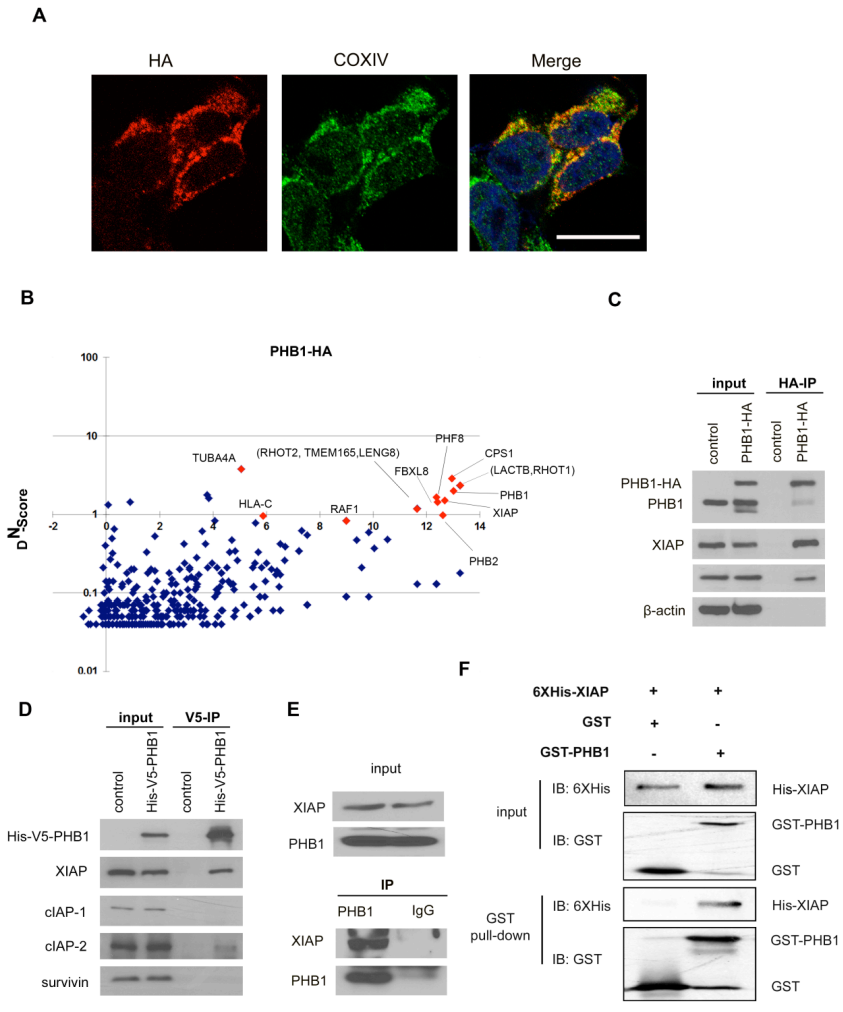

Figure 4:
A) Immunofluorescence assay of HEK293T cells with anti-HA (red) and anti-COXIV (green) antibodies. The nucleus is stained with DAPI (blue). Scale bar, 20um. B) IP-MS-*CompPASS* analysis of PHB1-HA interacting proteins in HEK293 cells. C) Co-IP of PHB1 and XIAP. Lysates of HEK293 transfected with PHB1-HA were subjected to HA agarose immunoprecipitation followed by Western blotting. D) IP of His-V5-PHB1 with V5 agarose in HEK293 cells. Immunoprecipitates were subjected to Western blotting using anti-IAP family antibodies. E) Co-IP of endogenous PHB1 and XIAP in Mes-Sa cells. F)*In vitro* GST-pull down. Direct binding of PHB1 to XIAP is shown in an *in vitro* assay using GST-PHB1 and purified recombinant His-XIAP protein. GST protein served as a negative control.

I next sought to determine the specific XIAP domain to which PHB1 binds. XIAP contains three BIR domains. BIR1 directly interacts with TAB1 to induce NF-kappaB activation. BIR2

mediates binding of XIAP to downstream effector caspases (caspases-3 and -7), whereas BIR3 binds to an upstream initiator caspase (caspase-9). BIR3 also mediates binding to functional XIAP antagonists such as DIABLO, ARTS and HtrA2/Omi. The RING domain of XIAP, which is adjacent to the BIR3 domain, demonstrates E3 ubiquitin ligase activity and enables IAPs to catalyze ubiquitination of substrate proteins, including themselves as well as other interactors. To identify the binding domain for PHB1 within XIAP, I performed co-immunoprecipitation (Co-IP) assays with His-V5-tagged PHB1 and different HA-tagged XIAP expression constructs including full-length XIAP, XIAPΔBIR, XIAP BIR1-2 and XIAP BIR2-3. The results indicated that PHB1 binds to full-length XIAP as well as to the XIAP BIR2-3 domain (Figure 5A). To more clearly define the PHB1 binding domain on XIAP, I utilized Co-IP assays to measure HA-tagged PHB1 binding to different GST-tagged XIAP expression constructs (full-length XIAP, XIAP BIR1, BIR2 and BIR3). These studies revealed that PHB1 binds principally to the BIR3 domain of XIAP (Figure 5B). I also observed a weak binding of PHB1 to the XIAP BIR2 domain. Thus, the principal PHB1 interaction site on XIAP appears to reside in the BIR3 domain.

Figure 5

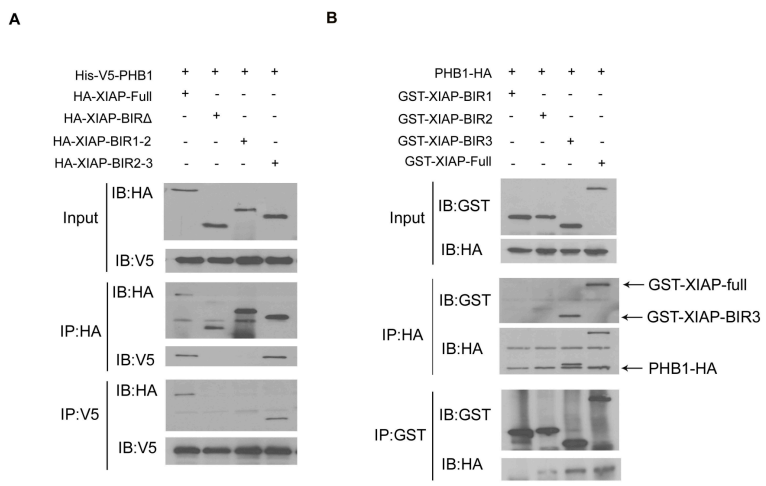

Figure 5: Immunoprecipitation assay. A) HEK293 cells were transiently transfected with the His-V5-PHB1 construct along with HA-tagged-XIAP-full-length (FL) and XIAP mutation constructs: HA-XIAP-FL, HA-XIAP-BIRΔ, HA-XIAP-BIR1-2 and HA-XIAP-BIR2-3. B) HEK293 cells were transiently transfected with PHB1-HA along with GST-tagged-XIAP-full-length (FL) and XIAP mutation constructs (GST-XIAP-BIR1, GST-XIAP-BIR2 and GST-XIAP-BIR3).

2B: To examine the cellular localization of PHB1, XIAP and the PHB1/XIAP complex

PHB1 is known to occupy multiple intracellular locales. To investigate the regions where PHB1 and XIAP are co-localized, we performed immunofluorescence double-labeling of cells with anti-PHB1 and anti-XIAP antibodies. In both Mes-Sa and PC3 cells, XIAP was localized primarily to the cytoplasm. PHB1 was detected predominantly in the mitochondria, although some cytoplasmic staining was apparent (Figure 6A). When cells were treated with paclitaxel to induce apoptosis, XIAP staining increased and showed co-localization with cytoplasmic PHB1 (Figure 6B). Subcellular fractionation followed by western blotting showed that after treatment with paclitaxel, PHB1 levels were significantly elevated, both in the mitochondria and cytosolic fraction (Figure 6C). These results are consistent with the co-localization of cytoplasmic XIAP with cytoplasmic PHB1 and suggests that PHB1 may be involved in the XIAP regulated apoptotic pathway. I am examining the co-localization of PHB1 and XIAP in prostate cancer now.

Figure 6

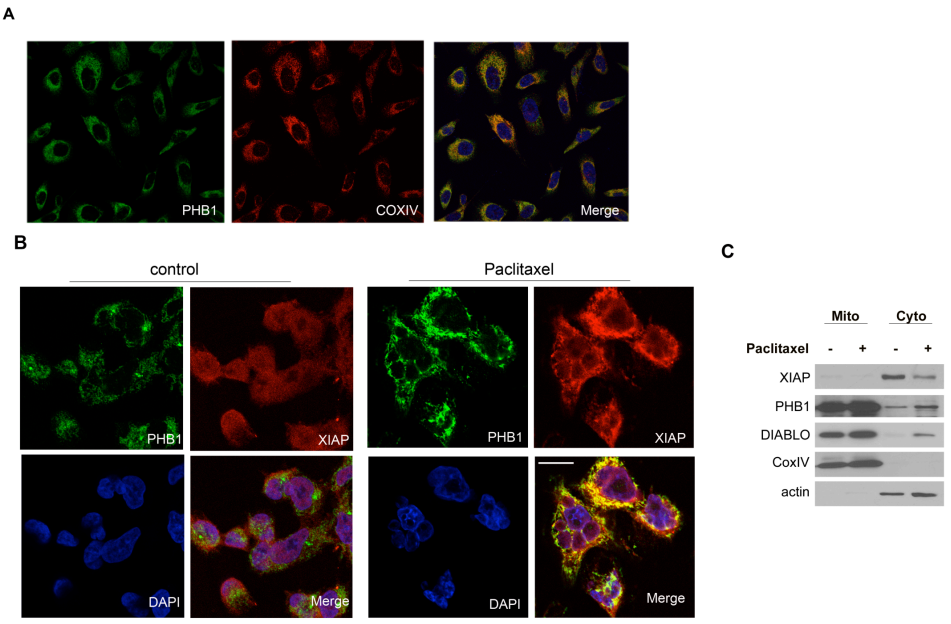

Figure 6: A) Immunofluorescence assay of PC3 cells with anti-PHB1 (green) and anti-COXIV (red) antibodies. The nucleus is stained with DAPI (blue). B) Immunofluorescence of Mes-Sa cells stained with anti-PHB1 (green) and anti-XIAP (red) antibodies. The nucleus is stained with DAPI (blue). Left panel: untreated cells; Right panel: cells treated with 500nM paclitaxel for 16 hrs. Scale bar, 20um. C) Mes-Sa cells were treated with vehicle or with 500nM paclitaxel followed by subcellular fractionation. An antibody against the cytochrome C oxidase subunit IV (COX IV) was used as a mitochondrial marker, and β-actin was used as a cytosolic marker.

2C: To investigate the effect of PHB1 on the apoptosis pathway

To confirm the involvement of PHB1 in apoptosis in the cells used in these studies, I silenced PHB1 in Mes-Sa cells using PHB1-specific siRNA followed by paclitaxel treatment to induce apoptosis. By flow cytometry analysis for Annexin-V, a marker of apoptosis, and 7-AAD, a marker of necrosis, I found that PHB1 silencing sensitized cells to paclitaxel-induced apoptosis (Figure 7A). The frequency of apoptosis, as demonstrated by the percentage of Annexin-V positive cells, increased markedly to 55.3% in cells treated with siPHB1 relative to 24.4% of siControl in the paclitaxel-treated cells. Early-stage apoptosis, marked by Annexin V-positive and 7-ADD-negative cells, also increased from 10.7% in controls to 24.9% in the paclitaxel-treated siPHB1 cells. Similar effects were observed when Mes-Sa cells were treated with staurosporine (STS), an apoptosis inducer (data not shown). One possible mechanism for PHB1's anti-apoptotic activity is through protection of XIAP function. This could occur if, for example, PHB1 competed with binding of an XIAP antagonist such as DIABLO. If this were the case, PHB1 silencing should result in increased levels of the XIAP-DIABLO complex. My results, however, showed decreased levels of XIAP-DIABLO interaction after PHB1 silencing (Figure 8), suggesting that PHB1 regulates XIAP functionality via other mechanisms. In this experiment, I noticed that the levels of full-length XIAP were modestly decreased after PHB1 silencing, suggesting a potential effect of PHB1 on XIAP cleavage or degradation.

It was shown previously that XIAP cleavage by caspases occurs at aspartic acid-242, which lies between the BIR2 and BIR3 domains. The resulting BIR1-2 cleavage product is degraded, while

the BIR3-RING domain product acts as a part of a positive feedback loop to increase apoptosis. I speculated that PHB1 binding to the XIAP-BIR3 domain may interfere with caspase-mediated XIAP cleavage. Both sicontrol (siCon) and siPHB1 treated Mes-Sa cells were treated with paclitaxel to induce apoptosis, and levels of XIAP and its downstream effectors were measured. Western blotting showed that PHB1 silencing leads to generation of a 30KDa cleaved-XIAP BIR3-RING domain, which results in enhanced caspase-3 processing into the catalytically active p17 fragment (cleaved caspase-3) and a consequent increase in cleaved PARP (poly ADP ribose polymerase), especially when paclitaxel is added (Figure 7B). This result suggests that the red fluorescent staining observed in paclitaxel-treated cells in Figure 6B likely represents both full-length and cleaved XIAP, as both would be recognized by antibody to the XIAP C-terminus. Moreover, caspase-3/7 activity, as measured by Caspase-Glo assay, revealed that PHB1 silencing increased activation of caspase-3/7 following paclitaxel treatment (Figure 7C) (*p<0.05; ***p<0.001). These findings are consistent with a role for PHB1 as an inhibitor of apoptosis and were verified further in prostate cancer cell lines (Figure 3). This study shows that, in contrast to the IBM protein family that antagonizes IAP action, PHB1 protects XIAP function by diminishing caspase-mediated XIAP cleavage. PHB1 was previously described as a chaperone for mitochondrial proteins. My results suggest a similar role for PHB1 in protecting cytoplasmic XIAP.

Figure 7

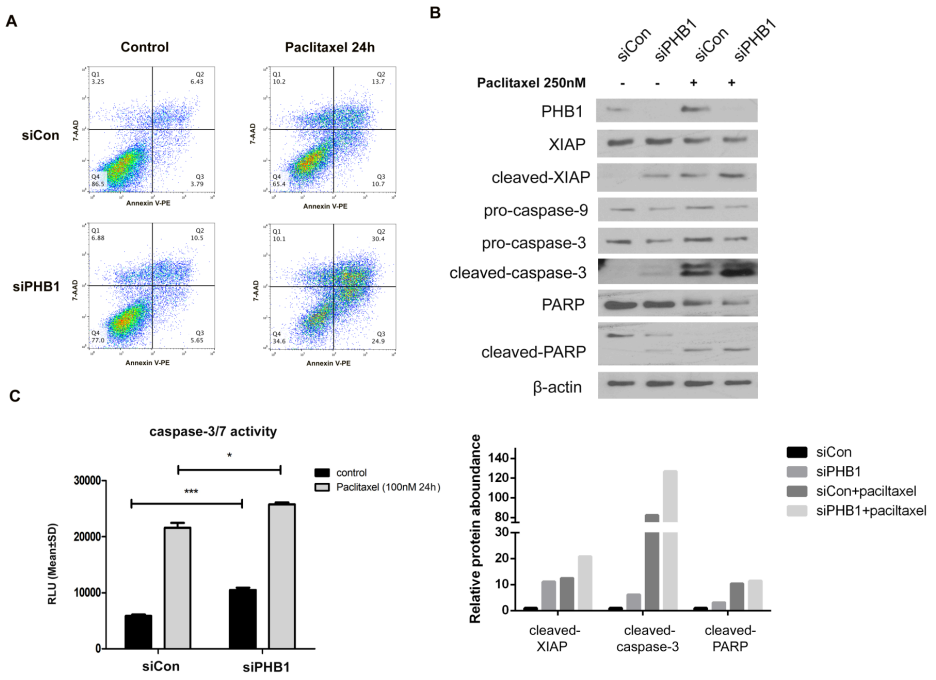

Figure 7: A) Mes-Sa cells were transfected with siCon or siPHB1 for 2 days, followed by paclitaxel (250nM) treatment for 24 hours. Results of flow cytometry analysis of apoptosis induction are presented in quadrants. B) Mes-Sa cells were transfected with siCon or siPHB1 for 2 days, followed by paclitaxel treatment for 24 hours. Western blotting of Mes-Sa cell lysates after treatment with 250nM paclitaxel for 24 hours. C) Caspase 3/7 activity after PHB1 silencing in Mes-Sa cells. *p<0.05; ***p<0.001. Error bars are SDs.

2D: To investigate whether PHB1 regulates apoptosis through its interaction with XIAP

I next investigated whether silencing of PHB1 and XIAP have similar functionality. PHB1 or XIAP were silenced in Mes-Sa cells, and the cells were then treated with paclitaxel. Figure 9A

shows successful knockdown of PHB1 and XIAP by specific siRNAs. I found that silencing either PHB1 or XIAP increased cell killing by paclitaxel (Figure 9B).

Figure 8

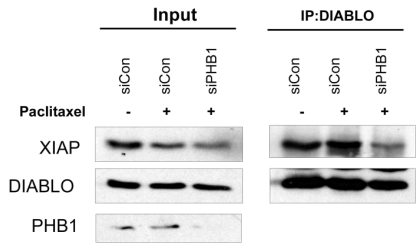

Figure 8: Silencing of PHB1 decreases interaction of XIAP with DIABLO. OVCAR5 cells were transfected with siCon or siPHB1 for 2 days followed by paclitaxel treatment for 24h. Immunoprecipitation assays with anti-DIABLO antibody and agarose beads, followed by Western blotting of DIABLO and XIAP antibodies.

Figure 9

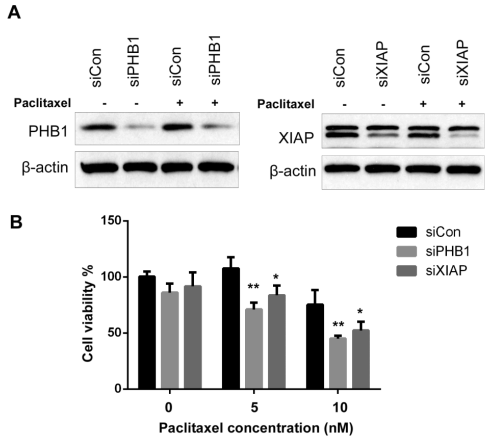

Figure 9: Effect of silencing PHB1 or XIAP on cancer cell sensitivity to paclitaxel. a) Mes-Sa cells were transfected with siCon, siPHB1 or siXIAP for 2 days, followed by paclitaxel treatment for 24 hours. Western blotting assessed the efficiency of PHB1 and XIAP knockdown. B) cell viability of siCon, siPHB1 and siXIAP-transfected cells under paclitaxel treatment was determined by CyQUANT cell viability assay in three independent experiments; $*p<0.05$; $**p<0.01$. Error bars are SDs.

In a previous study, we found that PHB1 is an important modulator of taxane resistance in non-small cell lung cancer (NSCLC) cells. In that report, silencing of PHB1 resensitized taxane-resistant cancer cells to paclitaxel treatment. I therefore investigated whether XIAP silencing mimics the effect of PHB1 silencing on chemoresistance to taxanes. In paclitaxel-resistant PC-3 (PC-3TR) prostate cancer cells, which have elevated PHB1 levels relative to parental PC-3 cells, sensitization to paclitaxel was restored by silencing with either siPHB1 or siXIAP (Figures 10A and 10B). Western blot analysis further showed that silencing PHB1 in paclitaxel-treated PC-3TR cells leads to diminished levels of XIAP, enhanced activation of caspase-3 (cleaved caspase-3) and increased PARP cleavage relative to siControl treated cells (Figure 10C). Next, I investigated whether overexpression of XIAP can rescue the apoptotic phenotype caused by PHB1. I found that overexpression of XIAP in PHB1-silenced cells partially rescued the cell death caused by siPHB1. In this experiment, PHB1 silencing resulted in a dramatic reduction of His-V5-XIAP protein compared to siControl-treated cells (Figure 11A). The level of His-V5-XIAP was restored in PHB1-silenced cells by treatment with proteasome inhibitor MG132. Together, these results suggest that XIAP is protected from proteasomal degradation in the presence of PHB1 (Figure 11B).

Figure 10

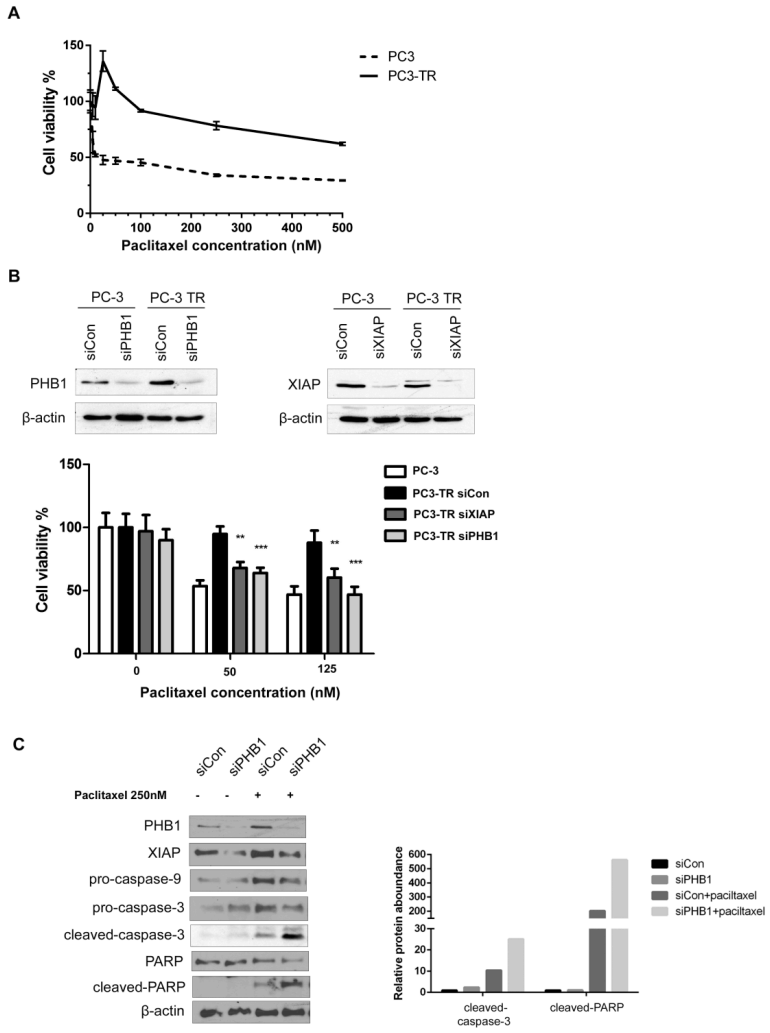

Figure 10: Silencing of PHB1 or XIAP restores chemosensitivity in taxane-resistant prostate cancer cells. A) PC3 and PC3-TR cells were treated with different concentrations of paclitaxel for 3 days, followed by cell viability measurement using CyQUANT assay. B) PC3 and PC3-TR cells were transfected with siCon, siPHB1 or siXIAP for 2 days, followed by paclitaxel treatment for 3 days. Cell number was determined by CyQUANT cell viability assay in three independent experiments; $^{**}p<0.01$; $^{***}p<0.001$. Error bars are SDs. C)PC-3-TR cells were transfected with siCon or siPHB1 for 2 days, followed by paclitaxel treatment for 24 hours. Left panel: Western blotting; Right panel: graph depicts densitometric quantification of the blot on the left.

Figure 11

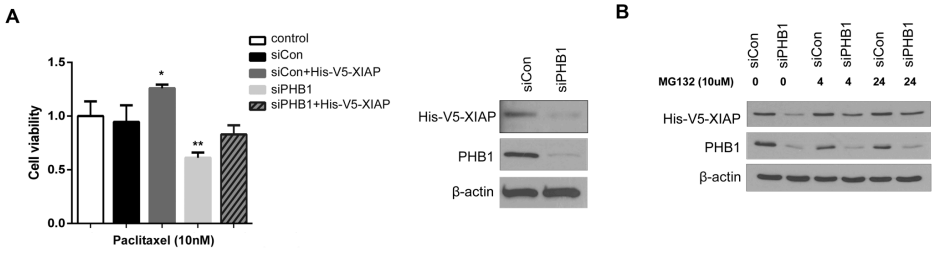

Figure 11: A) HEK293 cells were transfected with siCon, siCon+His-V5-XIAP, siPHB1, or siPHB1+His-V5-XIAP for 2 days, followed by paclitaxel treatment. Left panel: cell viability was measured 3 days after treatment using CyQUANT assay. $^{*}p<0.05$; $^{**}p<0.01$. Error bars are SDs. Right panel: lysates of His-V5-XIAP-transfected cells were subjected to Western blotting. B) In HEK293 cells, His-V5-XIAP was co-transfected with siCon or siPHB1 for 2 days, followed by MG132 (10uM) treatment for 4 hours or 24 hours. Cell lysates were subjected to Western blotting.

4) Other achievement

PHB1 and PHB2 bind to each other and form a complex that is anchored in the mitochondrial inner membrane (IM). Furthermore, PHB1 and PHB2 subunits are interdependent in various organisms, since depletion of either PHB1 or PHB2 does not affect the expression of the other, but results in its degradation and therefore the absence of the complex. Therefore, I am interested in exploring the biological role of the PHB complex in prostate cancer and chemoresistance. To do that, I have started to build the networks of the PHB complex using IP-MS interactome proteomics analysis (Figure 12).

Figure 12

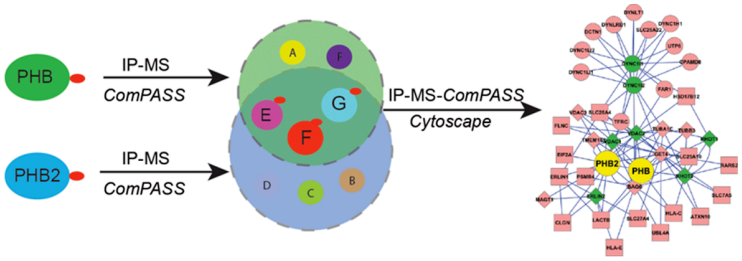

Figure 12: Workflow of construction of PHB complex network.

What opportunities for training and professional development has the project provided?

This project has provided me with the opportunity to attend the American Association of Cancer Research (AACR) Annual Meeting in April 2015 and to present my work at a poster section. More importantly, based on the quality of my abstract submitted for presentation at the 2015 AACR Annual Meeting, I was selected to receive an *AACR-Millennium Pharmaceuticals, Inc. Scholar-in-Training Award*. Later on, an abstract of the same work was selected as a poster presentation for Boston Children's Hospital's Dr. Judah Folkman Research Day, May 13, 2015.

- **How were the results disseminated to communities of interest?**

As this project comprehensively dissected the mechanism of PHB1 in regulation of apoptosis and chemoresistance, I had the chance to collaborate with other groups to further validate PHB1 as a potential target for cancer treatment. 1) In collaboration with Dr. Wistuba of MD Anderson, I examined PHB1 expression in 465 patients with non-small cell lung cancer (NSCLC). 2) A similar collaboration is ongoing with Dr. Sood of MD Anderson to look at PHB1 expression in ovarian cancer patients. 3) Moreover, Dr. Shi in the Laboratory of Nanomedicine and Biomaterials at Brigham and Women's Hospital developed novel nanoparticles to deliver siRNA to target PHB1 and found that siPHB1 inhibits tumor growth in the NSCLC xenograft model. I am planning to employ these nanoparticles in the treatment of prostate cancer. 4) Recently, Dr. Laurent Désaubry of the University Strasbourg sent me his synthesized flavaglines (FL3, FL23, FL40), potent anti-cancer reagents that directly target both PHB1 and PHB2. I am planning to test the therapeutic efficacy of flavaglines in the treatment of chemoresistant and metastatic prostate cancer as well.

- **What do you plan to do during the next reporting period to accomplish the goals?**

During the next reporting period, I will further investigate the mechanisms of how PHB1 regulates prostate cancer chemoresistance through its interaction with specific proteins,

determine whether PHB1 is widely overexpressed in human prostate cancer compared to normal surrounding tissue, and determine whether PHB1 expression or localization predicts response to chemotherapy.

IMPACT:

- **What was the impact on the development of the principal discipline(s) of the project?**

The research proposed here addresses the overarching challenge to develop effective treatments for advanced prostate cancer (i.e., disease relapse with no available curative therapy) and the focus area of therapy; including the identification of new biomarkers/targets and pathways, and understanding the mechanisms of chemoresistance.

This study could significantly impact the treatment of castrate-resistant prostate cancer patients who are candidates for taxane treatment. In Aim 1, I showed that prohibitin expression or localization correlates with taxane resistance in prostate cancer cells. After further examination of the expression of PHB1 in prostate cancer patient samples, I will identify a candidate biomarker for acquisition of the taxane-resistant phenotype, as well as a cell-surface epitope that could be used to target therapeutic agents specifically to taxane-resistant tumor cells. In Aim 2, I identified the prohibitin interactome and detailed dissected the role of PHB1-XIAP interaction, which will allow us to better understand the regulatory mechanisms involved in post-translational modifications of PHB1, its translocation to different cellular compartments, and its functional relevance. More importantly, the identification of the change in prohibitin interactors with the development of taxane resistance will bring new insight into the mechanism of taxane-resistant prostate cancer and will provide novel potential therapeutic targets (such as XIAP) for the development of agents that can extend sensitivity to taxanes or be effective in patients already resistant to taxane therapy.

.

- **What was the impact on other disciplines?**

In this study, I not only dissected the mechanism of some known functions of PHB1, such as its anti-apoptotic function, but also discovered novel functions of PHB1, such as its role in regulating the mTOR pathway. Given the fact that PHB1 and PHB2 exist interdependently in cells, my ongoing work on the construction of a PHB complex network will help us to further understand how these two proteins work as a complex and to explore their new functions. Since no work has been conducted to study PHB's function as a complex, I believe that this work will input some basic knowledge of the PHB complex as well as the SPFH (Stomatin, Prohibitin, Flotillin and HflK/C) family, to which PHB1 and PHB2 belong.

- **What was the impact on technology transfer?**

Given the importance of prohibitin's function in the regulation of apoptosis and chemoresistance, I am exploring the *in vivo* validation of PHB1 targeting in cancer treatment. In collaboration with Dr. Shi in the Laboratory of Nanomedicine and Biomaterials at Brigham and Women's Hospital, I am testing the systemic delivery of small interfering RNA (siRNA) targeting PHB1 in treatment of non-small cell lung cancer (NSCLC) using a nanoparticle (NP) platform. The lipid–polymer hybrid small interfering RNA (siRNA) NP is developed through a self-assembly approach and has a unique nanostructure comprising a cationic lipid/siRNA complex-containing poly(D,l-lactide-*co*-glycolide) (PLGA) polymer core and a lecithin/lipid-PEG shell. This hybrid NP is much smaller (≤100 nm) and exhibits promising *in vivo* features for systemic siRNA

delivery, including long circulation, high tumor accumulation, effective gene silencing, and modest side effects. I found that NP (siPHB1) knocked down the level of PHB1 more than 75% relative to NP(siControl), which greatly increased tumor cell apoptosis and resulted in the significant reduction of tumor growth of the NSCLC NCI-H460 xenograft model. Dr.Shi's lab will remain in close collaboration with our lab to further investigate the therapeutic efficacy of this NP platform in chemoresistant prostate cancer models.

Moreover, Dr. Laurent Désaubry from the University Strasbourg has sent me his laboratory's synthesized flavaglines (FL3, FL23, FL40), potent anti-cancer reagents that directly target both PHB1 and PHB2. I will use flavaglines as a tool to further study the functions of the PHB complex and to test the therapeutic efficacy of flavaglines in the treatment of chemoresistant and metastatic prostate cancer.

- **What was the impact on society beyond science and technology?**

Nothing to Report

CHANGES/PROBLEMS

- **Changes in approach and reasons for change**

Nothing to Report

- **Actual or anticipated problems or delays and actions or plans to resolve them**

In my previous study, I found that PHB1 is upregulated and also relocalizes to the plasma membrane in taxane-resistant lung cancer cells. I hypothesize that PHB1 may confer resistance to paclitaxel by increased accumulation on the cell surface. To test this hypothesis, I subcloned PHB1 into HA tagged- pDisplay plasmid (pDisplay-PHB-HA) to specifically express PHB1 on the plasma membrane of taxane-sensitive cancer cells, and I tested whether the overexpression of PHB on cell surface confers chemoresistance. My preliminary results showed that transient transfection of pDisplay-PHB1-HA does drive the expression of PHB1 on the plasma membrane; however, it does not confer resistance towards paclitaxel (data not shown). Stable expression of PHB1 at the plasma membrane may be needed for further examination. Another possibility as to how PHB1 may confer taxane-resistance may be the ratio of PHB1 in different subcellular localizations, such as mitochondria/cytosol vs. plasma membrane. I believed that the identification of plasma membrane-specific PHB1 may provide a clue; therefore, I used pDisplay-PHB-HA as bait for IP-MS in 293T cells and identified several plasma membrane-specific HCIPs of PHB. I employed 293T cells in all of my IP-MS/MS experiments, as the database used for *CompPASS* analysis is from 172 parallel IP-MS/MS experiments on 293T cells. Figure 13 summarizes the membrane-specific PHB1 interactome, which is quite different from the mitochondrial dominant PHB1 interactome (Figure 4B). Because cell surface prohibitin is expected to be more abundant in taxane-resistant cells, I will pay particular attention to differences in binding to interactors in taxane-resistant *vs*. taxane-sensitive tumor cells.

Figure 13

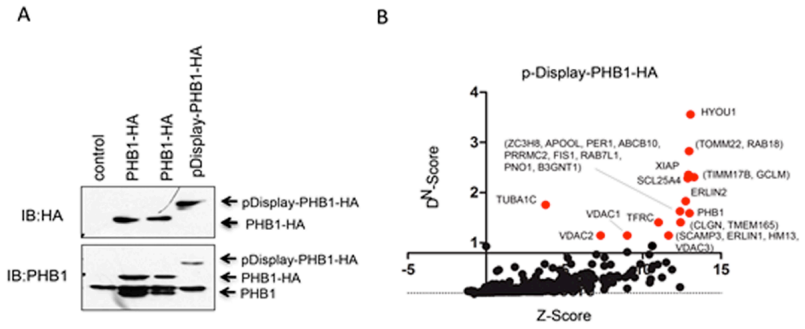

Figure 13: A) Western blot analysis of overexpressed PHB1-HA and pDisplay-PHB1-HA in HEK293 cells. B) Membrane specific PHB1 interactome identified in HEK293 cells by overexpression of pDisplay-PHB1-HA followed by IP-MS-*CompPASS*.

- **Changes that had a significant impact on expenditures**

Nothing to Report

- **Significant changes in use or care of human subjects, vertebrate animals, biohazards, and/or select agents**

Nothing to Report

- **Significant changes in use or care of human subjects**

Nothing to Report

- **Significant changes in use or care of vertebrate animals.**

Nothing to Report

- **Significant changes in use of biohazards and/or select agents**

I am planning to employ flavaglines as a tool to further study the functions of the PHB complex and to test the therapeutic efficacy of flavaglines in the treatment of chemoresistant and metastatic prostate cancer. In a recent study from Dr. Désaubry of the University Strasbourg, using an affinity chromatography approach, PHB1 and PHB2 were demonstrated to be direct targets of rocaglamides. My preliminary experiments tested the synthesized flavaglines (FL3, FL23, FL40) from Dr. Désaubry's lab and found that flavaglines significantly decreased the cell viability of multiple cancer cell lines, including those chemoresistant cells (Figure 14).

Figure 14

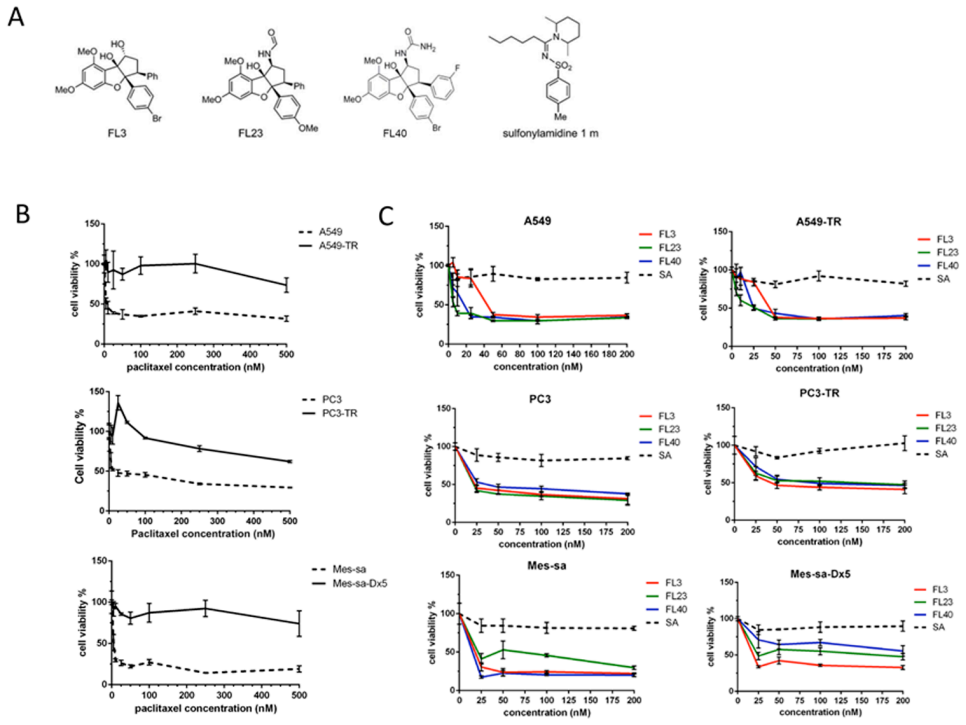

Figure 14: Flavaglines treatment of multiple cancer cell lines. A) structure of flavaglines and sulfonyl amidine. B) Cell viability of multiple chemosensitive and chemoresistant cell lines under paclitaxel treatment for 72 hours. C) Cell viability of above matched chemosensitive and chemoresistant cancer cells under flavaglines or SA treatment for 72 hours.

PRODUCTS

1. **Publications, conference papers, and presentations**

   - **Journal publications.**

   Zhu X, Xu Y*, Solis LM, Tao W, Wang L, Behrens C, Xu X, Zhao L, Liu D, Wu J, Zhang N, Wistuba II, Farokhzad OC, Zetter BR, Shi J. Long-circulating siRNA nanoparticles for validating Prohibitin1-targeted non-small cell lung cancer treatment. *Proc Natl Acad Sci U S A*. 2015 Jun 23;112(25):7779-84. doi: 10.1073/pnas.1505629112. Epub 2015 Jun 8. (*Co-first author); (Published); acknowledgement of federal support (yes).

   Islam MA, Reesor EK, Xu Y, Zope HR, Zetter BR, Shi J. Biomaterials for mRNA delivery. *Biomater Sci*. 2015. [Epub ahead of print Aug 17] (Published); acknowledgement of federal support (yes).

   Xu Y, Yang W, Shi J, Zetter BR. Prohibitin 1 regulates tumor cell apoptosis via interaction with X-linked inhibitor of apoptosis protein. *Journal of Molecular Cell Biology.* 2015 (under review); acknowledgement of federal support (yes).

   - **Books or other non-periodical, one-time publications.**

   Nothing to Report

   - **Other publications, conference papers, and presentations.**

   Poster presentation: Prohibitin 1 regulates apoptosis via its interaction with XIAP
   Author: Yingjie Xu[1], Wen Yang[2], Virginia Guarani[2], Jinjun Shi[3], J. Wade Harper[2], Bruce R. Zetter[1]. [1]Boston Children's Hospital, Harvard Medical School, Boston, MA; [2]Harvard Medical School, Boston, MA; [3]Brigham and Women's Hospital, Harvard Medical School, Boston, MA

   1. AACR Annual Meeting. April 18-22, 2015; Philadelphia, PA.
   2. Dr. Judah Folkman Research Day. May 13, 2015; Boston, MA.

2. **Website(s) or other Internet site(s)**
   Our work was presented in the poster section of the 2015 AACR Annual Meeting and subsequently was published online:
   http://www.abstractsonline.com/Plan/ViewAbstract.aspx?mID=3682&sKey=378f68bd-675a-4ae7-bea6-fbfc61ec3c0e&cKey=cf5feeca-c87c-4fba-a99f-2f0bb36345d4&mKey=19573a54-ae8f-4e00-9c23-bd6d62268424

3. **Technologies or techniques**
   Nothing to Report.

4. **Inventions, patent applications, and/or licenses**
   Nothing to Report.

5. **Other Products**
Nothing to Report.

PARTICIPANTS&OTHER COLLABORATING ORGANIZATIONS

What individuals have worked on the project?

No change.

Has there been a change in the active other support of the PD/PI(s) or senior/key personnel since the last reporting period?

Nothing to Report.

What other organizations were involved as partners?

Nothing to Report.

SPECIAL REPORTING REQUIREMENTS

Nothing to Report.

APPENDICES:

Zhu X, Xu Y*, Solis LM, Tao W, Wang L, Behrens C, Xu X, Zhao L, Liu D, Wu J, Zhang N, Wistuba II, Farokhzad OC, Zetter BR, Shi J. Long-circulating siRNA nanoparticles for validating Prohibitin1-targeted non-small cell lung cancer treatment. *Proc Natl Acad Sci U S A*. 2015 Jun 23;112(25):7779-84. doi: 10.1073/pnas.1505629112. Epub 2015 Jun 8. (*Co-first author).

Islam MA, Reesor EK, Xu Y, Zope HR, Zetter BR, Shi J. Biomaterials for mRNA delivery. *Biomater Sci*. 2015 Aug 17. [Epub ahead of print]

Xu Y, Yang W, Shi J, Zetter BR. Prohibitin 1 regulates tumor cell apoptosis via interaction with X-linked inhibitor of apoptosis protein. *Journal of Molecular Cell Biology* (under review, 2015).

Long-circulating siRNA nanoparticles for validating Prohibitin1-targeted non-small cell lung cancer treatment

Xi Zhu[a,b,1], Yingjie Xu[c,1], Luisa M. Solis[d], Wei Tao[a,e], Liangzhe Wang[c], Carmen Behrens[d], Xiaoyang Xu[a,f], Lili Zhao[a,g], Danny Liu[a,h], Jun Wu[a], Ning Zhang[i], Ignacio I. Wistuba[d], Omid C. Farokhzad[a,j], Bruce R. Zetter[c], and Jinjun Shi[a,2]

[a]Department of Anesthesiology, Brigham and Women's Hospital, Harvard Medical School, Boston, MA 02115; [b]West China School of Pharmacy, Sichuan University, Chengdu 610041, China; [c]Vascular Biology Program, Boston Children's Hospital, Harvard Medical School, Boston, MA 02115; [d]Department of Translational Molecular Pathology, The University of Texas MD Anderson Cancer Center, Houston, TX 77030; [e]School of Life Sciences, Tsinghua University, Beijing 100084, China; [f]Department of Chemical, Biological and Pharmaceutical Engineering, New Jersey Institute of Technology, Newark, NJ 07102; [g]The First Affiliated Hospital of Nanjing Medical University, Jiangsu Province Hospital, Nanjing 210029, China; [h]Department of Chemistry, University of Waterloo, Waterloo, ON N2L 3G1, Canada; [i]Department of Chemistry, University of Science and Technology of China, Hefei 230026, China; and [j]King Abdulaziz University, Jeddah 21589, Saudi Arabia

Edited by Liangfang Zhang, University of California, San Diego, La Jolla, CA, and accepted by the Editorial Board May 12, 2015 (received for review March 20, 2015)

RNA interference (RNAi) represents a promising strategy for identification and validation of putative therapeutic targets and for treatment of a myriad of important human diseases including cancer. However, the effective systemic in vivo delivery of small interfering RNA (siRNA) to tumors remains a formidable challenge. Using a robust self-assembly strategy, we develop a unique nanoparticle (NP) platform composed of a solid polymer/cationic lipid hybrid core and a lipid-poly(ethylene glycol) (lipid-PEG) shell for systemic siRNA delivery. The new generation lipid–polymer hybrid NPs are small and uniform, and can efficiently encapsulate siRNA and control its sustained release. They exhibit long blood circulation ($t_{1/2}$ ~8 h), high tumor accumulation, effective gene silencing, and negligible in vivo side effects. With this RNAi NP, we delineate and validate the therapeutic role of Prohibitin1 (PHB1), a target protein that has not been systemically evaluated in vivo due to the lack of specific and effective inhibitors, in treating non-small cell lung cancer (NSCLC) as evidenced by the drastic inhibition of tumor growth upon PHB1 silencing. Human tissue microarray analysis also reveals that high PHB1 tumor expression is associated with poorer overall survival in patients with NSCLC, further suggesting PHB1 as a therapeutic target. We expect this long-circulating RNAi NP platform to be of high interest for validating potential cancer targets in vivo and for the development of new cancer therapies.

siRNA delivery | nanoparticle | Prohibitin1 | non-small cell lung cancer

With the capability to silence any gene of interest, RNA interference (RNAi) technology has demonstrated enormous potential in medical research and applications (1, 2). RNAi-mediated gene silencing has revealed the functionality of specific genetic alterations in cancers (3–5). Many of these genes and pathways are considered "undruggable" targets or require complex and time-consuming development of effective inhibitors. The ubiquitous application of RNAi in cancer research and therapy is nevertheless hindered by the challenge of effective systemic in vivo delivery of siRNA to tumors, which requires overcoming of multiple physiological barriers, such as enzymatic degradation, rapid elimination by renal excretion or by the mononuclear phagocyte system (MPS), and poor cellular uptake and endosomal escape (2, 6, 7). To this end, a great number of cationic lipid/polymer-based nanoparticles (NPs) have been developed to protect siRNA from serum nucleases and facilitate its cytosolic delivery (8). Surface PEGylation has also been applied extensively to improve NP stability and reduce MPS recognition (9, 10). Several RNAi nanotherapeutics are now in clinical trial in cancer patients. However, the clinical stage anticancer RNAi NPs have shown relatively rapid clearance in blood (11, 12), which may reduce their extravasation into tumor tissue through the enhanced permeability and retention (EPR) effect (13). This could result in decreased in vivo silencing efficacy and consequently limit potential clinical impact.

Here we report the development of a long-circulating RNAi NP platform for exploring and validating PHB1 as a potential new therapeutic target in NSCLC treatment. This lipid–polymer hybrid small interfering RNA (siRNA) NP (Fig. 1*A*) is rationally developed through a robust self-assembly approach, and has a unique nanostructure comprising a cationic lipid/siRNA complex-containing poly(D,L-lactide-*co*-glycolide) (PLGA) polymer core and a lecithin/lipid-PEG shell. Unlike previous lipid–polymer hybrid RNAi NPs formulated by the double emulsion and solvent evaporation techniques (14–18), our self-assembled hybrid NP is much smaller (≤100 nm) and exhibits promising in vivo features for systemic siRNA delivery, including long circulation, high tumor accumulation, effective gene silencing, and modest side

Significance

This study developed a new generation lipid–polymer hybrid nanoparticle platform for effective systemic delivery of small interfering RNA (siRNA) to tumors, which represents a challenging hurdle for the widespread application of RNA interference (RNAi) in cancer research and therapy. With promising in vivo features such as long blood circulation, high tumor accumulation, and effective gene silencing, the hybrid siRNA nanoparticles were successfully used to reveal and validate a putative therapeutic target, Prohibitin1 (PHB1), in non-small cell lung cancer treatment. In vivo antitumor efficacy results and human tissue microarray analysis further suggested the feasibility of utilizing PHB1 siRNA nanoparticles as a novel therapeutic agent. This hybrid RNAi nanoparticle platform may serve as a valuable tool for validating potential cancer targets and developing new cancer therapies.

Author contributions: X.Z., Y.X., O.C.F., B.R.Z., and J.S. designed research; X.Z., Y.X., L.M.S., W.T., C.B., X.X., L.Z., D.L., J.W., N.Z., and I.I.W. performed research; X.Z., Y.X., L.M.S., L.W., C.B., I.I.W., O.C.F., B.R.Z., and J.S. analyzed data; and X.Z., Y.X., O.C.F., B.R.Z., and J.S. wrote the paper.

Conflict of interest statement: O.C.F. discloses financial interest in BIND Therapeutics, Selecta Biosciences, and Blend Therapeutics, which are developing nanoparticle therapeutics for medical applications. BIND, Selecta, and Blend did not support the aforementioned research, and currently these companies have no rights to any technology or intellectual property developed as part of this research.

This article is a PNAS Direct Submission. L.Z. is a guest editor invited by the Editorial Board.

[1]X.Z. and Y.X. contributed equally to this work.

[2]To whom correspondence should be addressed. Email: jinjun.shi@zeus.bwh.harvard.edu.

This article contains supporting information online at www.pnas.org/lookup/suppl/doi:10.1073/pnas.1505629112/-/DCSupplemental.

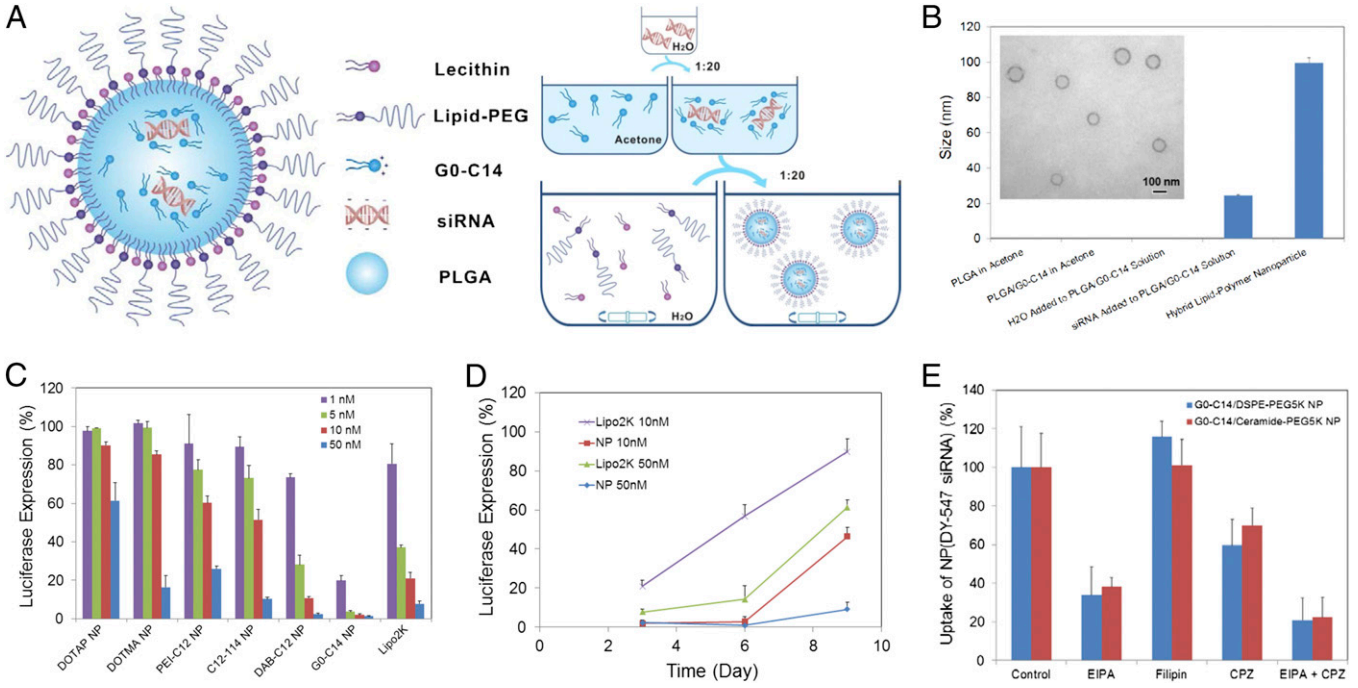

Fig. 1. Self-assembly of lipid–polymer hybrid NP for siRNA delivery. (*A*) Schematic diagram of the NP structure and the self-assembly process for NP formulation. (*B*) Monitoring of the NP formulation by dynamic light scattering (DLS). No particle formation was observed when H_2O was added to the acetone solution of PLGA/G0-C14 in a volume ratio of 1:20. When aqueous siRNA was added to the same solution, small complexes can be detected with a size of ~26 nm. After nanoprecipitation in the bulk aqueous solution of lecithin/lipid-PEG, the hybrid NPs show a size of ~100 nm. *Inset* is the transmission electron microscopy (TEM) image of the NPs. (*C*) Luciferase expression in Luc-HeLa cells transfected with NP(siLuc) composed of different cationic lipids or lipid-like compounds. All siRNA NPs were made with the N/P ratio of 10/1. Lipo2K was used as a positive control. (*D*) Sustained luciferase silencing by NP(siLuc) vs. Lipo2K–siLuc complexes. (*E*) NP uptake in the presence of specific endocytic inhibitors.

effects. We also reveal that the cationic lipid component and the surface lipid-PEG have a critical role in controlling gene silencing efficacy and pharmacokinetics (PK) of the new generation hybrid NPs. After systematic investigation and screening, this siRNA NP is successfully applied to define the role of PHB1 as a potential cancer target. Although proposed to modulate tumor cell proliferation and chemoresistance (19–21), systemic in vivo validation of PHB1 for cancer treatment remains elusive. In this work, we demonstrate antitumor activity following systemic delivery of PHB1 siRNA and propose this approach as a novel therapeutic modality for NSCLC treatment.

Results

A Robust Self-Assembly Strategy for NP Formulation. As illustrated in Fig. 1*A*, the lipid–polymer hybrid NPs are self-assembled together with siRNA through a simple two-step approach. Aqueous siRNA was first mixed with the acetone solution containing cationic lipids (or lipid-like compounds) and PLGA polymer in a 1:20 volume ratio. With water rapidly and homogeneously dispersing in acetone, the negatively charged siRNA molecules spontaneously assembled with cationic lipids (e.g., G0-C14) into small nanocomplexes with a size of ~26 nm (Fig. 1*B*). It is worth noting that acetone has no effect on the integrity and bioactivity of siRNA (*SI Appendix*, Fig. S1). By adding the acetone solution to a rapidly mixing, bulk aqueous solution of lecithin and lipid-PEG, the PLGA polymer and cationic lipid/siRNA complex were co-nanoprecipitated to form a solid NP core surrounded by a lecithin/lipid-PEG shell.

Different cationic lipids/lipid-like compounds were tested for NP formulation and were demonstrated to have an influence on the particle size, siRNA encapsulation, and release kinetics (*SI Appendix*, Figs. S2 and S3). The lipid-like compounds are cationic molecules consisting of polar amine-containing hydrophilic head groups and nonpolar hydrophobic hydrocarbon tails, which were synthesized through the ring opening of epoxides by amine substrates (*SI Appendix*, Fig. S2 *B* and *C*) (22). With G0-C14 as the cationic lipid component, the hybrid NP was ~100 nm in size (Fig. 1*B*), with siRNA encapsulation efficiency at ~80% and a loading of ~640 pmol siRNA/mg PLGA. Compared with traditional lipid–polymer hybrid RNAi NPs that were prepared by the double emulsion/solvent evaporation methods (14–18), this self-assembled hybrid NP is much smaller and more uniform, and can be easily made, while retaining comparable siRNA encapsulation efficiency. In addition, the solid PLGA polymer core offers a more rigid and stable nanostructure that can better protect the encapsulated siRNA than the lipid–siRNA complex (lipoplex) structure (*SI Appendix*, Fig. S4*A*). Stability tests showed that the siRNA within the NPs underwent no obvious degradation in serum within 24 h, whereas ~70% siRNA degradation was observed in the lipoplexes.

NP-Mediated siRNA Delivery in Vitro. Firefly luciferase-expressed HeLa (Luc-HeLa) cells were used for optimizing and understanding the hybrid NP platform for siRNA delivery. As shown in the luciferase silencing experiments, the choice of cationic lipids (or lipid-like compounds) greatly influenced the silencing efficacy of the siRNA NPs (Fig. 1*C*). A highly potent NP formulation was prepared with G0-C14, which is much more effective than the commercial transfection agent lipofectamine 2000 (Lipo2K). Nearly complete (>95%) luciferase silencing was obtained with 5–50 nM siRNA. No obvious cytotoxicity was observed under these conditions (*SI Appendix*, Fig. S4*B*). Moreover, G0-C14 NPs could maintain luciferase silencing for a longer period relative to Lipo2K (Fig. 1*D*). Over 90% silencing could still be retained 9 d after transfection with G0-C14 NPs (50 nM siRNA), whereas only ~38% was silenced for Lipo2K under the same condition. In addition, the effect of N/P ratio, which was defined as the ratio of cationic amino groups (N) of G0-C14 to phosphate groups (P) of siRNA, was examined for optimal encapsulation and gene silencing with the use of a minimal amount of cationic lipids (*SI Appendix*, Fig. S4 *C* and *D*). The N/P ratio of 10 was selected for following NP formulations.

We then studied the cellular internalization of G0-C14 NPs. Fluorophore DY547-labeled siRNA NPs, denoted as NP(DY547-siRNA), were incubated with Luc-HeLa cells in the presence of different endocytic inhibitors [5-*N*-ethyl-*N*-isoproamiloride (EIPA), filipin, or chlorpromazine (CPZ)], which represent three endocytic pathways: macropinocytosis and caveolae- and clathrin-mediated endocytosis, respectively. We observed a ∼50–65% reduction of uptake upon the treatment of EIPA, and ∼30–40% reduction upon CPZ, for G0-C14 NPs with either ceramide-PEG or 1,2-distearoyl-sn-glycero-3-phosphoethanolamine-N-[methoxy(polyethylene glycol)] (DSPE-PEG) on the surface (Fig. 1*E*). This suggests the role of macropinocytosis and clathrin-mediated endocytosis in NP uptake. Moreover, these two pathways may, to some extent, function independently, as higher inhibition of uptake (∼80%) was observed when coincubating the two inhibitors (EIPA and CPZ) with NPs.

Effect of Lipid-PEG on Systemic siRNA Delivery. To evaluate the in vivo performance of these hybrid NPs for systemic siRNA delivery, we first examined the PK by injecting NP(DY647-siRNA) to healthy BALB/c mice via tail vein. The circulation profile of three different NP(DY647-siRNA) formulations, with ceramide-PEG5K, DSPE-PEG5K, or DSPE-PEG3K as the surface lipid-PEG, was measured and compared with that of naked DY647-siRNA. Fig. 2*A* shows naked siRNA was rapidly cleared from blood within 30 min. Ceramide-PEG5K NPs extended the circulation of siRNA with a half-life ($t_{1/2}$) of ∼30 min. More impressively, DSPE-PEG5K NPs exhibited a prolonged circulation $t_{1/2}$ of ∼8.1 h. The change of surface lipid-PEG to DSPE-PEG3K ($t_{1/2}$ ∼7.1 h) modestly altered the NP circulation profile. Both DSPE-PEG NPs demonstrated ∼100-fold greater measurement for area under the curve (AUC) than that of naked siRNA (*SI Appendix*, Fig. S5*A*). To assess the NP biodistribution (BioD) and tumor accumulation, nude mice carrying human NSCLC NCI-H460 tumor were injected i.v. with NP(DY677-siRNA) or naked DY677-siRNA. Long-circulating DSPE-PEG5K NPs demonstrated high tumor accumulation in the xenograft, whereas ceramide-PEG5K NPs and naked siRNA exhibited low or negligible signal in tumor (Fig. 2*B* and *SI Appendix*, Fig. S5). Quantification analysis further showed a 10-fold higher accumulation of DSPE-PEG5K NPs per gram of tumor tissue than ceramide-PEG5K NPs (Fig. 2*C*).

To explain the drastic difference in PK/BioD between DSPE-PEG and ceramide-PEG NPs, the effect of lipid-PEG on NP properties and performance was systematically studied. Through quantitative analysis of PEG molecules (23), both NPs carried a similar amount of lipid-PEG on the surface, with ∼9.5 weight% of PLGA polymer (*SI Appendix*, Fig. S6*A*). We then measured the dissociation kinetics of lipid-PEG from NPs in the presence of serum albumin, which is abundant in blood and can bind with diacyl lipids (24). Fig. 2*D* illustrated a much more rapid release of ceramide-PEG5K than DSPE-PEG5K from NPs. Owing to the dissociation of lipid-PEGs and exposure of PLGA/cationic lipid/siRNA hybrid core, the NP surface charge (or zeta potential) also changed over time (Fig. 2*E*). Both DSPE-PEG5K and ceramide-PEG5K NPs were relatively neutral initially. After incubation with albumin, the surface charge increased rapidly from 2.2 to 31.4 mV in 3 h for ceramide-PEG5K NPs, but gradually from –4.0 to 11.9 mV for DSPE-PEG5K NPs in 24 h. The trend of surface charge change is consistent with the lipid-PEG dissociation kinetics.

We next investigated the uptake kinetics of these two NPs in a mouse macrophage cell line. The ceramide-PEG5K NP displayed significantly faster uptake kinetics than the DSPE-PEG5K counterpart (Fig. 2*F*), which may account for its much shorter residence life in blood. The effect of lipid-PEG on NP uptake by tumor cells was also tested (*SI Appendix*, Fig. S6 *B* and *C*). Again, rapid cell uptake was seen with ceramide-PEG5K NPs after 1-h incubation, whereas DSPE-PEG5K NPs exhibited slow uptake within the first 6 h of incubation followed by accelerated internalization. This effect correlates with the lipid-PEG release

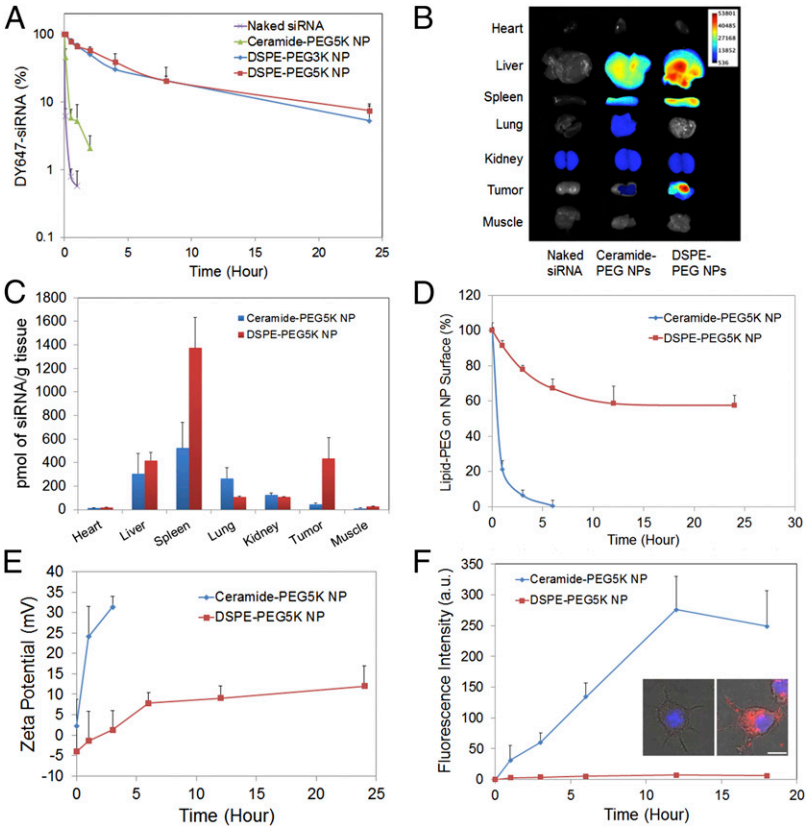

Fig. 2. Effect of lipid-PEG on in vivo PK and BioD of the hybrid NPs. (*A*) Circulation profile of naked siRNA and three different siRNA NP formulations composed of DSPE-PEG3K, DSPE-PEG5K, or ceramide-PEG5K in normal BALB/c mice after i.v. injection. The siRNA was labeled with near infrared (NIR) dye DY647. (*B*) Ex vivo fluorescence image of representative tissues from mice bearing NCI-H460 tumor 24 h postinjection. (*C*) BioD of NP(siRNA) quantified from *B*. (*D*) Dissociation kinetics of DSPE-PEG5K vs. ceramide-PEG5K from respective NPs in the presence of serum albumin. (*E*) The change of zeta potential of DSPE-PEG5K vs. ceramide-PEG5K NPs vs. time. (*F*) NP uptake kinetics on RAW264.7 macrophage cells. *Inset* shows fluorescence images of RAW264.7 cells treated with DSPE-PEG5K (*Left*) and ceramide-PEG5K (*Right*) siRNA NPs at 18 h. The siRNA was labeled with dye DY547. (Scale bar, 10 μm.)

profiles in Fig. 2*D*. It should be noted also that there is no substantial difference in endocytosis pathways for these two NPs (Fig. 1*E*). The difference in uptake kinetics also affects gene silencing in tumor cells. Luciferase silencing was more effective after a 6-h incubation with ceramide-PEG NPs relative to DSPE-PEG NPs (*SI Appendix*, Fig. S6*D*). When the incubation time was extended to 24 h, however, the two NPs exhibited comparable silencing efficacy.

In Vitro Validation of PHB1-Targeted NSCLC Treatment. Next, we examined whether the hybrid siRNA NP platform could be used to silence a potential therapeutic target in NSCLC cell lines. PHB1 is a 32-kDa protein found in organisms ranging from yeast to humans and has been implicated in aging, obesity, diabetes, cancer, and inflammatory diseases (25–27). Up-regulation of PHB1 has been reported in cancers of the stomach, esophagus, urinary bladder, breast, prostate, lung, and others (25, 28), and is also associated with drug resistance (21). Nonetheless, the validity of PHB1 as a therapeutic target is not well established due to the absence of specific and effective PHB1 systemic inhibitors.

We first silenced PHB1 expression in NCI-H460 cells in vitro using the anti-PHB1 siRNA (siPHB1) hybrid NPs. Immunofluorescence staining illustrated that NP(siPHB1) successfully knocked down PHB1 by >90% (Fig. 3*A*). By flow cytometry analysis, we found that PHB1 silencing induced apoptosis in vitro (Fig. 3*B*). After 3 d, the frequency of apoptotic cells (Annexin-V positive) increased markedly to 50.4% in the NP(siPHB1) group compared with 10.9% of NP(siControl)-treated cells, along with an increase of early-stage apoptosis (Annexin-V positive and 7-ADD negative) from 2.28% to 13.4%. Western blot analysis showed that NP (siPHB1) dramatically reduced caspase-3 and -9 protein levels, and led to increased levels of catalytically active caspase-3 and cleaved poly(ADP ribose) polymerase (PARP) (Fig. 3*C*), as well as a significant increase in caspase-3/7 activities (Fig. 3*D*).

In cell proliferation analysis, NP(siPHB1) treatment for 6 h resulted in drastic inhibition of cell proliferation compared with NP(siControl) (Fig. 3*E*). The cell number in the NP(siPHB1) group was only ∼4% of that in the control groups after 12 d. Similarly, in soft agar colony formation assay, NP(siPHB1)-treated cells formed much smaller and fewer colonies, indicating that PHB1 silencing reduced the ability of anchorage-independent growth of NSCLC (Fig. 3*F*). To understand the underlying mechanism, we further explored whether PHB1 silencing affected mitochondrial structure, as PHB1 is reported to maintain mitochondrial integrity (29). Seventy-two hours after short-term NP(siPHB1) transfection, we observed an absence of PHB1 protein and vesicular punctuated mitochondria structure, whereas NP(siControl)-treated cells exhibited a normal mitochondrial morphology (Fig. 3*G*). Similar findings were also observed in a second NSCLC cell line, A549 (*SI Appendix*, Fig. S7).

In Vivo Therapeutic Efficacy and Safety Profile. For in vivo validation of PHB1-targeted cancer therapy, we first tested whether the NP(siPHB1) can silence PHB1 in tumor tissue after systemic administration. Immunocompromised mice bearing a s.c. NCI-H460 (human NSCLC) tumor xenograft were injected with NPs via tail vein for three consecutive days. Western blot analysis of tumor tissue showed that NP(siPHB1) induced ∼76% decrease in PHB1 expression relative to NP(siControl) (Fig. 4*A* and *SI Appendix*, Fig. S8*A*), which greatly increased tumor cell apoptosis as confirmed by TUNEL staining (*SI Appendix*, Fig. S8*B*). We then examined whether the NP-mediated PHB1 silencing had anti-tumor effect. Rapid tumor growth was observed in mice that received saline, naked siPHB1 or NP(siControl) (Fig. 4*B*). In contrast, NP(siPHB1) treatment resulted in a significant suppression of tumor growth. The average tumor weight in the NP(siPHB1) group was ∼70% less at day 16, compared with others; and no obvious change in body weight was observed for all groups (*SI Appendix*, Fig. S8 *C–E*).

To examine whether greater efficacy would result from combining NP(siPHB1) with known chemotherapeutics, we chose cisplatin, a drug commonly used in the treatment of NSCLC. When tested in vitro, the combination group showed enhanced cytotoxicity in A549 and NCI-H460 cells (Fig. 4*C* and *SI Appendix*, Fig. S9*A*). The combinatorial apoptotic effect was confirmed in assays showing increased levels of cleaved caspase-3 and PARP (Fig. 3*C*). In the in vivo experiments, mice bearing A549 tumor were treated with saline, NP(siPHB1), or NP(siControl) at an i.v. dose of 600 μg siRNA per kilogram per injection with or without cisplatin at an i.p. dose of

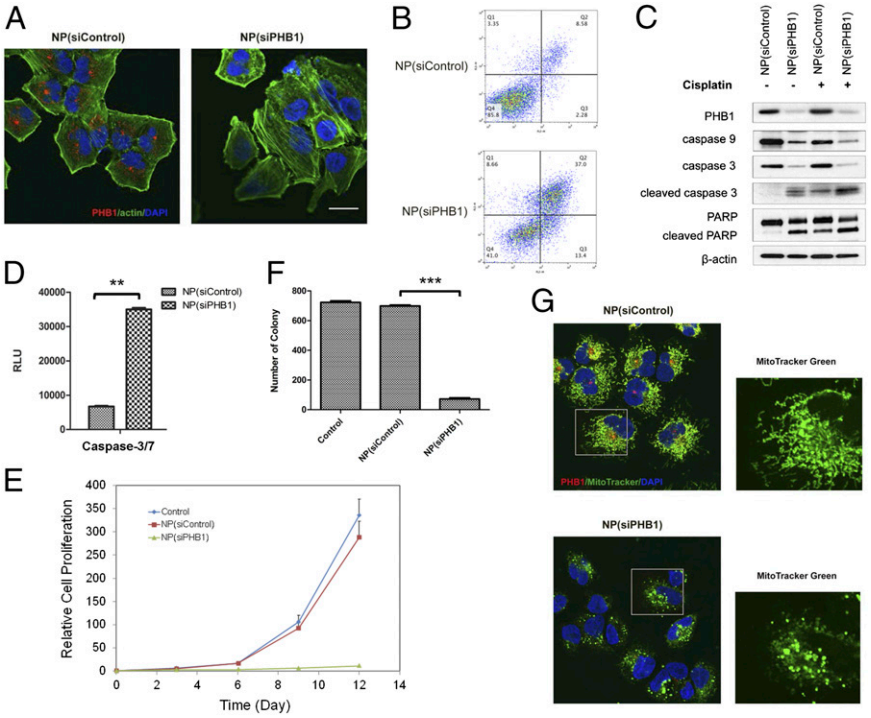

Fig. 3. NP-mediated PHB1 silencing in NSCLC cells. (*A*) Immunofluorescence images of NCI-H460 cells after treatment with NP(siControl) or NP(siPHB1). PHB1, red; actin, green; and nucleus, blue. (*B*) Flow cytometry analysis of cell apoptosis 72 h post-NP treatment. The *x* axis represents the level of phycoerythrin (PE)-conjugated Annexin V, and the *y* axis for 7-AAD. Living cells accumulate in Q4, cells undergoing apoptosis in Q3, cells in end-stage apoptosis or dead cells in Q2, and necrotic cells in Q1. (*C*) Representative Western blot analysis of PHB1, caspase-9, caspase-3, cleaved caspase-3 (or active caspase-3), and PARP cleavage after NP treatment alone or in combination with cisplatin. β-Actin was used as a control. (*D*) Caspase-3/7 activities measured by caspase-Glo 3/7 assay, after NP treatment (**$P < 0.01$). (*E*) Inhibition of cell proliferation of NCI-H460 cells upon PHB1 silencing. (*F*) Quantitative analysis of colony numbers in soft agar colony formation assay 3 wk post-NP treatment (***$P <$ 0.001). (*G*) Mitochondrial staining of NCI-H460 cells after NP treatment. MitoTracker, green; PHB1, red; and nucleus, blue. Enlarged MitoTracker pictures depict (*Top*) long tubular mitochondrial network for NP(siControl), and (*Bottom*) punctuated form of mitochondria for NP(siPHB1). (Scale bar, 20 μm.)

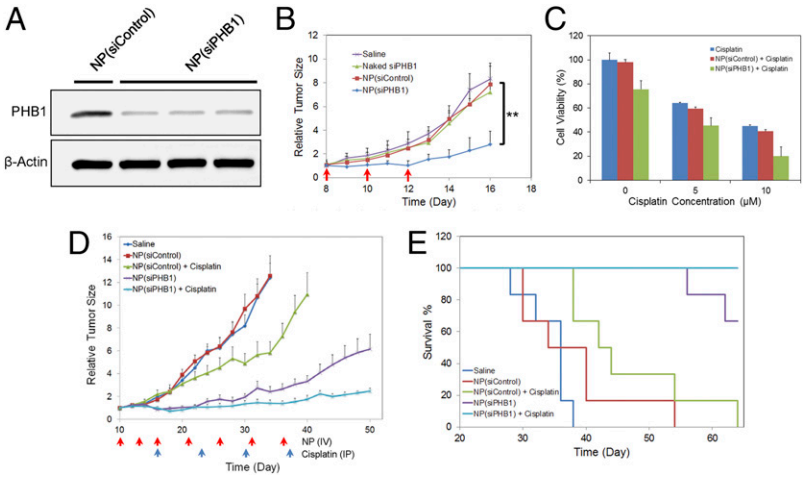

Fig. 4. In vivo validation of PHB1-targeted NSCLC therapy. (*A*) Representative Western blot analysis of PHB1 expression in NCI-H460 tumor tissue after systemic NP treatment. (*B*) Therapeutic efficacy of NP(siPHB1) in NCI-H460 xenograft [$n = 4$ per group; $^{**}P < 0.01$ vs. NP(siControl)]. Three i.v. injections are indicated by the arrows. (*C*) In vitro cytotoxicity of NP(siPHB1) in combination with free cisplatin in A549 cells. (*D*) Inhibition of A549 tumor growth after combinatorial treatment with NP(siPHB1) and cisplatin. The arrows indicate the timeline for i.v. injection of NP(siPHB1) (red) and i.p. injection of cisplatin (blue). Data are shown as the mean ± SEM ($n = 6$ per group). (*E*) The Kaplan–Meier survival curve of the cohorts in *D*.

3 mg/kg/wk. The administration timeline for NP(siRNA) and cisplatin is shown in Fig. 4*D*. As can be seen, tumor growth was significantly inhibited by monotherapy with NP(siPHB1) (Fig. 4*D* and *SI Appendix*, Fig. S9 *B–D*). More impressively, combination treatment with NP(siPHB1) and cisplatin nearly completely inhibited tumor growth during the treatment period. Moreover, mice that received the combination treatment survived over the entire 64-d duration (Fig. 4*E*). These results suggest that effective PHB1 silencing by the long-circulating RNAi NPs represents a potential strategy for NSCLC treatment, which may be further combined with chemotherapeutics for even better antitumor efficacy.

In addition to therapeutic efficacy, we also evaluated in vivo side effects of the NP(siPHB1). After three i.v. injections, blood serum samples were obtained for hematological analysis, and the histopathology of different organs was evaluated. Multiple hematological parameters, including alanine aminotransferase (ALT), aspartate aminotransferase (AST), blood urine nitrogen (BUN), creatinine and Troponin-1, were in the normal range in all groups (*SI Appendix*, Fig. S10). H&E staining results further demonstrated no noticeable histological change in the tissues from heart, liver, spleen, lung, and kidney between saline and NP(siPHB1) groups, indicating no organ toxicity (*SI Appendix*, Fig. S11).

To exclude the possibility that the antitumor effect of NP(siPHB1) might be confounded by siRNA-mediated immune stimulation (30, 31), we studied the immunostimulatory effect of the NPs in immunocompetent mice. The results showed no obvious change of IL-12 level in serum for all groups (*SI Appendix*, Fig. S12). Serum levels of TNF-α and IL-6 were similarly increased for blank NP and NP(siPHB1) 6 h postinjection, suggesting that the cytokine responses may be attributed to NP itself rather than encapsulated siRNA. Both TNF-α and IL-6 concentrations in the two NP groups returned to the baseline level of saline group after 24 h. Note that the transient immune response was also observed in the clinical stage siRNA nanotherapeutics for cancer treatment (11, 12).

PHB1 Expression in Patients with NSCLC. To validate the relevance of PHB1 as a potential target in human NSCLC, we examined PHB1 levels in 465 patients with NSCLC (*SI Appendix*, Table S1). Immunohistochemical (IHC) staining intensity was quantified as negative, low, moderate, or high on a scale of 0–3 (*SI Appendix*, Figs. S13 and S14). In these specimens, PHB1 staining was predominantly cytoplasmic. We then analyzed the PHB1 expression using a score (0–300) calculated from staining intensity (0–3) multiplied by extension of expression (0–100%). High PHB1 was recorded when the score was higher than 50. Fig. 5*A* reveals that patients with NSCLC with high PHB1 tumor expression clearly demonstrate poorer overall survival (OS), relative to patients with low PHB1. Whereas the recurrence-free survival (RFS) is similar to OS, the difference is not statistically significant between the high-PHB1 and low-PHB1 cohorts when analyzed for all patients (Fig. 5*B*). However, among patients with NSCLC with advanced disease stage III–IV, patients with high PHB1 expression have significantly worse OS and RFS compared with those expressing lower levels (Fig. 5 *C* and *D*). PHB1 levels do not differ demonstrably between NSCLC tumor type (adenocarcinoma vs. squamous cell carcinoma) and are not sex specific.

Discussion

The lack of systemic siRNA delivery vehicles with long circulating half-lives, effective tumor accumulation, and gene silencing represents a significant barrier for the widespread applications of RNAi in oncology. The new generation lipid–polymer hybrid NP platform developed herein has several unique features. In contrast to previously reported hybrid polymer NPs loaded with cationic lipid/polyamine–siRNA complexes (14–18, 32), which are formulated by emulsion techniques and are relatively large, our robust self-assembly strategy leads to the synthesis of hybrid NPs with relatively small size (≤100 nm) and long circulation time ($t_{1/2}$ ~8 h). Smaller NPs are considered to be more efficient in crossing leaky microvasculature and show higher tumor accumulation than larger NPs (33, 34). Compared with siRNA lipoplexes, the solid polymer/cationic lipid core of our hybrid NPs can better protect siRNA from degradation and control its release kinetics for sustained gene silencing. Surprisingly, we noticed a change in the silencing efficacy of cationic lipids (or lipid-like compounds) after combining into the hybrid NPs. For example, the C12-114

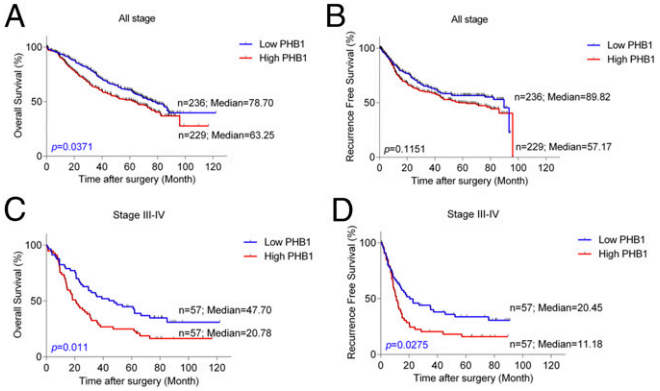

Fig. 5. Kaplan–Meier estimates of overall survival (OS) and recurrence-free survival (RFS) of patients with NSCLC in (*A* and *B*) all stage or (*C* and *D*) stages III–IV. Comparison was made among patients with high vs. low PHB1 tumor expression. Marks on graph lines represent censored samples.

lipid, which is ineffective for luciferase silencing in a lipoplex formulation (22), can achieve ~90% silencing in our NP system (Fig. 1*C*). We therefore speculate that the hybrid NP system could be used to revisit previously abandoned cationic lipids or lipid-like compounds for siRNA delivery. Notably, the siRNA hybrid NPs can be kept at −80 °C for at least 12 mo without causing obvious changes of particle size and silencing activity (*SI Appendix*, Fig. S15), suggesting another translationally promising feature of this NP platform.

An additional unique feature of the hybrid NPs is the dissociation of lipid-PEG molecules from the NP surface. PEGylation is widely used to minimize NP interaction with serum proteins, which can promote elimination of circulating NPs by the MPS (9, 10). PEGylation may, however, also prevent the interaction of NPs with the target cell membrane and thus decrease their uptake by tumor cells. In our hybrid NP system, the lipid-PEGs that self-assembled on the particle surface by hydrophobic interaction with PLGA polymer, can detach from NPs in serum. The dissociation kinetics are controlled by the length and/or saturation of lipophilic tails (Fig. 2*D*). In vivo results of PK, BioD, and efficacy suggest that slow de-PEGylation such as in the case of DSPE-PEG NPs may lead to more effective systemic delivery.

PHB1 has been proposed as a promising biomarker and potential therapeutic target for cancer prognosis (25, 28) and therapy (19, 20, 35). Moreover, PHB1 has been associated with chemoresistance in NSCLC cells (21). Our findings here show a significant correlation between high PHB1 expression and poor OS and RFS in patients with late-stage NSCLC. We further provide the first demonstration to our knowledge of tumor inhibition following systemic in vivo delivery of PHB1 siRNA. Our results verify that the RNAi hybrid NP system offers a means for rapid in vivo validation of potential cancer targets, particularly those considered undruggable. As the hybrid NPs can also simultaneously carry small molecular drugs (e.g., cisplatin prodrug) in the PLGA polymer core (15, 36), the co-delivery of siRNA/drug combinations may present a therapeutic advantage in cancer treatment (37, 38). In summary, we have rationally developed a distinctive lipid–polymer hybrid NP platform for effective systemic siRNA delivery, through a simple and robust self-assembly strategy, and expect that it provides a useful toolkit for both fundamental cancer research and clinical development of novel RNAi therapeutics.

Materials and Methods

Detailed materials and methods are provided in *SI Appendix, SI Materials and Methods*, including the synthesis of cationic lipid-like compounds; preparation and characterization of lipid–polymer hybrid NPs; a serum stability study; siRNA release kinetics; lipid-PEG dissociation kinetics and NP surface charge measurement; in vitro gene silencing; NP cellular uptake; immunofluorescent staining; cell proliferation and NP cytotoxicity; flow cytometry and Western blot analysis; animal studies; analysis of PHB1 tumor expression in patients with NSCLC; and statistics.

Animal protocol was approved by the Institutional Animal Care and Use Committee at Harvard Medical School. Utilization of human tissues was approved by the University of Texas MD Anderson Cancer Center Institutional Review Board.

ACKNOWLEDGMENTS. This work was supported by the National Institutes of Health (NIH) Grants R00CA160350 (to J.S.), R01CA37393 (to B.R.Z.), EB015419 (to O.C.F.), and U54-CA151884 (to O.C.F.); the Movember-Prostate Cancer Foundation (PCF) Challenge Award (to J.S. and O.C.F.); a PCF Young Investigator Award (to J.S.) and the David Koch–PCF Program in Nanotherapeutics (O.C.F.); the National Research Foundation of Korea Grant K1A1A2048701 (to O.C.F.); and the University of Texas Lung Specialized Programs of Research Excellence Grant P50CA70907 (to I.I.W.). X.Z., L.Z., and L.W. received financial support from the China Scholarship Council. Y.X. received a Department of Defense Prostate Cancer Research Program Postdoctoral Training Award (W81XWH-14-1-0268). X.X. received postdoctoral support from an NIH National Research Service Award (F32CA168163).

1. Pecot CV, Calin GA, Coleman RL, Lopez-Berestein G, Sood AK (2011) RNA interference in the clinic: Challenges and future directions. *Nat Rev Cancer* 11(1):59–67.
2. Whitehead KA, Langer R, Anderson DG (2009) Knocking down barriers: Advances in siRNA delivery. *Nat Rev Drug Discov* 8(2):129–138.
3. Whitehurst AW, et al. (2007) Synthetic lethal screen identification of chemosensitizer loci in cancer cells. *Nature* 446(7137):815–819.
4. Barbie DA, et al. (2009) Systematic RNA interference reveals that oncogenic KRAS-driven cancers require TBK1. *Nature* 462(7269):108–112.
5. Ren Y, et al. (2012) Targeted tumor-penetrating siRNA nanocomplexes for credentialing the ovarian cancer oncogene ID4. *Sci Transl Med* 4(147):147ra112.
6. Davis ME (2009) The first targeted delivery of siRNA in humans via a self-assembling, cyclodextrin polymer-based nanoparticle: From concept to clinic. *Mol Pharm* 6(3):659–668.
7. Zhang Y, Satterlee A, Huang L (2012) In vivo gene delivery by nonviral vectors: Overcoming hurdles? *Mol Ther* 20(7):1298–1304.
8. Kanasty R, Dorkin JR, Vegas A, Anderson D (2013) Delivery materials for siRNA therapeutics. *Nat Mater* 12(11):967–977.
9. Knop K, Hoogenboom R, Fischer D, Schubert US (2010) Poly(ethylene glycol) in drug delivery: Pros and cons as well as potential alternatives. *Angew Chem Int Ed Engl* 49(36):6288–6308.
10. Guo X, Huang L (2012) Recent advances in nonviral vectors for gene delivery. *Acc Chem Res* 45(7):971–979.
11. Tabernero J, et al. (2013) First-in-humans trial of an RNA interference therapeutic targeting VEGF and KSP in cancer patients with liver involvement. *Cancer Discov* 3(4):406–417.
12. Zuckerman JE, et al. (2014) Correlating animal and human phase Ia/Ib clinical data with CALAA-01, a targeted, polymer-based nanoparticle containing siRNA. *Proc Natl Acad Sci USA* 111(31):11449–11454.
13. Bertrand N, Wu J, Xu X, Kamaly N, Farokhzad OC (2014) Cancer nanotechnology: The impact of passive and active targeting in the era of modern cancer biology. *Adv Drug Deliv Rev* 66:2–25.
14. Shi J, Xiao Z, Votruba AR, Vilos C, Farokhzad OC (2011) Differentially charged hollow core/shell lipid-polymer-lipid hybrid nanoparticles for small interfering RNA delivery. *Angew Chem Int Ed Engl* 50(31):7027–7031.
15. Xu X, et al. (2013) Enhancing tumor cell response to chemotherapy through nanoparticle-mediated codelivery of siRNA and cisplatin prodrug. *Proc Natl Acad Sci USA* 110(46):18638–18643.
16. Shi J, et al. (2014) Hybrid lipid-polymer nanoparticles for sustained siRNA delivery and gene silencing. *Nanomedicine (Lond Print)* 10(5):897–900.
17. Díez S, Miguéliz I, Tros de Ilarduya C (2009) Targeted cationic poly(D,L-lactic-co-glycolic acid) nanoparticles for gene delivery to cultured cells. *Cell Mol Biol Lett* 14(2):347–362.
18. Wilson DS, et al. (2010) Orally delivered thioketal nanoparticles loaded with TNF-α-siRNA target inflammation and inhibit gene expression in the intestines. *Nat Mater* 9(11):923–928.
19. Rajalingam K, et al. (2005) Prohibitin is required for Ras-induced Raf-MEK-ERK activation and epithelial cell migration. *Nat Cell Biol* 7(8):837–843.
20. Sievers C, Billig G, Gottschalk K, Rudel T (2010) Prohibitins are required for cancer cell proliferation and adhesion. *PLoS ONE* 5(9):e12735.
21. Patel N, et al. (2010) Rescue of paclitaxel sensitivity by repression of Prohibitin1 in drug-resistant cancer cells. *Proc Natl Acad Sci USA* 107(6):2503–2508.
22. Love KT, et al. (2010) Lipid-like materials for low-dose, in vivo gene silencing. *Proc Natl Acad Sci USA* 107(5):1864–1869.
23. Cheng TL, Chuang KH, Chen BM, Roffler SR (2012) Analytical measurement of PEGylated molecules. *Bioconjug Chem* 23(5):881–899.
24. Liu H, et al. (2014) Structure-based programming of lymph-node targeting in molecular vaccines. *Nature* 507(7493):519–522.
25. Theiss AL, Sitaraman SV (2011) The role and therapeutic potential of prohibitin in disease. *Biochim Biophys Acta* 1813(6):1137–1143.
26. Kolonin MG, Saha PK, Chan L, Pasqualini R, Arap W (2004) Reversal of obesity by targeted ablation of adipose tissue. *Nat Med* 10(6):625–632.
27. Thuaud F, Ribeiro N, Nebigil CG, Désaubry L (2013) Prohibitin ligands in cell death and survival: Mode of action and therapeutic potential. *Chem Biol* 20(3):316–331.
28. Kapoor S (2013) Prohibitin and its rapidly emerging role as a biomarker of systemic malignancies. *Hum Pathol* 44(4):678–679.
29. Gregory-Bass RC, et al. (2008) Prohibitin silencing reverses stabilization of mitochondrial integrity and chemoresistance in ovarian cancer cells by increasing their sensitivity to apoptosis. *Int J Cancer* 122(9):1923–1930.
30. Judge AD, et al. (2005) Sequence-dependent stimulation of the mammalian innate immune response by synthetic siRNA. *Nat Biotechnol* 23(4):457–462.
31. Robbins M, et al. (2008) Misinterpreting the therapeutic effects of small interfering RNA caused by immune stimulation. *Hum Gene Ther* 19(10):991–999.
32. Woodrow KA, et al. (2009) Intravaginal gene silencing using biodegradable polymer nanoparticles densely loaded with small-interfering RNA. *Nat Mater* 8(6):526–533.
33. Kong G, Braun RD, Dewhirst MW (2000) Hyperthermia enables tumor-specific nanoparticle delivery: Effect of particle size. *Cancer Res* 60(16):4440–4445.
34. Alexis F, Pridgen E, Molnar LK, Farokhzad OC (2008) Factors affecting the clearance and biodistribution of polymeric nanoparticles. *Mol Pharm* 5(4):505–515.
35. Mishra S, Murphy LC, Nyomba BL, Murphy LJ (2005) Prohibitin: A potential target for new therapeutics. *Trends Mol Med* 11(4):192–197.
36. Dhar S, Gu FX, Langer R, Farokhzad OC, Lippard SJ (2008) Targeted delivery of cisplatin to prostate cancer cells by aptamer functionalized Pt(IV) prodrug-PLGA-PEG nanoparticles. *Proc Natl Acad Sci USA* 105(45):17356–17361.
37. Hu CM, Zhang L (2012) Nanoparticle-based combination therapy toward overcoming drug resistance in cancer. *Biochem Pharmacol* 83(8):1104–1111.
38. Creixell M, Peppas NA (2012) Co-delivery of siRNA and therapeutic agents using nanocarriers to overcome cancer resistance. *Nano Today* 7(4):367–379.

Biomaterials Science

REVIEW

Biomaterials for mRNA delivery

Cite this: DOI: 10.1039/c5bm00198f

Mohammad Ariful Islam,[a] Emma Reesor,[a,c] Yingjie Xu,[b] Harshal Zope,[a] Bruce R. Zetter*[b] and Jinjun Shi*[a]

Received 21st June 2015,
Accepted 4th August 2015

DOI: 10.1039/c5bm00198f

www.rsc.org/biomaterialsscience

Messenger RNA (mRNA) has recently emerged with remarkable potential as an effective alternative to DNA-based therapies because of several unique advantages. mRNA does not require nuclear entry for transfection activity and has a negligible chance of integrating into the host genome which excludes the possibility of potentially detrimental genomic alternations. Chemical modification of mRNA has further enhanced its stability and decreased its activation of innate immune responses. Additionally, mRNA has been found to have rapid expression and predictable kinetics. Nevertheless, the ubiquitous application of mRNA remains challenging given its unfavorable attributes, such as large size, negative charge and susceptibility to enzymatic degradation. Further refinement of mRNA delivery modalities is therefore essential for its development as a therapeutic tool. This review provides an exclusive overview of current state-of-the-art biomaterials and nanotechnology platforms for mRNA delivery, and discusses future prospects to bring these exciting technologies into clinical practice.

Introduction

Messenger RNA (mRNA), a natural biomolecule, is a transient entity that mediates the translation of genetic information from genes encoded in DNA to proteins located throughout the cell. The physical and temporal qualities of mRNA have allowed its use as a safe genetic material for gene-based therapy which does not require genomic integration.[1,2] It is suitable for this use because of its potential to avoid nuclear localization and because it allows rapid protein expression even in non-dividing and hard-to-transfect cells (*e.g.* dendritic cells and macrophages). These properties also make mRNA an attractive molecule for immunotherapy.[3] Another advantage of mRNA as a genetic element is its predictable, consistent protein expression kinetics, especially compared to DNA transfection which follows random onset time courses.[4–7] However, relative to the technologies developed for DNA delivery, mRNA delivery strategies still require much more improvement and testing. Fortunately some of the carriers and biomaterials established for DNA and small interfering RNA (siRNA) have also been exhibiting a promising foundation for the development of mRNA delivery technologies.

mRNA has been investigated for more than half a century, but its widespread applications in medical research and in the development of novel therapeutic modalities have been limited due to its perceived instability, susceptibility to degradation, insufficient translatability and immunostimulatory effects.[8–10] Such challenges have partially been resolved thanks to an improved understanding of the structure of mRNA and its relationship to mRNA stability, as well as the development of a variety of chemical modification methods.[10–15] These breakthroughs have subsequently facilitated the synthesis of mRNA with many different structural modifications (*e.g.*, anti-reverse cap analogues (ARCA), 3′-globin UTR and poly-A tail), which still possess functional activity for immunotherapy and gene-based therapy. With these advances in stability and functionality, the use of mRNA as a therapeutic tool is now becoming a reality.[14]

Nevertheless, like other nucleic acids (*e.g.*, DNA and siRNA), naked mRNA cannot readily cross the cell membrane on its own and thus requires delivery systems to enhance its cell permeation.[16] Viral vectors have been used as mRNA carriers but may suffer from their potential immunologic side effects and toxicity as well as the vector-size limitations.[1,17] Non-viral strategies such as electroporation, gene gun and sonoporation have been more thoroughly investigated as mRNA delivery systems.[16,18,19] However, the *ex vivo* manipulation of cells with mRNA transfection using such approaches, while feasible, is highly laborious, expensive and overall ill-suited for extensive applications.[20–22]

Biomaterials represent an important step forward from the aforementioned non-viral strategies and have demonstrated

[a]*Laboratory for Nanoengineering & Drug Delivery, Brigham and Women's Hospital, Harvard Medical School, Boston, MA 02115, USA. E-mail: jinjun.shi@zeus.bwh.harvard.edu*
[b]*Vascular Biology Program, Boston Children's Hospital, Harvard Medical School, Boston, MA 02115, USA. E-mail: bruce.zetter@childrens.harvard.edu*
[c]*Nanotechnology Engineering Program, University of Waterloo, Waterloo, ON N2L 3G1, Canada*

promising potential for the delivery of various biomacromolecules such as DNA and siRNA.[1,23] Compared to viral vectors and *ex vivo* technologies mentioned above, biomaterials are more biocompatible and diversified, and can be easily formulated for effective *in vivo* delivery and controlled release of therapeutics. Recently, biomaterials have also attracted considerable attention for mRNA delivery.[5,24,25] For example, protamine has demonstrated remarkable abilities to ameliorate the transfection capabilities of mRNA and several protamine–mRNA complexes are now under clinical trials in cancer patients.[26,27] Moreover, biomaterials-based nanoparticle platforms have in recent years been gradually applied to mRNA vaccine development and mRNA-based gene therapy.[1,28,29]

In this review, we summarize the strategies for chemical modification of mRNA, provide an overview of the currently available biomaterials and nanotechnology platforms for mRNA delivery and a critical analysis of how these mRNA delivery systems may be further improved to potentiate their therapeutic utility and discuss the challenges and opportunities in this exciting field.

mRNA modification for clinical translation

Owing primarily to its instability, mRNA was originally considered to be unsuitable for use as a therapeutic molecule, despite the fact that research on mRNA delivery into cells was pioneered over three decades ago.[30,31] Recent advances in molecular and structural biology, along with substantial progress in the understanding of mRNA biology and its degradation mechanism, have promoted the development of various chemical modification methods to improve mRNA stability and translation capacity.[8,32] Below we briefly outline the various modifications of mRNA's structure, including different capping techniques and elements that can be included to improve stability.

In eukaryotic cells, mature mRNA is generally comprised of five distinct portions (Fig. 1a): (i) a cap structure, (ii) a 5′ untranslated region (5′ UTR), (iii) an open reading frame (ORF), (iv) a 3′ untranslated region (3′ UTR) and (v) a poly(A) tail (a tail of 100–250 adenosine residues).[33,34] With recent progresses in molecular biology techniques, *in vitro* transcription is commonly utilized to produce functional mRNA using a bacteriophage promoter.[5] During *in vitro* mRNA transcription it has been observed that almost half of the caps are oriented in reverse which makes them unrecognizable to the cap-binding protein.[35,36] Anti-reverse cap analogs (ARCAs) were developed to solve this problem. These are modifications in which OCH_3 is used to replace or remove natural 3′ OH cap groups to avoid inappropriate cap orientation (Fig. 1b and c).[11] It was found, moreover, that modification in the C2′ position, as well as the C3′ position, can also prevent inappropriate cap orientation.[12] Additional modifications of ARCA structure have been reported for the purpose of improving the efficiency and stability of mRNA.[5] For example, tetraphosphate ARCAs are reported to improve translation efficiency relative to that of other cap

Mohammad Ariful Islam

Dr Mohammad Ariful Islam obtained his Bachelor in Biotechnology and Genetic Engineering from Bangladesh in 2007. He earned his Master (Feb 2010) and Doctoral degree (Feb 2013) from Seoul National University, South Korea under Prof. Chong-Su Cho and Prof. Cheol-Heui Yun. He developed several smart polymeric carriers to deliver gene (DNA, siRNA, microRNA) for cancer therapy and subunit antigens for vaccine therapy to prevent infectious diseases. He achieved several research awards for outstanding research performances include "Brain Korea 21 (BK21) Award" in 2012, the "Best Young Scientist Award" in 2013 from Seoul National University and some others in various scientific meetings. He has authored about 25 peer-reviewed articles and 3 of his research works have been issued/pending national and international patents. Currently, he is a Postdoctoral Fellow under Prof. Jinjun Shi and Prof. Omid Farokhzad at Harvard Medical School and Brigham & Women's Hospital, USA since Feb 2014, and working on developing mRNA nanotherapeutics for cancer immunotherapy & gene therapy, immunosenescence and asthma nanotherapeutics.

Emma Reesor

Emma K. G. Reesor worked as a research assistant under the mentorship of Dr Mohammad Ariful Islam in the Omid Farokhzad and Jinjun Shi Laboratory at Harvard Medical School as a part of her Bachelor of Applied Sciences degree from the University of Waterloo, Canada. She is specialized in Nanotechnology Engineering, in the Departments of Chemistry, Chemical Engineering and Electrical Engineering of University of Waterloo, with a focus on Nanoscale Biosystems.

analogs,[12] as well as phosphorothioate ARCAs, which confer hydrolysis resistance to mRNA, thus increasing translational stability.[13]

Polyadenylation, the addition of a poly adenine (A) tail to the 3′ end of mRNA, is catalyzed by poly(A) polymerase and is part of the process that produces mature mRNA in eukaryote cells. The poly(A) tail acts as the binding site for poly(A)-binding protein (PABP) which is exported with mRNA from nucleus to cytoplasm where it further binds to and recruit proteins that facilitate translation, such as translation initiation factor 4F (eIF4F).[37] The poly-A tail makes the mRNA molecule more stable as shortening or removal of the poly (A) tail accelerates mRNA degradation *via* enhanced exonucleotide digestion.[38] *E. coli* poly(A) polymerase I (E-PAP) has been optimized to add a poly(A) tail of at least 150 adenines to the 3′ terminal of *in vitro* transcribed mRNA. In some reports, instead of enzymatically attached poly(A) tail, *in vitro* transcribed RNA generated from plasmid templates consists of coding sequencing and a poly(A) tail with 30 to 120 nucleotides in length.[39–42] The additional adenine residues confer stability to the *in vitro* transcribed capped mRNA and may increase its translational efficiency.[43] Where direct comparisons have been made, longer poly A tails >100 adenines have generally been found to be preferable to smaller ones.[40,41,44]

The widely studied adenylate–uridylate rice elements (AREs) are important mRNA decay signals in the 3′ untranslated regions (3′ UTRs) of most eukaryotic mRNAs. mRNAs which contain AREs demonstrate reduced stability, perhaps due to the removal of the poly(A) tail. Stability is increased, however, when AREs are replaced with the 3′ UTR of a stable mRNA species such as β-globin mRNA.[45] Iron responsive elements (IREs) represent an additional type of 3′ UTR which affect mRNA stability depending on their precise location in mRNA structure. In this case, the mRNA half-life increases when IREs occupy the 3′ UTR, whereas when they are located at 5′ position its translational abilities improve.[46]

The multiple means of modulating structural elements of the mRNA, including the 5′ cap, 5′- and 3′-UTRs, the coding region, and the poly(A) tail, improve the intracellular stability and translational efficiency of *in vitro* transcribed (IVT) mRNA. Although the degree of improvement for modulation of IVT mRNA appears to depend on the means of modification, the cell type and cell differentiation state, reports range from modest levels of improvement to 2–3 orders of magnitude,[12,40–42,47] which leads to the significantly higher protein expression and prolonged persistence of the protein from a range of a few minutes to longer than 1 week.[40,47,48] Moreover, the incorporation of chemically modified nucleotides, such as substitution of cytidine triphosphate and uridine triphosphate with naturally occurring 5-methylcytidine and pseudouridine (ψ) triphosphate, respectively, into mRNA further suppresses the immune-stimulating property of *in vitro* transcription (IVT) mRNA.[10]

It is also noteworthy to clearly distinguish the different immune-stimulating effects that mRNA can have. First, there is an inherent response of the body to foreign, non-self mRNA. This is the type of response that the body uses to prevent threats such as RNA viruses, through the endosomal recognition.[49] These RNA molecules can be encountered through immune sensors such as Toll-like receptors (TLRs).[50] Some of

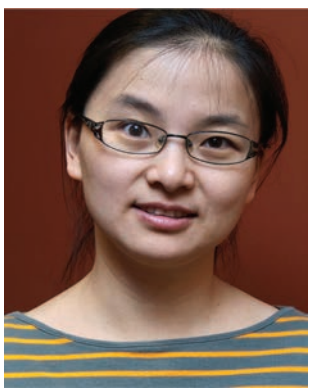

Yingjie Xu

Dr Yingjie Xu obtained her doctoral degree in the Department of Experimental Medicine at McGill University, under the supervision of Dr Moulay Alaoui-Jamali in 2011. After that, she joined Prof. Bruce Zetter's Laboratory as a Postdoctoral research fellow in the Vascular Biology Program at Boston Children's Hospital and Harvard Medical School. Yingjie's studies are focused on identifying the diagnostic and prognostic markers for cancer progression and chemoresistance and dissecting the underlying molecular mechanisms.

Harshal Zope

Dr Harshal Zope was born in Bhusawal, India on 26th Jan 1986. He pursued his interest in research by joining Institute of Biotechnology and Bioinformatics, University of Pune, India. In Pune University, he obtained a 5 years integrated M.Sc. degree in Biotechnology (2008) as well as M. Tech degree in Biotechnology (2009). Next, he pursued his interest by joining Leiden University for his PhD research under the supervision of Dr Alexander Kros (Feb 2010). During his PhD, he worked on peptide based functional biomaterials for various applications such as understanding membrane fusion, drug delivery and vaccine development. Currently, Harshal Zope is a postdoctoral fellow at laboratory of nanomedicine, Harvard Medical School/ Brigham and Women's Hospital (HMS/BWH), Boston, USA. In the group of Prof. Omid Farokhzad and Prof. Jinjun Shi, he is developing a novel nanotechnology platform for HIV vaccine and cancer therapy.

the aforementioned mRNA modifications are specifically designed to reduce this innate immune response to minimize inherent host response. Second, the delivered therapeutic mRNA molecules can induce the desired immune response through stimulating appropriate immune cells and presentation of the specific antigen. This can also be referred to as the immune-stimulating effect of the mRNA, but in this case is a designed antigen-specific effect as opposed to an inherent reaction to foreign materials. It is also important to mention that the innate immunity is not preferable for mRNA-based gene therapy applications, where we only need to transfer mRNA into the cells and facilitate the expression of the protein of interest for therapeutic purpose. The results of these actions will be henceforth discussed with a variety of mRNA molecules and delivery methods.[10,51–53]

Naked mRNA, in different modified forms, has already been tested in clinical settings. The direct intradermal injections of naked mRNA were applied as a phase I/II non-randomized clinical trial in patients with stage IV renal cell cancer.[54] In this study, granulocyte-macrophage colony stimulating factor (GM-CSF) was used as an adjuvant with mRNA encoding several tumor-associated antigens including mucin 1, carcinoembryonic, human epidermal growth factor receptor 2, telomerase, survivin and melanoma-associated antigen 1. Results revealed that vaccinations were well tolerated with no severe side effects and induced clinical responses.[54] Recently, CureVac has developed self-adjuvanted two-component mRNA vaccines comprised of both free mRNA and protamine-complexed mRNA for the treatment of castration-resistant prostate cancer and stage IIIB/IV non-small cell lung cancer. They have demonstrated excellent safety as well as high levels of cellular immunity with T and B cell responses in several clinical trials.[55–59] Moderna is another company that has been investigating mRNA as a vaccine and therapeutic technology, with two ventures Onkaido Therapeutics and Valera actively exploring the discovery and development of mRNA-based treatments in oncology and infectious diseases, respectively. Some representative studies using modified naked mRNA are summarized in Table 1.

Whereas naked modified mRNA shows feasibility in their application as vaccines, several challenging issues remain elusive, such as enzymatic degradation, rapid elimination by renal excretion or by the mononuclear phagocyte system (MPS), as well as poor cellular uptake and endosomal escape, in particular for systemic mRNA delivery. Hence, to achieve more efficient mRNA delivery, a great number of biomaterials and nanoparticle platforms have been developed to protect mRNA from nuclease degradation and facilitate its cytosolic delivery for improved protein expression (Fig. 2 and 3). In the remainder of this review, we focus on recent advances in the delivery of mRNA to cells and tissues by means of contemporary biomaterials and nanotechnologies, including protamine complexes, lipid nanoparticles, polymeric nanoparticles, lipid–polymer hybrid nanoparticles, and gold nanoparticles.

Protamine–mRNA complexes

Protamine is a natural cationic protein, which gives it an excellent ability to complex nucleic acid including mRNA (Fig. 3a)

Bruce R. Zetter

Dr Bruce Zetter is the Charles Nowiszewski Professor of Cancer Biology at Boston Children's Hospital and Harvard Medical School. He is highly regarded nationally and internationally as a leader in the research of tumor progression, cancer diagnosis, cancer metastasis, and tumor angiogenesis. His current research interests are focused on tumor metastasis, novel cancer treatments and on tests that predict future outcomes for cancer patients. Dr Zetter serves on numerous editorial boards of scientific journals, grant review panels for federal agencies and private foundations and scientific advisory boards of biotechnology companies.

Jinjun Shi

Dr Jinjun Shi holds an academic appointment as Assistant Professor at Harvard Medical School and directs the Laboratory for Nanoengineering & Drug Delivery in the Department of Anesthesiology at Brigham and Women's Hospital. He is also a research affiliate at Harvard-MIT Division of Health Sciences & Technology. His research involves an interdisciplinary combination of biomaterials, drug delivery, nanomedicine, and immunotherapy. Dr Shi has developed many multifunctional nanoparticle systems for the delivery of chemotherapeutics, proteins, vaccines, and nucleic acids, one of which has led to the first-in-human clinical trial of a synthetic nanoparticle vaccine for smoking cessation and relapse prevention. He has authored more than 30 papers, and holds over 25 issued/pending national and international patents. He has also received many awards, such as the NIH K99/R00 Career Development Award, the AACR Scholar-in-Training Award, the Movember-PCF Challenge Award, and the PCF Young Investigator Award.

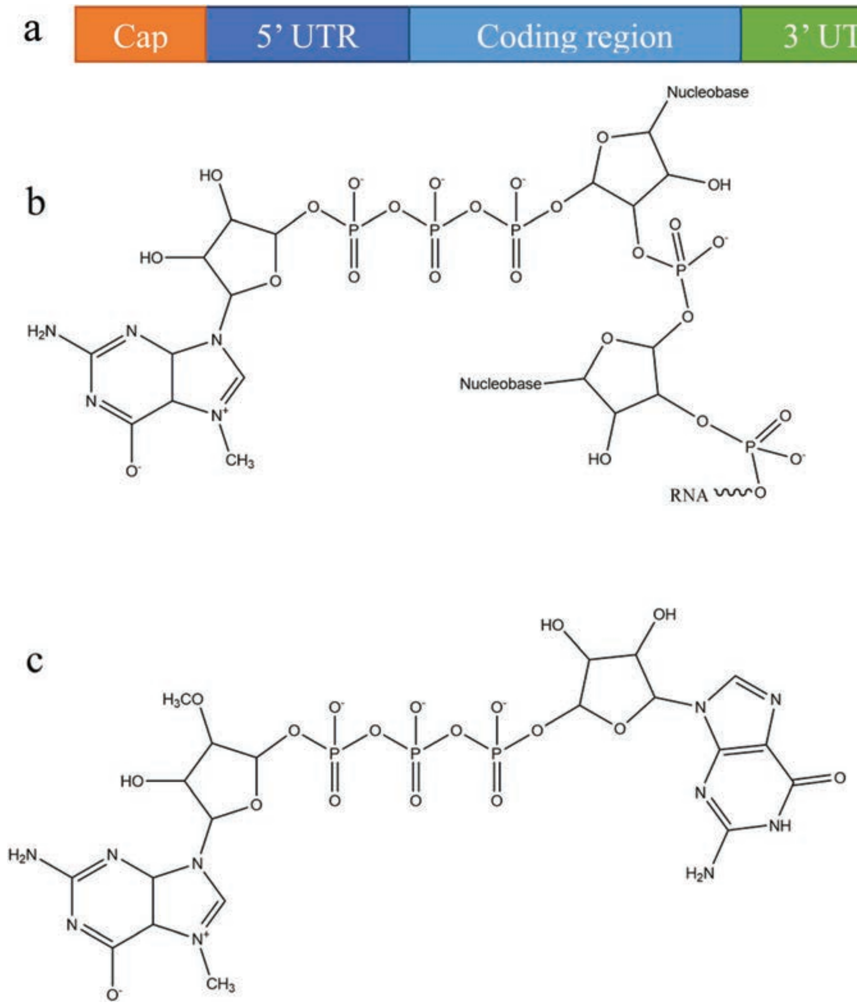

Fig. 1 mRNA structural features: (a) a basic structure of a eukaryotic mRNA with five distinct components, (b) the cap structure of the 5′ end of eukaryotic mRNA, and (c) the structure of anti-reverse cap analogues (ARCA): 3′-O-Me-m7G(5′)ppp(5′)G.

Table 1 Naked mRNA and its activity in animal models and patients

Category	Stage	mRNA	Activity and efficiency	Ref.
Naked mRNA	C57BL/6 mice	Luciferase and human CEA	After intramuscular injection mice demonstrated anti-CEA antibody response	119
	CAF_1 (H-2^a) mice	S1509a	Intradermal injection induced immunity in tumors	120
	Mice	Chloramphenicol acetyltransferase and luciferase	After intramuscular injection CAT activity was detected and, in a separate experiment, a dose–response effect with luciferase was determined	121
	Genetically engineered mice (C57BL6/CFW background)	Human VEGF-A	After intramyocardial injection there was improved heart function and long-term survival because of the directed differentiation of endogenous heart progenitors	122
	Patients with stage IIIB/IV non-small cell lung cancer	MAGE-C1, MAGE-C2, NY-ESO-1, BIRC5, 5T4	No dose limiting toxicity and good safety profile, along with significant induction of T and B cell responses in 65% of patients.	59
Naked mRNA with GM-CSF	Patients with stage IV renal cell cancer	MUC1, CEA, Her-2/neu, telomerase, survivin and MAGE-A1	The intradermal mRNA injections resulted in clinical response without any severe side effects and induced CD4+ and CD8+ T cell responses for the specific antigens.	54
	Patients with stage III and IV metastatic melanoma	Autologous mRNA	Intradermal injection; safe and feasible; increase in antitumor humoral immune response in some patients;	24

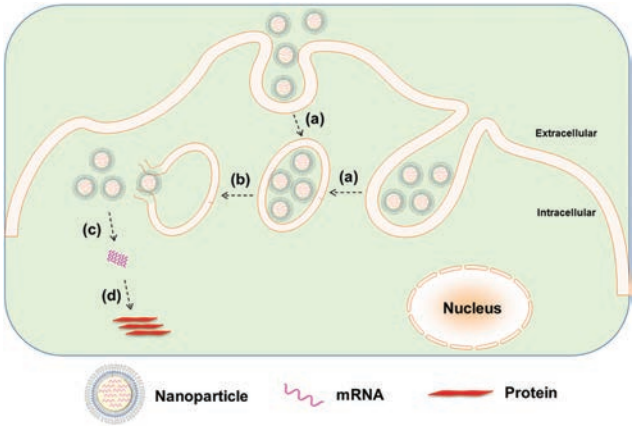

Fig. 2 Nanoparticle-mediated delivery of mRNA: (a) cellular internalization of nanoparticles into endosome, (b) endosomal escape, (c) release of mRNA from nanoparticles, and (d) mRNA translation to protein without genomic integration.

and provides mRNA increased uptake and transfection capabilities.[60] It has been shown that protamine can effectively complex with mRNA and these complexes can act as a danger signal that activates murine cells through a MyD88-dependent pathway involving TLR7 and TLR8.[60] Hoerr *et al.* demonstrated that these complexes degrade within 2 h when incubated in serum, which limits their abilities for survival in the circulation *in vivo*.[53] Nevertheless, they later showed that even partially degraded mRNA–protamine complexes can still exhibit immunostimulatory activity for over 100 h.[60] Moreover, it was found that protamine–mRNA complexes strongly activated a variety of white blood cells (such as granulocytes, B cells and NK cells) and overall significantly stimulated immune response compared to that of protamine–DNA systems.[53,60] In a clinical study by Weibe *et al.* the efficacy of this system was demonstrated by testing intradermally administered protamine-complexed mRNAs coding for Melan-A (a melanoma

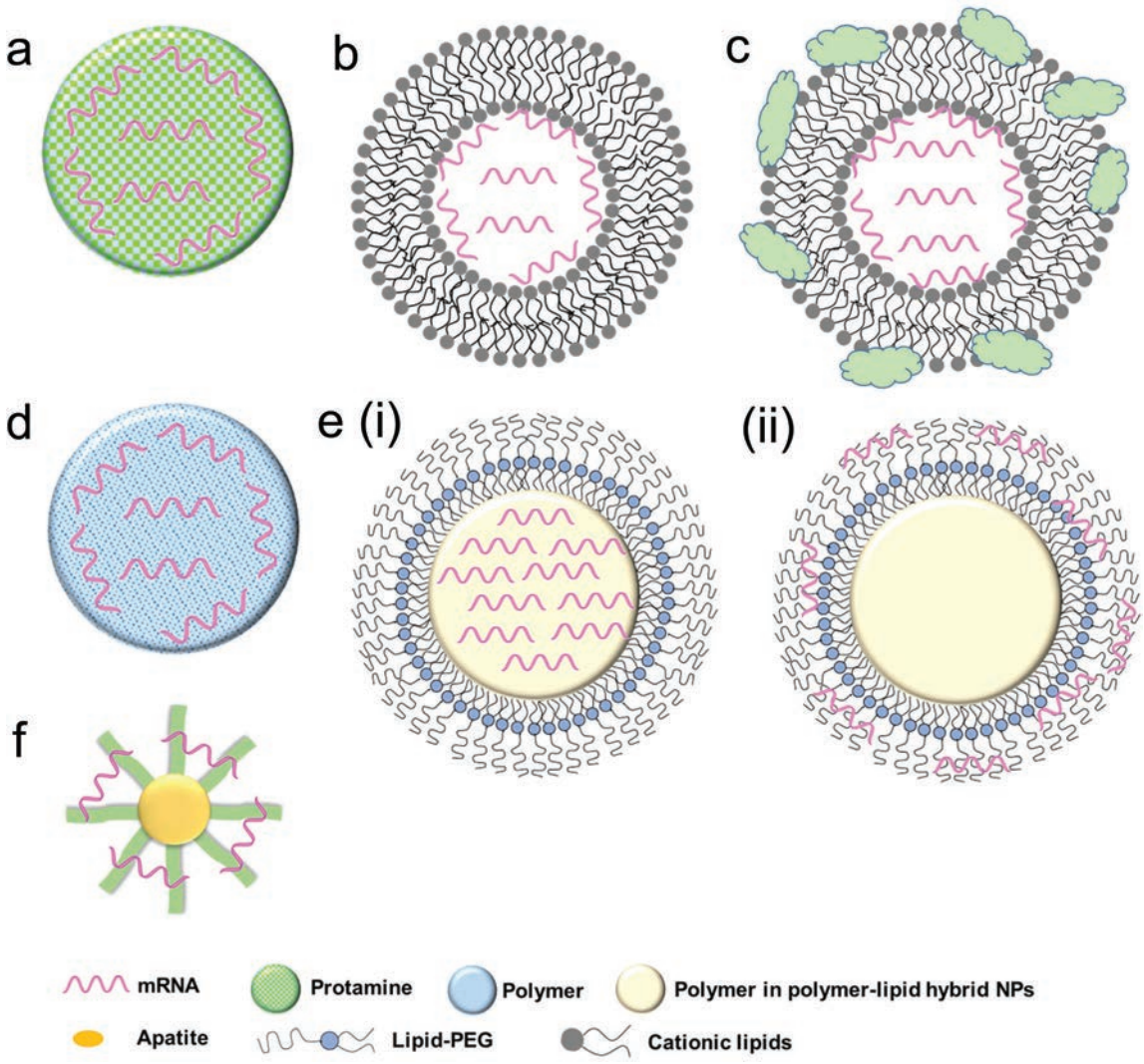

Fig. 3 Schematic representation of various biomaterial-based systems for mRNA delivery: (a) protamine–mRNA complex; (b) lipid nanoparticle; (c) lipid nanoparticle with inorganic compounds (*e.g.* apatite); (d) cationic polymeric nanoparticle; (e) lipid–polymer hybrid nanoparticles including (i) mRNA–polymer complex core surrounded by a lipid shell and (ii) polymer core surrounded by a lipid shell with mRNA absorbed onto the surface; and (f) gold nanoparticle.

antigen), Tyrosinase (an enzyme which catalyzes the production of melanin), gp100 (a protein involved in melanosome maturation), Mage-A1 (a melanoma antigen), Mage-A3 (a melanoma antigen) and Survivin (a protein involved in the regulation of apoptosis) metastatic melanoma patients.[26] No side effects greater than grade II (mild to moderate) were observed and overall there was a complete clinical response, including significant effect on the frequency of immunosuppressive cells and increase of antigen-specific T cells.[26]

Recently, CureVac has also explored the use of protamine-complexed mRNA. It was found in an *in vivo* study that a two-component mRNA vaccine composed of both free and protamine-complexed mRNA resulted in successful antigen expression and immune stimulation, which were mediated by Toll-like receptor 7.[51] A balanced adaptive immunity with both cellular (T cell-mediated) and humoral immunity was achieved which not only showed prophylactic activity but also exhibited therapeutic efficacy against tumor. CureVac has also put forward a clinical trial for patients with castrate-resistant prostate cancer using mRNA-encoding for prostate-specific antigen (PSA), prostate-specific membrane antigen (PSMA), prostate stem cell antigen PSCA and six transmembrane epithelial antigen of the prostate 1 (STEAP1).[27] After intradermal vaccination, 80% of the subjects demonstrated immune response to the delivered mRNA antigen and 60% against multiple antigens, which ultimately correlated with longer survival.[27] The currently investigated protamine–complexed mRNA systems and their therapeutic efficacy are summarized in Table 2.

Lipid nanoparticles

The field of lipid nanoparticles for nucleic acid delivery is relatively mature compared to other nanotechnologies. As such, quite a variety of different lipid formulations have been tested for mRNA delivery. Cationic lipids are used ubiquitously owing to their favourable electrostatic interactions with negatively charged mRNA to form nanoparticles (Fig. 3b). This field was pioneered in 1989 with a study of the use of DOTMA (*N*-[1-(2,3-dioleyloxy)propyl]-*N*,*N*,*N*-trimethylammonium chloride) to transfect human, rat, mouse, xenopus (frog) and drosophila cells with luciferase mRNA.[31] The clinical development of such cationic lipid tools has however been hampered by their toxicity.[31] Despite these concerns, DOTMA remains a commonly used material, along with DOTAP (1,2-dioleoyloxy-3-trimethylammonium propane chloride).[61] An important note about these cationic lipids is that while positively charged lipid nanoparticles can be effective *in vitro*, *in vivo* results are less promising because cationic liposomes can be quickly eliminated by the mononuclear phagocyte system (MPS).

The coating of poly(ethylene) glycol (PEG) layer on lipid carriers has been widely used for the delivery of nucleic acid payloads, such as siRNA[62] and DNA,[63] to improve the formulation process, reduce aggregation and increase the blood circulation time.[64–67] However, the surface PEGylation has also been shown to decrease cellular uptake, an effect which may be minimized by optimizing PEG size and content.[63,68,69] PEG modification has also been applied to nanoparticle-based mRNA delivery, particularly to polymer nanoparticles[70] and lipid–polymer hybrid nanoparticles,[71,72] both of which will be discussed in later sections. The application of PEGylation to lipid-based mRNA delivery systems to improve their *in vivo* efficacy remains elusive. Another strategy is the incorporation of a helper lipid such as 1,2-dioleoyl-*sn*-glycero-3-phosphoethanolamine (DOPE) to reduce aggregation of the lipid systems (as well as to improve endosomal escape).[73–76]

To further enhance mRNA transfection potency in both mitotic and non-mitotic cells, Akaike and co-workers developed a different approach by coating inorganic carbonate apatite nanoparticles on liposomal carriers (Fig. 3c). It was evident that these inorganic additives helped to increase mRNA uptake through effective endocytosis. They also demonstrated that decorating mRNA-containing DOTAP-apatite particles with RGD, which is known for its ability to bind integrins,[77] enhanced cytoplasmic expression of delivered mRNA. This method is versatile and holds a great potential due to its abilities for targeting and efficient delivery of mRNA.[61,78–80]

More recently, a novel lipid/protamine/mRNA nanoparticle platform was proposed and comprehensively explored for systemic delivery to tumors.[10] In this study DOTAP liposomes were used to encapsulate mRNA–protamine complexes and then coated with DSPE-PEG and DSPE-PEG-anisamide.[10] These particles demonstrated stability against degradation in serum, high *in vitro* transfection ability in NCI-H460 cells, low cytotoxicity (even at a concentration 50 times higher than the dose they found to induce effective transfection), accumulation in tumor site and anticancer action *in vivo*.[10] Together this approach presents a very promising hybrid system for the systemic delivery of mRNA. Currently, Tekmira Pharmaceuticals is also investigating lipid nanoparticles for systemic mRNA delivery to the liver.

Until now, lipid nanoparticles have been widely utilized, particularly to introduce mRNA to immune cells for vaccine purposes. The detailed overview of currently available lipid-based nanoparticles for mRNA delivery was presented in several recent reports,[3,16,25,81] and a summary of these advances is presented in Table 2. As the lipid nanoparticles represent a more thoroughly explored system, their further development and optimization may open up the foundation for the creation of more effective mRNA delivery systems.

Polymeric nanoparticles

Polymeric nanoparticles have emerged as effective delivery vehicles for a variety of payloads, such as DNA,[82] siRNA,[83] mRNA,[28] proteins,[84] chemotherapeutic agents[85] and others. To date, cationic polymers have been used primarily because of their favourable electrostatic interactions with negatively charged nucleic acids (Fig. 3d) and cell membranes. As compared with other delivery vehicles such as liposomes, multiple parameters must be considered in their design. Pack *et al.* enumerated some of these in their recent report in which they emphasized optimization with respect to synthesis of mRNA carriers, transfection and endosomal escape capabilities.[86]

Table 2 Biomaterials for mRNA delivery

Category	Platform	Stage	mRNA	Activity and efficiency	Ref.
Protamine–mRNA complex	Protamine complexed β-gal mRNA	HeLa-K^b cells injected into B6 ($H2^b$) mice and BALB/c mice	β-Gal and GFP	Successful CTL response, dependent on injection site	53
		Human PBMC	β-Gal, EGFP or CMV pp65	Complexes triggered strong IL-6 and TNF-α release, activation of innate immune system and other APCs	60
		Murine BM-DC	β-Gal or CMV pp65	Stimulated mouse BM-DC: release of IL-6 and IL-12 and up-regulation of CD86	123
	Protamine complexed Melan-A, Tyrosinase, gp100, Mage-A1, Mage-A3, and Survivin mRNA	Patients with metastatic melanoma	Melan-A, Tyrosinase, gp100, Mage-A1, Mage-A3, and Survivin	Increased frequency of immunosuppressive and vaccine-directed T cells	26
	CureVac®: A two-component mRNA vaccine composed of free mRNA and mRNA complexed with protamine	BALB/c and C57BL/6 mice	OVA (GgOVA), control (Ecβ-gal sh), PSMA (HsPSMA) and STEAP (HsSTEAP)	Demonstrated antitumor effects after intravenous injection; activated the adaptive and innate immune systems Ability to inhibit established tumors	51
	CureVac® (CV9201)	Patients with stage IIIB/IV non-small cell lung cancer	MAGE-C1, MAGE-C2, NY-ESO-1, survivin and 5T4	This is a phase I/IIa open, uncontrolled, international, prospective clinical trial	58
	CureVac® (CV9202)	Patients with stage IV non-small cell lung cancer	NY-ESO-1, MAGEC1, MAGEC2, 5 T4, Survivin, and MUC1	mRNA vaccines potentially induced immune response to antigens expressed in tumors	57
	CureVac® (CV9202) in combination with radiotherapy	Patients with stage IV non-small cell lung cancer	NY-ESO-1, MAGEC1, MAGEC2, 5 T4, Survivin, and MUC1	19 patients have been recruited thus far, recruitment finished by the end of 2014	57
	CureVac® (CV9103)	Patients with castrate-resistant prostate cancer	PSA, PSCA, PSMA and STEAP1	Intradermal injections; maximum tolerated dose not defined; activation of TLR7 Antigen-specific T-cells were detected in 79% of patients and 58% of the immunological responders reacted against multiple antigens; Increased antigen-specific T-cells and antigen-unspecific B cells in 74% of patients Safe, well-tolerated and induces high levels of cellular immunogenicity	27,55
	CureVac® (CV9104)	Patients with metastatic castrate-refractory prostate cancer	mRNA-encoding six antigens (this is an advancement of CV9103 encoding two more antigens)	This is a randomised, double-blind, placebo-controlled, Phase I/II trial scheduled to be finished in 2016.	27,124
Lipid nanoparticle	DOTAP liposomes covered with apatite nanoparticles	HeLa	Luciferase	Together with ARCA (over cap) had over 100-fold improvement compare to DOTAP, percentage not determined	78
		HeLa	Luciferase	9–14 better than mRNA liposome alone, percentage not determined	79
		NIH 3T3			
		HeLa	Luciferase	DOTAP-apatite outperformed DOTAP alone and Lipofectamine 2000, percentage not determined	80
		HUVEC			
	Fibronectin complexed to DOTAP liposomes covered with apatite nanoparticles	HeLa	Luciferase	Fn-DOTAP-apatite more than 50-times better than DOTAP, percentage not determined	61
	DOTAP/DOPE/DSPE-PEG-2000-biotin	Primary murine bone marrow-derived DC from C57BL/6 mice	TriMix mRNA encoding CD40-ligand,TLR4 and CD70	19%	19
	DOTAP/DOPE/DSPE-PEG-2000-biotin lipoplex loaded microbubbles	DC primary cultures from the bone marrow of C57BL/6 mice	Luciferase	24%	21
	DOTMA	NIH 3T3	Luciferase	Percentage not determined, at least 20–30% RNase resistant	31

Table 2 *(Contd.)*

Category	Platform	Stage	mRNA	Activity and efficiency	Ref.
	Lipofectamine 2000 and TransIT	Neurospheres from subventricular zone of adult C57BL/6 mice	EGFP	40–50%	125
	MLRI/DOPE and TransFast	CHO	GFP and luciferase	>50%	126
		NIH 3T3		>45%	
	Novel cationic lipids: X2, S1, S2, S3, 2X3 and 2D3 with DOPE (helper lipid)	DC cells cultured from the bone marrow of C57BL/6 mice	EGFP and B-16	Up to 47% of DC progenitors	127
				Up to 57% of immature DCs	
	DOTAP/cholesterol liposome with DSPE-PEG and DSPE-PEG-AA, encapsulating protamine/mRNA cores	NCI-H460 xenograft	Herpes simplex virus 1-thymidine kinase (HSV1-tk)	68–78%	10
	DOTAP/DOPE	HeLa	Luciferase, GFP and CXCR4	~80%	92
	Stemfect	JAWS II	Luciferase and GFP	80%	128
		DC2.4	Luciferase and GFP	>97%	
		Human primary DCs	Luciferase and GFP	>50%	
		Murine primary DCs	Luciferase and GFP	>60%	
Polymeric nanoparticle	Linear PEI	BEAS-2B	Luciferase	5-Fold higher than Lipo 2000	70
	Poly(DMAEMA-*co*-OEGMA)	BEAS-2B	Luciferase	Same level as Lipo 2000	
	Poly(DMAEMA) with PEG	BEAS-2B	Luciferase	3-Fold improvement after PEGylation	
	Branched PEI (25 kDa)	PC3	GFP	~30%	93
	Linear PEI	HeLa	Luciferase, GFP and CXCR4	40%	92
	Branched PEI (2 kDa) conjugated to melittin, with chloroquine	HeLa	GFP	52.2%	91
		HUVEC		71.6%	
	Triblock copolymer (comprising DMAEMA, PEGMA, DEAEMA and BMA)	DC2.4	EGFP and OVA	50%	28
		RAW264.7		77%	
Polymer-lipid hybrid nanoparticle	Poly-(β-amino ester) core, phospholipid bilayer shell	DC2.4	Luciferase and GFP	30%	106
	Mannosylated histidylated lipopolyplexes	DC2.4	EGFP and MART-1	60%	71
	DMDHP	CHO	Luciferase and GFP	70–80%	129
Gold nanoparticle	DNA oligonucleotide-conjugated gold nanoparticle	HeLa	BAX	Fluorescent signal uniformly detected, percentage not determined.	29
		HepG2			

Abbreviations: (*N*,*N*-[bis(2-hydroxyethyl)]-*N*-[2,3-bis(tetradecanoyloxy) propyl] ammonium chloride (DMDHP); 1,2-dioleoyl-3-trimethylammonium-propane (DOTAP); 1,2-dioleoyl-*sn*-glycero-3-phosphoethanolamine (DOPE); 1,2-distearoyl-*sn*-glycero-3-phosphoethanolamine-*N*-[biotinyl(polyethylene glycol)-2000] (ammonium salt); 1,2-distearoy-phosphatidylethanolamine-polyethylene glycol (DSPE-PEG); 1,2-distearoy-phosphatidylethanolamine-polyethylene glycol-anisamide (DSPE-PEG-AA); Antigen-presenting cell (APC); Anti-Reverse Cap Analog (ARCA); Bone-marrow-derived dendritic cell (BM-DC); Carcinoembryonic antigen (CEA); Cluster of differentiation 70 (CD70); Cluster of differentiation 86 (CD86); C–X–C chemokine receptor type 4 (CXCR-4); Cytomegalovirus (CMV); Cytotoxic T cell (CTL); Dendritic cell (DC); Diethylaminoethyl methacrylate (DEAEMA) and butyl methacrylate (BMA); Diethylaminoethyl methacrylate (DMAEMA); Enhanced green fluorescent protein (EGFP); Granulocyte-macrophage colony stimulating factor (GM-CSF); Green fluorescent protein (GFP); Human bronchial epithelia cell line (BEAS-2B); Human epidermal growth factor receptor 2 (Her-2/neu); Interleukin 12 (IL-12); Interleukin 6 (IL-6); Melanoma-associated antigen 1 (MAGE-A1); Melanoma-associated antigen family C1 (MAGE-C1); Melanoma-associated antigen family C2 (MAGE-C2); Mucin 1 (MUC1); New York esophageal squamous cell carcinoma 1 (NY-ESO-1); *N*-[1-(2,3-dioleyloxy)propyl]-*N*,*N*,*N*-trimethylammonium chloride (DOTMA); Oligo(ethylene glycol) methyl ether methacrylate (OEGMA); Ovalbumin (OVA); Peripheral blood mononuclear cell (PBMC); Poly(ethylene glycol) methyl ether methacrylate (PEGMA); Polyethylenimine (PEI); Prostate-specific antigen (PSA); Prostate-specific membrane antigen (PSMA); Prostate stem cell antigen (PSCA); Six transmembrane epithelial antigen of the prostate 1 (STEAP1); Toll-like receptor (TLR); Tumor necrosis factor alpha (TNF-α); Tumor-associated antigen (TAA); Vascular endothelial growth factor-A (VEGF-A); β-Galactosidase (β-gal); Trophoblast glycoprotein (5T4).

Additionally, polymers to be used for pharmaceutical purposes should be biocompatible, non-toxic and non-immunogenic.

Generally, polymeric nanoparticles are prepared by nanoprecipitation[87,88] or emulsion techniques.[89,90] When properly optimized, these polymeric carriers may serve as a highly functional delivery vehicle for mRNA. The surfaces can be easily modified with other materials such as ligands to confer targeting abilities and other polymers to afford properties such as pH-responsive release for tuning the release profile.[91] The particles themselves must overcome extra- and intracellular barriers to ensure that the mRNA is available for protein expression (Fig. 2). Additionally, specific to polymeric particles, the charge and size of the polymers used must be carefully considered since the binding strength between the mRNA and polymer is a key factor in mRNA expression efficiency.[91]

Among various polymeric carriers for gene delivery, polyethylenimine (PEI) (Fig. 4a) is a classic material and is always used as a standard control in nucleic acid transfection. Rejman *et al.* explored the use of linear PEI polyplexes in HeLa cells and found moderate mRNA transfection efficiency of approximately 40% using C–X–C chemokine receptor (CXCR) type 4. This was exceeded by a cationic lipid formulation (DOTAP/DOPE) (Fig. 4b and c).[92] However, concerns regarding PEI include non-degradability and potential toxicity (depending on the molecular weight and type of PEI). Recently, a few different studies have investigated the efficiency of modified PEI as an mRNA delivery system with high transfection efficiency and reduced toxicity. Read *et al.* explored the use of reducible polycations with histidine and polylysine residues (HIS-RPCs) and, with their optimised formulations, found

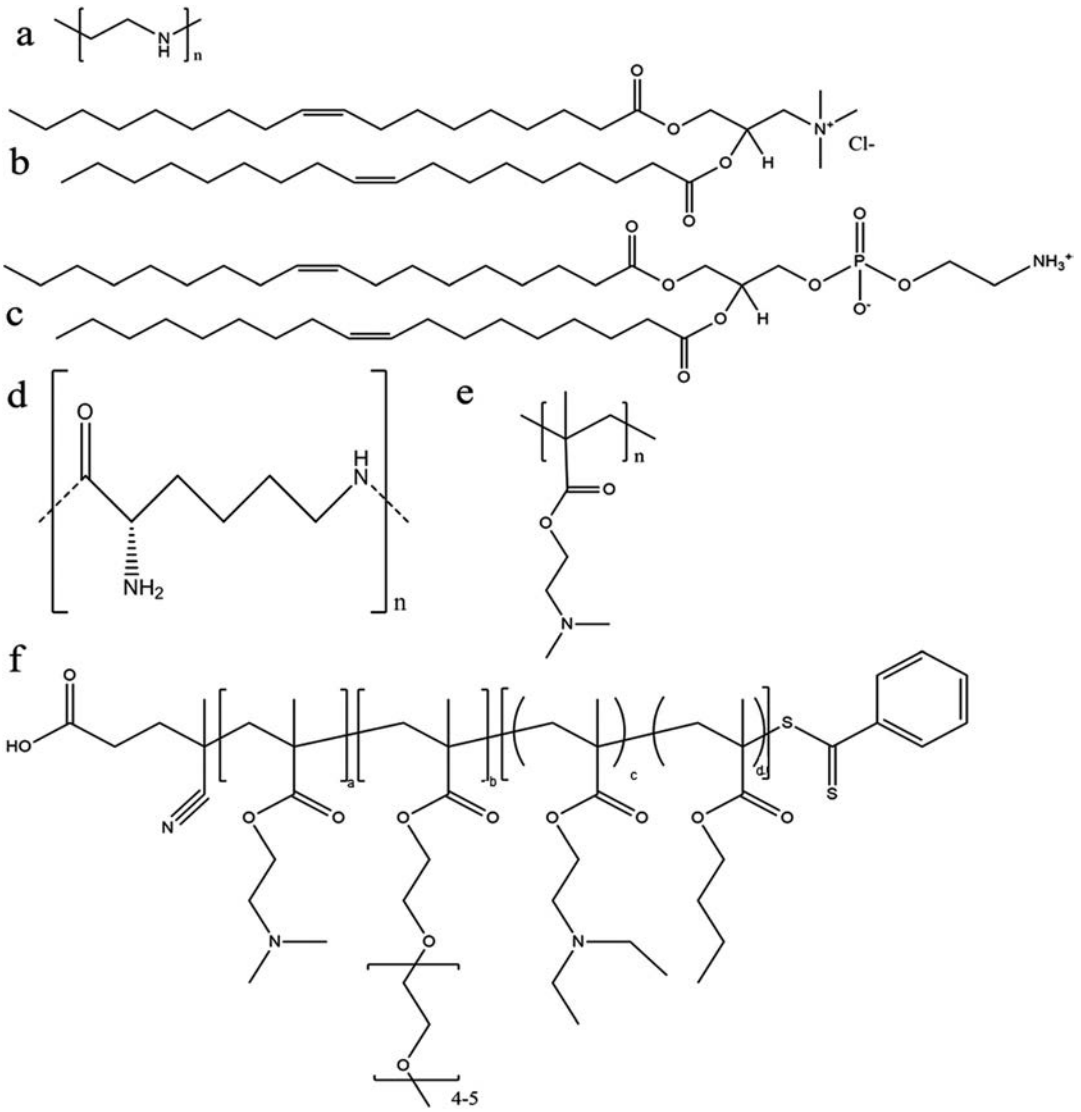

Fig. 4 Chemical structure of some representative polymers and lipids used for mRNA delivery: (a) polyethylenimine (PEI); (b) 1,2-dioleoyl-3-trimethylammonium-propane (chloride salt) (DOTAP); (c) 1,2-dioleoyl-*sn*-glycero-3-phosphoethanolamine (DOPE); (d) poly(L-lysine) (PLL); (e) poly-(2-(dimethylamino)ethyl methacrylate) (p(DMAEMA)); and (f) poly(DMAEMA-PEGMA-DEAEMA-*co*-BMA).

transfection efficiencies of over 90% in human prostate cancer cells (PC3).[93] In contrast, they found that nanoparticles made of unmodified branched PEI (25 kDa) were only able to achieve efficiencies of about 30%.[93] Bettinger *et al.* also investigated the transfection activity of PEI (branched but with low molecular weight of 2 kDa) along with another well-known cationic polymer, poly(L-lysine) (Fig. 4d). In this study, they included additive compounds to increase transfection capability of PEI and, here, they found that the polymer in the presence of chloroquine (an agent to aid endosomolysis) and in conjugation to melittin (a membrane-active peptide) significantly increased the transfection efficiency.[91] With these additives, transfection efficiencies of 52.2% and 71.6% were achieved in HeLa and HUVEC cells, respectively, and were greater than with the cationic lipid (DOTAP) alone.[91] The effect of molecular weight of PEI was also investigated with the conclusion that overall higher MW polymers had better endosomolytic activity but bound mRNA too tightly for it to be released.[91] These studies and their conflicting results also bring forward the important note that the efficacy and utility of a polymer candidate can be markedly improved through the use of additives and tuning of the MW and size of the particle.

The effect of PEGylation on the polymer–mRNA binding efficacy and mRNA transfection abilities was also investigated. It was demonstrated that adding PEG side chains to poly(*N*,*N*-diethylaminoethyl methacrylate) (P(DMAEMA)) (Fig. 4e) increased its ability to complex mRNA and tendency to form monodispersed particles, as compared to their unmodified variants as well as linear PEI (used as a positive control).[70] Nonetheless, linear PEI displayed the highest mRNA transfection capabilities and the PEGylated mRNA nanoparticle exhibited significantly higher transfection capability over its non-PEGylated counterpart.[70] Moreover, through testing with an influenza-peptide 7 (an endolysosomal release peptide), it was found that the PEGylated copolymer further supported the endosomal release of their mRNA payload and improved transfection efficiency,[70] suggesting further investigation into this polymer chemistry may be fruitful.

With rapid advances in polymer chemistry, a vast variety of other cationic polymers have been synthesized and applied to mRNA delivery. Recently a novel triblock polymer has been developed (Fig. 4f) using: (i) diethylaminoethyl methacrylate (DMAEMA) to promote mRNA condensation, (ii) poly(ethylene glycol) methyl ether methacrylate (PEGMA) to enhance stability and biocompatibility and (iii) a copolymer of diethylaminoethyl methacrylate (DEAEMA) and butyl methacrylate (BMA) to facilitate cytosolic entry.[28] The triblock polymer nanoparticles were ranging in size from 86 to 216 nm after complexation with mRNA and achieved transfection efficiency of up to 77% in RAW264.7 macrophage cells and 50% in DC2.4 dendritic cells, compared with approximately 30% in both cell lines while commercial transfection agent Lipofectamine 2000 was used.[28] A further study was performed using a number of differing formulations made of the similar three polymers and found that the optimal arrangement was DMAEMA-PEGMA-DEAEMA-*co*-BMA, which provided an ideal balance between stability and charge shielding.[28] With this arrangement, the copolymers showed decreased cytotoxicity *in vitro* with the decreasing of molecular weights for the second (PEGMA) block.[28]

The use of polymeric nanoparticles for mRNA delivery is still in its infancy but has shown great potential. The field of polymeric mRNA delivery began with the use of diethylaminoethyl-dextran[30] and has now evolved to rival the abilities of many well-established lipid systems. Various novel polymeric carriers as mRNA delivery systems are summarized in Table 2. The future of this field largely depends on the further discovery and optimization of more efficient polymers to improve mRNA transfection efficiency, as well as safety and biocompatibility.

Lipid–polymer hybrid nanoparticles

The lipid–polymer hybrid nanoparticle platform has several potential advantages when compared with either lipid- or polymer-based nanoparticles for the delivery of therapeutic compounds including small molecules, peptides, proteins and oligonucleotides, and has gained significant attention in last decade.[94–98] Structurally, the core of the nanoparticle is made up of a polymeric material coated with lipids and/or lipid–PEGs which can enhance the nanoparticle stability and pharmacokinetics, and confer surface tunable properties.[94,99–101] Alternatively, the properties of the core can be tuned in order to respond to external stimuli which can help to facilitate endosomal escape.[71,102,103] We have also recently reported the development of several such systems which exhibited sustained delivery of siRNA and enhanced gene silencing.[104,105] Lipid–polymer hybrid nanoparticle systems have also been employed as delivery vehicles for mRNA.[71,72,102]

There are two structural strategies which have been employed to design lipid–polymer hybrid nanoparticles for mRNA delivery. In the first method, negatively charged mRNA is complexed with the cationic polymer and then the surface can be decorated with lipids or lipid–PEG conjugates (Fig. 3e (i)).[10,106] In the second method, mRNA is adsorbed to the surface of the cationic nanoparticle core (Fig. 3e (ii)).[107] Using both methods, mRNA delivery can be achieved; however release profiles may vary and it has been hypothesized by Su *et al.*[102] that surface adsorbed mRNA has a faster release profile. They also showed that adsorbed mRNA has increased stability compared to naked mRNA which suggests that even if the mRNA is on the surface of nanoparticle, degradation can still be reduced due to the complexation.

To increase endosomal mRNA delivery, various pH-responsive polymers have been used. Upon endocytosis, changes in pH cause a conformational change in the polymer which results in osmotic shock followed by endosome disruption. For example, a PEGylated derivative of histidylated polylysine and L-histidine-(*N*,*N*-di-*n*-hexadecylamine)ethylamide liposomes (termed as 'histidylated lipopolyplexes') was prepared to for mRNA-based cancer vaccine in which polylysine was used to complex mRNA, and histidylation contributed in charge

switching at endosomal pH condition due to the imidazole group with pI of 6. Additionally, they found that mannosylation of this delivery system significantly enabled targeted mRNA delivery to dendritic cells through interaction with the mannose receptor.[71] The PEGylated histidylated mRNA lipopolyplexes were also efficient in inducing an anti-B16 specific cellular immune response and conferring protection against B16F10 melanoma in mice.[72] In another report, poly-β-amino ester (PBAE), developed by Su *et al.*, also used pH-responsiveness to disrupt endosomal membrane.[106] The PBAE polymer was coated with lipids containing DOTAP which was used to adsorb mRNA on the particle as described earlier. Both of the pH-responsive systems have great potential for developing an effective delivery system for mRNA.[102]

A summary of the advances on lipid–polymer hybrid nanoparticles is presented in Table 2. As of now it is difficult to postulate which is the most efficient method for mRNA delivery since there is a lack of sufficient studies to compare different mRNA delivery systems and determine the optimum one. Evidently, there is a compelling need to investigate various delivery options and establish quick optimization methods to screen a large number of mRNA delivery systems at once. This would accelerate the developmental progress of this highly promising biomedical research field.

Gold nanoparticles

Another type of nanoparticle delivery system for mRNA delivery is gold nanoparticle-DNA oligonucleotide (AuNP–DNA) conjugates (Fig. 3f).[29] This novel system has demonstrated significant transfection activity in HeLa (cervical carcinoma) and HepG2 (hepatocyte carcinoma) cells (detected using confocal fluorescent microscopy). The nanoparticles were tested *in vivo* using direct injection into xenograft tumors and the results showed that the AuNP–DNA–mRNA nanoparticles were able to induce the production of biologically functionalized Bcl-2-associated X (BAX) protein,[29] suggesting a promising start for this unique mRNA nanoparticle formulation. While gold nanoparticles have not been extensively studied for mRNA delivery, their promising results with other nucleic acids (*e.g.*, siRNA and DNA) indicate that they have significant potential for the delivery of mRNA.

Indeed, the gold nanoparticle-oligonucleotide system has been more widely studied with DNA and siRNA.[108–110] This system has demonstrated significant cellular uptake in a number of cell lines.[109,111–113] Recently, the mechanism behind the uptake of gold oligonucleotide particles was further elucidated. It has been shown that their uptake is highest in serum-free conditions and the membrane proteins responsible for the uptake of these particles are the scavenger receptors.[111] Other delivery systems based upon gold nanoparticles include gold nanoparticles passivated with BSA-SV40 large T antigen conjugates,[114] layer-by-layer gold nanoparticles with polymers for the delivery of siRNA[115,116] and plasmid DNA delivery using carbon dot-gold nanoparticles conjugated with PEI.[117] These exciting techniques and technologies all may have the potential to be applied to mRNA delivery, demonstrating that the field of gold nanoparticle-mediated mRNA transport is rich with new possibilities.

Conclusion

mRNA-based vaccine and gene therapy technologies are innovative, promising and rapidly emerging strategies in biomedical research for the purpose of treating acquired and congenital diseases. Although naked mRNA has prospective clinical efficacy, this field faces various challenges such as the delivery issues, targeting administration and short-term gene expression, all of which are critical drawbacks and could be the major limitations to translate this field to widespread clinical application. The rapid advancements in biomaterials and nanotechnology could significantly help overcome these obstacles. This review has receptively presented the progress of cutting-edge biomaterials and nanotechnology platforms to improve the efficacy of mRNA delivery. While further improvements are necessary, it is encouraging to see that some of the mRNA-based treatment strategies[24,26,118] have already reached into the clinical trials stage within a short phase of their development. More efforts are still required to find novel biomaterials/nanoparticles and optimized formulations which can provide high transfection activity and biocompatibility with minimal carrier-specific toxicity/immunostimulation, high selectivity and specificity, and effective systemic *in vivo* delivery and prolonged protein expression (particularly for gene therapy). With the advancement and proper design of biomaterials, it is expected that mRNA technology will be of high interest in clinical applications for years to come.

Acknowledgements

This work was supported by the National Institutes of Health (NIH) grants R00CA160350 (J. S.) and R01CA37393 (B. R. Z.), and the Movember-PCF Challenge Award (J. S.) and PCF Young Investigator Award (J. S.). Y. X. received DoD PCRP Postdoctoral Training Award (W81XWH-14-1-0268).

References

1 H. Yin, R. L. Kanasty, A. A. Eltoukhy, A. J. Vegas, J. R. Dorkin and D. G. Anderson, *Nat. Rev. Genet.*, 2014, **15**, 541–555.
2 E. S. Quabius and G. Krupp, *Nat. Biotechnol.*, 2015, **32**, 229–235.
3 R. P. Deering, S. Kommareddy, J. B. Ulmer, L. A. Brito and A. J. Geall, *Expert Opin Drug Deliv.*, 2014, **11**, 885–899.
4 J. Lee, D. Boczkowski and S. Nair, *Methods Mol. Biol.*, 2013, **969**, 111–125.
5 A. Yamamoto, M. Kormann, J. Rosenecker and C. Rudolph, *Eur. J. Pharm. Biopharm.*, 2009, **71**, 484–489.

6 C. Leonhardt, G. Schwake, T. R. Stogbauer, S. Rappl, J. T. Kuhr, T. S. Ligon and J. O. Radler, *Nanomedicine*, 2014, **10**, 679–688.

7 T. S. Ligon, C. Leonhardt and J. O. Radler, *PLoS One*, 2014, **9**, e107148.

8 X. Wu and G. Brewer, *Gene*, 2012, **500**, 10–21.

9 E. Grudzien-Nogalska, J. Kowalska, W. Su, A. N. Kuhn, S. V. Slepenkov, E. Darzynkiewicz, U. Sahin, J. Jemielity and R. E. Rhoads, *Methods Mol. Biol.*, 2013, **969**, 55–72.

10 Y. Wang, H. H. Su, Y. Yang, Y. Hu, L. Zhang, P. Blancafort and L. Huang, *Mol. Ther.*, 2013, **21**, 358–367.

11 J. Stepinski, C. Waddell, R. Stolarski, E. Darzynkiewicz and R. E. Rhoads, *RNA*, 2001, **7**, 1486–1495.

12 J. Jemielity, T. Fowler, J. Zuberek, J. Stepinski, M. Lewdorowicz, A. Niedzwiecka, R. Stolarski, E. Darzynkiewicz and R. E. Rhoads, *RNA*, 2003, **9**, 1108–1122.

13 E. Grudzien-Nogalska, J. Jemielity, J. Kowalska, E. Darzynkiewicz and R. E. Rhoads, *RNA*, 2007, **13**, 1745–1755.

14 J. Peng, E. L. Murray and D. R. Schoenberg, *Methods Mol. Biol.*, 2008, **419**, 215–230.

15 M. S. Kormann, G. Hasenpusch, M. K. Aneja, G. Nica, A. W. Flemmer, S. Herber-Jonat, M. Huppmann, L. E. Mays, M. Illenyi, A. Schams, M. Griese, I. Bittmann, R. Handgretinger, D. Hartl, J. Rosenecker and C. Rudolph, *Nat. Biotechnol.*, 2011, **29**, 154–157.

16 G. Tavernier, O. Andries, J. Demeester, N. N. Sanders, S. C. De Smedt and J. Rejman, *J. Controlled Release*, 2011, **150**, 238–247.

17 C. E. Thomas, A. Ehrhardt and M. A. Kay, *Nat. Rev. Genet.*, 2003, **4**, 346–358.

18 M. D. Mattozzi, M. J. Voges, P. A. Silver and J. C. Way, *J. Visualized Exp.*, 2014, DOI: 10.3791/51234. Q5

19 H. Dewitte, S. Van Lint, C. Heirman, K. Thielemans, S. C. De Smedt, K. Breckpot and I. Lentacker, *J. Controlled Release*, 2014, **194**, 28–36.

20 S. Van Meirvenne, L. Straetman, C. Heirman, M. Dullaers, C. De Greef, V. Van Tendeloo and K. Thielemans, *Cancer Gene Ther.*, 2002, **9**, 787–797.

21 M. L. De Temmerman, H. Dewitte, R. E. Vandenbroucke, B. Lucas, C. Libert, J. Demeester, S. C. De Smedt, I. Lentacker and J. Rejman, *Biomaterials*, 2011, **32**, 9128–9135.

22 H. Dewitte, S. Van Lint, C. Heirman, K. Thielemans, S. C. De Smedt, K. Breckpot and I. Lentacker, *J. Controlled Release*, 2014, **194c**, 28–36.

23 R. Kanasty, J. R. Dorkin, A. Vegas and D. Anderson, *Nat. Mater.*, 2013, **12**, 967–977.

24 B. Weide, J. P. Carralot, A. Reese, B. Scheel, T. K. Eigentler, I. Hoerr, H. G. Rammensee, C. Garbe and S. Pascolo, *J. Immunother.*, 2008, **31**, 180–188.

25 P. Midoux and C. Pichon, *Expert Rev. Vaccines*, 2015, **14**, 221–234.

26 B. Weide, S. Pascolo, B. Scheel, E. Derhovanessian, A. Pflugfelder, T. K. Eigentler, G. Pawelec, I. Hoerr, H. G. Rammensee and C. Garbe, *J. Immunother.*, 2009, **32**, 498–507.

27 K. J. Kallen, U. Gnad-Vogt, B. Scheel, G. Rippin and A. Stenzl, *J. Immunother. Cancer*, 2013, **1**, 1–1.

28 C. Cheng, A. J. Convertine, P. S. Stayton and J. D. Bryers, *Biomaterials*, 2012, **33**, 6868–6876.

29 J. H. Yeom, S. M. Ryou, M. Won, M. Park, J. Bae and K. Lee, *PLoS One*, 2013, **8**, e75369.

30 G. Koch, *Curr. Top. Microbiol. Immunol.*, 1973, **62**, 89–138.

31 R. W. Malone, P. L. Felgner and I. M. Verma, *Proc. Natl. Acad. Sci. U. S. A.*, 1989, **86**, 6077–6081.

32 M. Strenkowska, J. Kowalska, M. Lukaszewicz, J. Zuberek, W. Su, R. E. Rhoads, E. Darzynkiewicz and J. Jemielity, *New J. Chem.*, 2010, **34**, 993–1007.

33 A. K. Banerjee, *Microbiol. Rev.*, 1980, **44**, 175–205.

34 R. J. Jackson, *Cell*, 1993, **74**, 9–14.

35 A. E. Pasquinelli, J. E. Dahlberg and E. Lund, *RNA*, 1995, **1**, 957–967.

36 A. Cai, M. Jankowska-Anyszka, A. Centers, L. Chlebicka, J. Stepinski, R. Stolarski, E. Darzynkiewicz and R. E. Rhoads, *Biochemistry*, 1999, **38**, 8538–8547.

37 L. Weill, E. Belloc, F. A. Bava and R. Mendez, *Nat. Struct. Mol. Biol.*, 2012, **19**, 577–585.

38 D. Schwartz, C. J. Decker and R. Parker, *RNA*, 2003, **9**, 239–251.

39 V. F. Van Tendeloo, P. Ponsaerts, F. Lardon, G. Nijs, M. Lenjou, C. Van Broeckhoven, D. R. Van Bockstaele and Z. N. Berneman, *Blood*, 2001, **98**, 49–56.

40 S. Holtkamp, S. Kreiter, A. Selmi, P. Simon, M. Koslowski, C. Huber, O. Tureci and U. Sahin, *Blood*, 2006, **108**, 4009–4017.

41 M. Mockey, C. Goncalves, F. P. Dupuy, F. M. Lemoine, C. Pichon and P. Midoux, *Biochem. Biophys. Res. Commun.*, 2006, **340**, 1062–1068.

42 U. Sahin, K. Kariko and O. Tureci, *Nat. Rev. Drug Discovery*, 2014, **13**, 759–780.

43 G. J. Cao and N. Sarkar, *Proc. Natl. Acad. Sci. U. S. A.*, 1992, **89**, 10380–10384.

44 A. C. Beckel-Mitchener, A. Miera, R. Keller and N. I. Perrone-Bizzozero, *J. Biol. Chem.*, 2002, **277**, 27996–28002.

45 G. Shaw and R. Kamen, *Cell*, 1986, **46**, 659–667.

46 R. D. Klausner, T. A. Rouault and J. B. Harford, *Cell*, 1993, **72**, 19–28.

47 K. J. Kallen and A. Thess, *Therapeutic Advances in Vaccines*, 2014, vol. 2, pp. 10–31.

48 K. Kariko, A. Kuo and E. Barnathan, *Gene Ther.*, 1999, **6**, 1092–1100.

49 S. S. Diebold, T. Kaisho, H. Hemmi, S. Akira and C. Reis e Sousa, *Science*, 2004, **303**, 1529–1531.

50 S. R. Nallagatla, R. Toroney and P. C. Bevilacqua, *RNA Biol.*, 2008, **5**, 140–144.

51 M. Fotin-Mleczek, K. M. Duchardt, C. Lorenz, R. Pfeiffer, S. Ojkic-Zrna, J. Probst and K. J. Kallen, *J. Immunother.*, 2011, **34**, 1–15.

52 M. Fotin-Mleczek, K. Zanzinger, R. Heidenreich, C. Lorenz, A. Thess, K. M. Duchardt and K. J. Kallen, *J. Gene Med.*, 2012, **14**, 428–439.

53 I. Hoerr, R. Obst, H. G. Rammensee and G. Jung, *Eur. J. Immunol.*, 2000, **30**, 1–7.

54 S. M. Rittig, M. Haentschel, K. J. Weimer, A. Heine, M. R. Muller, W. Brugger, M. S. Horger, O. Maksimovic, A. Stenzl, I. Hoerr, H. G. Rammensee, T. A. Holderried, L. Kanz, S. Pascolo and P. Brossart, *Mol. Ther.*, 2011, **19**, 990–999.

55 H. Kubler, T. Maurer, A. Stenzl, S. Feyerabend, U. Steiner, M. Schostak, W. Schultze-Seemann, F. Vom Dorp, L. Pilla and G. Viatali, *J. Clin. Oncol.*, 2011, (Supp)), Abstract: 4535.

56 S. Rausch, C. Schwentner, A. Stenzl and J. Bedke, *Hum. Vaccin. Immunother.*, 2014, **10**, 3146–3152.

57 M. Sebastian, A. Papachristofilou, C. Weiss, M. Fruh, R. Cathomas, W. Hilbe, T. Wehler, G. Rippin, S. D. Koch, B. Scheel, M. Fotin-Mleczek, R. Heidenreich, K. J. Kallen, U. Gnad-Vogt and A. Zippelius, *BMC Cancer*, 2014, **14**, 748.

58 ClinicalTrials.gov, Trial of an RNActive®-Derived Cancer Vaccine in Stage IIIB/IV Non Small Cell Lung Cancer (NSCLC), https://clinicaltrials.gov/ct2/show/NCT00923312?term=cV9201&rank=1, (accessed 06 April, 2015).

59 M. Sebastian, L. V. Boehmer, A. Zippelius, F. Mayer, M. Reck, D. Atanackovic, M. Thomas, F. Schneller, S. W. Jan, E. Goekkurt, H. Bernhard, A. Groeschel, B. Scheel, S. D. Koch, T. Lander, G. Rippin, V. Wiegand, U. S. Gnad-Vogt, K. J. Kallen and A. Knuth, *J. Clin. Oncol.*, 2012, **2012**, 30, Abstract: 2573.

60 B. Scheel, R. Teufel, J. Probst, J. P. Carralot, J. Geginat, M. Radsak, D. Jarrossay, H. Wagner, G. Jung, H. G. Rammensee, I. Hoerr and S. Pascolo, *Eur. J. Immunol.*, 2005, **35**, 1557–1566.

61 F. T. Zohra, Y. Maitani and T. Akaike, *Biol. Pharm. Bull.*, 2012, **35**, 111–115.

62 Y. Bao, Y. Jin, P. Chivukula, J. Zhang, Y. Liu, J. Liu, J. P. Clamme, R. I. Mahato, D. Ng, W. Ying, Y. Wang and L. Yu, *Pharm. Res.*, 2013, **30**, 342–351.

63 P. Harvie, F. M. Wong and M. B. Bally, *J. Pharm. Sci.*, 2000, **89**, 652–663.

64 J. Heyes, K. Hall, V. Tailor, R. Lenz and I. MacLachlan, *J. Controlled Release*, 2006, **112**, 280–290.

65 M. C. Woodle, *Adv. Drug Delivery Rev.*, 1998, **32**, 139–152.

66 V. P. Torchilin, *Nat. Rev. Drug Discovery*, 2005, **4**, 145–160.

67 M. L. Immordino, F. Dosio and L. Cattel, *Int. J. Nanomedicine*, 2006, **1**, 297–315.

68 H. Hatakeyama, H. Akita, K. Kogure, M. Oishi, Y. Nagasaki, Y. Kihira, M. Ueno, H. Kobayashi, H. Kikuchi and H. Harashima, *Gene Ther.*, 2007, **14**, 68–77.

69 L. Y. Song, Q. F. Ahkong, Q. Rong, Z. Wang, S. Ansell, M. J. Hope and B. Mui, *Biochim. Biophys. Acta*, 2002, **1558**, 1–13.

70 S. Uzgun, G. Nica, C. Pfeifer, M. Bosinco, K. Michaelis, J. F. Lutz, M. Schneider, J. Rosenecker and C. Rudolph, *Pharm. Res.*, 2011, **28**, 2223–2232.

71 F. Perche, T. Benvegnu, M. Berchel, L. Lebegue, C. Pichon, P. A. Jaffres and P. Midoux, *Nanomedicine*, 2011, **7**, 445–453.

72 M. Mockey, E. Bourseau, V. Chandrashekhar, A. Chaudhuri, S. Lafosse, E. Le Cam, V. F. Quesniaux, B. Ryffel, C. Pichon and P. Midoux, *Cancer Gene Ther.*, 2007, **14**, 802–814.

73 D. Hirsch-Lerner, M. Zhang, H. Eliyahu, M. E. Ferrari, C. J. Wheeler and Y. Barenholz, *Biochim. Biophys. Acta*, 2005, **1714**, 71–84.

74 L. Wasungu, M. C. Stuart, M. Scarzello, J. B. Engberts and D. Hoekstra, *Biochim. Biophys. Acta*, 2006, **1758**, 1677–1684.

75 H. Farhood, N. Serbina and L. Huang, *Biochim. Biophys. Acta*, 1995, **1235**, 289–295.

76 L. Wasungu and D. Hoekstra, *J. Controlled Release*, 2006, **116**, 255–264.

77 S. E. D'Souza, M. H. Ginsberg and E. F. Plow, *Trends Biochem. Sci.*, 1991, **16**, 246–250.

78 F. T. Zohra, E. H. Chowdhury, S. Tada, T. Hoshiba and T. Akaike, *Biochem. Biophys. Res. Commun.*, 2007, **358**, 373–378.

79 F. T. Zohra, E. H. Chowdhury, M. Nagaoka and T. Akaike, *Anal. Biochem.*, 2005, **345**, 164–166.

80 F. T. Zohra, E. H. Chowdhury and T. Akaike, *Biomaterials*, 2009, **30**, 4006–4013.

81 K. K. Phua, S. K. Nair and K. W. Leong, *Nanoscale*, 2014, **6**, 7715–7729.

82 J. U. Menon, P. Ravikumar, A. Pise, D. Gyawali, C. C. Hsia and K. T. Nguyen, *Acta Biomater.*, 2014, **10**, 2643–2652.

83 H. Gul-Uludag, J. Valencia-Serna, C. Kucharski, L. A. Marquez-Curtis, X. Jiang, L. Larratt, A. Janowska-Wieczorek and H. Uludag, *Leuk. Res.*, 2014, **38**, 1299–1308.

84 M. C. Chen, K. Sonaje, K. J. Chen and H. W. Sung, *Biomaterials*, 2011, **32**, 9826–9838.

85 A. A. Ranade, P. P. Bapsy, S. Nag, D. Raghunadharao, V. Raina, S. H. Advani, S. Patil, A. Maru, V. P. Gangadharan, C. Goswami, J. S. Sekhon, K. Sambasivaiah, P. Parikh, A. Bakshi and R. Mohapatra, *Asia Pac. J. Clin. Oncol.*, 2013, **9**, 176–181.

86 D. W. Pack, A. S. Hoffman, S. Pun and P. S. Stayton, *Nat. Rev. Drug Discovery*, 2005, **4**, 581–593.

87 L. Zhang, J. M. Chan, F. X. Gu, J. W. Rhee, A. Z. Wang, A. F. Radovic-Moreno, F. Alexis, R. Langer and O. C. Farokhzad, *ACS Nano*, 2008, **2**, 1696–1702.

88 J. Wu, N. Kamaly, J. Shi, L. Zhao, Z. Xiao, G. Hollett, R. John, S. Ray, X. Xu, X. Zhang, P. W. Kantoff and O. C. Farokhzad, *Angew. Chem., Int. Ed.*, 2014, **53**, 8975–8979.

89 M. G. Nava-Arzaluz, E. Pinon-Segundo, A. Ganem-Rondero and D. Lechuga-Ballesteros, *Recent Pat. Drug Delivery Formulation*, 2012, **6**, 209–223.

90 E. Pinon-Segundo, M. G. Nava-Arzaluz and D. Lechuga-Ballesteros, *Recent Pat. Drug Delivery Formulation*, 2012, **6**, 224–235.

91 T. Bettinger, R. C. Carlisle, M. L. Read, M. Ogris and L. W. Seymour, *Nucleic Acids Res.*, 2001, **29**, 3882–3891.

92 J. Rejman, G. Tavernier, N. Bavarsad, J. Demeester and S. C. De Smedt, *J. Controlled Release*, 2010, **147**, 385–391.

93 M. L. Read, S. Singh, Z. Ahmed, M. Stevenson, S. S. Briggs, D. Oupicky, L. B. Barrett, R. Spice, M. Kendall, M. Berry, J. A. Preece, A. Logan and L. W. Seymour, *Nucleic Acids Res.*, 2005, **33**, e86.

94 L. Zhang, J. M. Chan, F. X. Gu, J.-W. Rhee, A. Z. Wang, A. F. Radovic-Moreno, F. Alexis, R. Langer and O. C. Farokhzad, *ACS Nano*, 2008, **2**, 1696–1702.

95 S. Krishnamurthy, R. Vaiyapuri, L. Zhang and J. M. Chan, *Biomater. Sci.*, 2015.

96 C. Salvador-Morales, L. Zhang, R. Langer and O. C. Farokhzad, *Biomaterials*, 2009, **30**, 2231–2240.

97 B. Mandal, H. Bhattacharjee, N. Mittal, H. Sah, P. Balabathula, L. A. Thoma and G. C. Wood, *Nanomedicine*, 2013, **9**, 474–491.

98 S. D. Kong, M. Sartor, C. M. Hu, W. Zhang, L. Zhang and S. Jin, *Acta Biomater.*, 2013, **9**, 5447–5452.

99 C. Salvador-Morales, L. Zhang, R. Langer and O. C. Farokhzad, *Biomaterials*, 2009, **30**, 2231–2240.

100 D. E. Owens Iii and N. A. Peppas, *Int. J. Pharm.*, 2006, **307**, 93–102.

101 B. T. Luk, R. H. Fang and L. Zhang, *Theranostics*, 2012, **2**, 1117–1126.

102 X. Su, J. Fricke, D. G. Kavanagh and D. J. Irvine, *Mol. Pharm.*, 2011, **8**, 774–787.

103 C. Clawson, L. Ton, S. Aryal, V. Fu, S. Esener and L. Zhang, *Langmuir*, 2011, **27**, 10556–10561.

104 J. Shi, Z. Xiao, A. R. Votruba, C. Vilos and O. C. Farokhzad, *Angew. Chem., Int. Ed.*, 2011, **123**, 7165–7169.

105 J. Shi, Y. Xu, X. Xu, X. Zhu, E. Pridgen, J. Wu, A. R. Votruba, A. Swami, B. R. Zetter and O. C. Farokhzad, *Nanomedicine*, 2014, **10**, 897–900.

106 X. Su, J. Fricke, D. G. Kavanagh and D. J. Irvine, *Mol. Pharm.*, 2011, **8**, 774–787.

107 D. M. Anderson, L. L. Hall, A. R. Ayyalapu, V. R. Irion, M. H. Nantz and J. G. Hecker, *Hum. Gene Ther.*, 2003, **14**, 191–202.

108 S. M. Ryou, S. Kim, H. H. Jang, J. H. Kim, J. H. Yeom, M. S. Eom, J. Bae, M. S. Han and K. Lee, *Biochem. Biophys. Res. Commun.*, 2010, **398**, 542–546.

109 N. L. Rosi, D. A. Giljohann, C. S. Thaxton, A. K. Lytton-Jean, M. S. Han and C. A. Mirkin, *Science*, 2006, **312**, 1027–1030.

110 J. H. Kim, J. H. Yeom, J. J. Ko, M. S. Han, K. Lee, S. Y. Na and J. Bae, *J. Biotechnol.*, 2011, **155**, 287–292.

111 P. C. Patel, D. A. Giljohann, W. L. Daniel, D. Zheng, A. E. Prigodich and C. A. Mirkin, *Bioconjugate Chem.*, 2010, **21**, 2250–2256.

112 D. A. Giljohann, D. S. Seferos, W. L. Daniel, M. D. Massich, P. C. Patel and C. A. Mirkin, *Angew. Chem., Int. Ed.*, 2010, **49**, 3280–3294.

113 D. A. Giljohann, D. S. Seferos, P. C. Patel, J. E. Millstone, N. L. Rosi and C. A. Mirkin, *Nano Lett.*, 2007, **7**, 3818–3821.

114 J. A. Ryan, K. W. Overton, M. E. Speight, C. N. Oldenburg, L. Loo, W. Robarge, S. Franzen and D. L. Feldheim, *Anal. Chem.*, 2007, **79**, 9150–9159.

115 A. Elbakry, A. Zaky, R. Liebl, R. Rachel, A. Goepferich and M. Breunig, *Nano Lett.*, 2009, **9**, 2059–2064.

116 E. Zhao, Z. Zhao, J. Wang, C. Yang, C. Chen, L. Gao, Q. Feng, W. Hou, M. Gao and Q. Zhang, *Nanoscale*, 2012, **4**, 5102–5109.

117 J. Kim, J. Park, H. Kim, K. Singha and W. J. Kim, *Biomaterials*, 2013, **34**, 7168–7180.

118 H. Kübier, A. Stenzl, W. Schultze-Seemann, F. vom Dorp, L. Pilla, C. Hampel, D. Jocham and K. Miller, *Eur. J. Cancer*, 2011, **47**, S498–S499.

119 R. M. Conry, A. F. LoBuglio, M. Wright, L. Sumerel, M. J. Pike, F. Johanning, R. Benjamin, D. Lu and D. T. Curiel, *Cancer Res.*, 1995, **55**, 1397–1400.

120 R. D. Granstein, W. Ding and H. Ozawa, *J. Invest. Dermatol.*, 2000, **114**, 632–636.

121 J. A. Wolff, R. W. Malone, P. Williams, W. Chong, G. Acsadi, A. Jani and P. L. Felgner, *Science*, 1990, **247**, 1465–1468.

122 L. Zangi, K. O. Lui, A. von Gise, Q. Ma, W. Ebina, L. M. Ptaszek, D. Spater, H. Xu, M. Tabebordbar, R. Gorbatov, B. Sena, M. Nahrendorf, D. M. Briscoe, R. A. Li, A. J. Wagers, D. J. Rossi, W. T. Pu and K. R. Chien, *Nat. Biotechnol.*, 2013, **31**, 898–907.

123 B. Scheel, S. Braedel, J. Probst, J. P. Carralot, H. Wagner, H. Schild, G. Jung, H. G. Rammensee and S. Pascolo, *Eur. J. Immunol.*, 2004, **34**, 537–547.

124 ClinicalTrials.gov, Trial of RNActive®-Derived Prostate Cancer Vaccine in Metastatic Castrate-refractory Prostate Cancer, https://www.clinicaltrials.gov/ct2/show/NCT01817738?term=curevac&rank=2, (accessed 12 May, 2015).

125 S. McLenachan, D. Zhang, A. B. Palomo, M. J. Edel and F. K. Chen, *PLoS One*, 2013, **8**, e83596.

126 S. Zou, K. Scarfo, M. H. Nantz and J. G. Hecker, *Int. J. Pharm.*, 2010, **389**, 232–243.

127 O. O. Markov, N. L. Mironova, M. A. Maslov, I. A. Petukhov, N. G. Morozova, V. V. Vlassov and M. A. Zenkova, *J. Controlled Release*, 2012, **160**, 200–210.

128 K. K. Phua, K. W. Leong and S. K. Nair, *J. Controlled Release*, 2013, **166**, 227–233.

129 D. M. Anderson, L. L. Hall, A. R. Ayyalapu, V. R. Irion, M. H. Nantz and J. G. Hecker, *Hum. Gene Ther.*, 2003, **14**, 191–202.

OXFORD UNIVERSITY PRESS | Journal of Molecular Cell Biology

Prohibitin 1 regulates tumor cell apoptosis via interaction with X-linked Inhibitor of Apoptosis Protein

Journal:	*Journal of Molecular Cell Biology*
Manuscript ID	JMCB-2015-0330
Manuscript Type:	Letter to the Editor
Date Submitted by the Author:	05-Oct-2015
Complete List of Authors:	Xu, Yingjie; Boston Children's Hospital, Vascular Biology Program Yang, Wen; Harvard Medical School, Cell Biology Shi, Jinjun; Brigham and Women's Hospital, Laboratory of Nanomedicine and Biomaterials, Department of Anesthesiology Zetter, Bruce; Boston Children's Hospital, Vascular Biology Program
Keyword:	Prohibitin 1, X-linked Inhibitor of Apoptosis Protein (XIAP), apoptosis, cancer, interactome

Prohibitin 1 regulates tumor cell apoptosis via interaction with X-linked Inhibitor of Apoptosis Protein

Yingjie Xu[1], Wen Yang[2], Jinjun Shi[3], and Bruce R. Zetter[1,*]

[1]*Vascular Biology Program, Boston Children's Hospital, Harvard Medical School, Boston, MA 02115, USA*

[2]*Department of Cell Biology, Harvard Medical School, Boston, MA 02115, USA*

[3]*Laboratory of Nanomedicine and Biomaterials, Department of Anesthesiology, Brigham and Women's Hospital, Harvard Medical School, Boston, MA 02115, USA*

Keywords: Prohibitin 1; X-linked Inhibitor of Apoptosis Protein (XIAP); apoptosis; cancer; interactome

*Corresponding Author: Bruce R. Zetter, Ph.D., Boston Children's Hospital and Harvard Medical School, 300 Longwood Avenue, Boston, MA 02115; *E-mail:* bruce.zetter@childrens.harvard.edu; *Phone:* 617-919-2320; *Fax*: 617-730-0268

Abstract

Prohibitin 1 (PHB1) is a member of a highly conserved eukaryotic protein family containing the stomatin/prohibitin/flotillin/HflK/C (SPFH) domain. PHB1 has been functionally linked to diverse cellular processes, including cell-cycle progression, apoptosis, mitochondrial biogenesis and tumor chemoresistance. To better understand the role of PHB1, we performed proteomic experiments to identify the PHB1 interactome. We here report that the X-linked inhibitor of apoptosis protein (XIAP) is a novel PHB1-interacting protein. The interaction was confirmed by GST pull-down assay, showing a direct interaction between the two proteins. This interaction is functionally significant, as silencing PHB1 decreases XIAP stability, resulting in consequent elevation of apoptotic pathway members, including active caspase-3 and cleaved poly ADP ribose polymerase (PARP). Using deletion constructs of XIAP, we showed that PHB1 binds principally to the BIR3 domain of XIAP. These results suggest that the natural interaction of PHB1 and XIAP represents a novel mechanism for the regulation of apoptosis and may influence tumor expansion and response to chemotherapeutic agents.

Dear Editor,

Prohibitin 1 (PHB1) was identified previously as a protein that is both upregulated and translocated to the plasma membrane in taxane-resistant cancer cells. We found that PHB1 silencing resensitized taxane-resistant cells to apoptosis and paclitaxel treatment both *in vitro* and *in vivo* (Patel et al., 2010). In line with our findings, overexpression of PHB1 has been shown to markedly attenuate ceramide, staurosporine (STS), camptothecin and serum withdrawal-induced apoptosis via the intrinsic apoptotic pathway. In complementary studies, PHB1 silencing sensitized several cancer cell types to stress- or drug-induced apoptosis (Peng et al., 2015). Despite these advances, the mechanism whereby PHB1 regulates apoptosis and chemoresistance remains unclear. In this letter, we identify XIAP as a novel binding partner of PHB1 based on immunoprecipitation followed by mass spectrometry (IP-MS). This interaction is functionally relevant and can modulate the apoptotic process and influence tumor response to chemotherapeutic agents.

The identity of potential PHB1-interacting proteins was revealed by IP-MS-based proteomic analysis (Sowa et al., 2009). We found that PHB1-HA was predominantly, but not solely, expressed in mitochondria, consistent with previous findings (Figure S1A). The PHB1 interaction network determined by our experiments (Figure S1B) includes several known PHB1-binding proteins, such as PHB2 and RAF1 (Peng et al., 2015), providing internal validation of the approach. The screen further identified several novel PHB1-interacting proteins, including the serine beta-lactamase-like protein LACTB, the mitochondrial carbamoyl phosphate synthase 1 (CPS1), the mitochondrial ras family

GTPases Rho T1 and T2 and the apoptosis inhibitor XIAP. These proteins participate in cellular functions consistent with previously known roles of PHB1, including apoptosis, mitochondrial homeostasis, the unfolded protein response and signal transduction (Thuaud et al., 2013). The new identification of XIAP, a well-characterized anti-apoptosis factor (Eckelman et al., 2006), as a PHB1 interactor offers the possibility that this interaction may mediate the known effects of PHB1 on apoptosis (Patel et al., 2010). Immunoprecipitation of HEK293 cells with anti-HA agarose validated the intracellular association of PHB1-HA with XIAP (Figure 1A). PHB2, a known PHB1 binding partner, also was found in the immunoprecipitates. More importantly, our results demonstrated that XIAP interacts with endogenous PHB1 in both Mes-Sa uterine sarcoma cells (Figure 1B) as well as OVCAR5 ovarian cancer cells (Figure S1C). GST pull-down assays further revealed an interaction between 6XHis-XIAP and GST-PHB1 *in vitro* (Figure 1C). Together, these results demonstrate that PHB1 binds directly to XIAP, both *in vivo* and *in vitro*.

XIAP contains three BIR domains. BIR1 directly interacts with TAB1 to induce NF-kappaB activation (Lu et al., 2007). BIR2 mediates binding of XIAP to downstream effector caspases (caspases-3 and -7), whereas BIR3 binds to an upstream initiator caspase (caspase-9). BIR3 also mediates binding to functional XIAP antagonists such as DIABLO, ARTS and HtrA2/Omi (Eckelman et al., 2006). Co-immunoprecipitation (Co-IP) assays with His-V5-tagged PHB1 and multiple HA-tagged XIAP expression constructs, including full-length XIAP, XIAPΔBIR, XIAP BIR1-2 and XIAP BIR2-3, revealed that PHB1 binds to full-length XIAP as well as to the XIAP BIR2-3 domain (Figure S1D). Examination of HA-tagged PHB1 binding to additional GST-tagged XIAP

expression constructs, including full-length XIAP, XIAP BIR1, BIR2 and BIR3 showed that PHB1 binds principally to the BIR3 domain of XIAP (Figure 1D), along with weak binding to the XIAP BIR2 domain. We conclude that the principal PHB1 interaction site on XIAP resides within the BIR3 domain.

PHB1 is present in multiple compartments of the cell, principally in the mitochondria, but also in the cytosol, nucleus and plasma membrane (Thuaud et al., 2013). To determine in which regions PHB1 and XIAP co-localize, we performed immunofluorescence double-labeling of cells with anti-PHB1 and anti-XIAP antibodies. In both Mes-Sa and OVCAR5 cells, XIAP was localized primarily to the cytoplasm, and PHB1 was detected predominantly in the mitochondria, although some cytoplasmic staining was apparent (Figure S2A). Moreover, when cells were treated with paclitaxel to induce apoptosis, cytoplasmic PHB1 staining increased and showed co-localization with cytoplasmic XIAP (Figure 1E, Figure S2B). Subcellular fractionation followed by Western blotting showed that, after treatment with paclitaxel, PHB1 levels were significantly elevated, both in the mitochondria and cytosolic fraction (Figure S2C). These results suggest that co-localization of XIAP with PHB1 takes place predominantly in the cytoplasm.

To confirm the involvement of PHB1 in apoptosis in the cells used in these studies, we silenced PHB1 in Mes-Sa cells using PHB1-specific siRNA followed by paclitaxel treatment to induce apoptosis. By flow cytometry analysis for Annexin-V, a marker of apoptosis, and 7-AAD, a marker of necrosis, we found that PHB1 silencing sensitized cells to paclitaxel-induced apoptosis (Figure 1F). The frequency of apoptosis, as demonstrated by the finding that the percentage of Annexin-V positive cells, increased

markedly to 55.3% in cells treated with siPHB1 relative to 24.4% in the paclitaxel-treated siControl cells. Early-stage apoptosis, marked by Annexin V-positive and 7-ADD-negative cells, also increased from 10.7% in controls to 24.9% in the paclitaxel-treated siPHB1 cells. Similar effects were observed when Mes-Sa cells were treated with staurosporine (STS), an apoptosis inducer (Figure S3A).

One possible mechanism for PHB1's anti-apoptotic activity is through protection of XIAP function. This could occur if, for example, PHB1 competed with binding of an XIAP antagonist such as DIABLO. If this were the case, PHB1 silencing should result in increased levels of the XIAP-DIABLO complex. Our results, however, showed decreased XIAP-DIABLO interaction after PHB1 silencing (Figure S4), suggesting that PHB1 regulates XIAP functionality via other mechanisms. In this experiment, we noticed that the levels of full-length XIAP were partly decreased after PHB1 silencing, suggesting a potential effect of PHB1 on XIAP cleavage or degradation.

It was shown previously that XIAP cleavage by caspases occurs at aspartic acid-242, which lies between the BIR2 and BIR3 domains. The resulting BIR1-2 cleavage product is degraded, while the BIR3-RING domain product acts as a part of a positive feedback loop to increase apoptosis (Hornle et al., 2011). We speculated that PHB1 binding to the XIAP-BIR3 domain could interfere with caspase-mediated XIAP cleavage. We treated siControl (siCon) and siPHB1 Mes-Sa cells with paclitaxel to induce apoptosis, and measured the levels of XIAP and its downstream effectors. Western blotting showed that PHB1 silencing leads to generation of a 30KDa cleaved-XIAP BIR3-RING

domain, which resulted in enhanced caspase-3 processing into the catalytically active p17 fragment (cleaved caspase-3) and a consequent increase in cleaved PARP (poly ADP ribose polymerase), especially when paclitaxel is added (Figure 1G, left panel). The red fluorescent staining observed in paclitaxel-treated cells in Figure 1E likely represents both full-length and cleaved XIAP, as both would be recognized by antibody to the XIAP C-terminus. Moreover, caspase-3/7 activity, as measured by Caspase-Glo assay, revealed that PHB1 silencing led to increased caspase-3/7 activation following paclitaxel treatment (Figure 1G, right panel) (*p<0.05; ***p<0.001). These findings are consistent with a role for PHB1 as an inhibitor of apoptosis and were verified further in multiple cell lines (Figure S3B-C). Our study shows that, in contrast to the IBM protein family that antagonizes IAP action, PHB1 protects XIAP function by diminishing caspase-mediated XIAP cleavage. PHB1 was previously described as a chaperone for mitochondrial proteins. Our results suggest a similar role for PHB1 in protecting cytoplasmic XIAP.

We next investigated whether silencing of PHB1 and XIAP have similar functionality. PHB1 or XIAP were silenced in Mes-Sa cells, and the cells were then treated with paclitaxel. Figure 1H shows successful knockdown by PHB1 and XIAP-specific siRNAs. Silencing either PHB1 or XIAP increased cell killing by paclitaxel. Next, we investigated whether overexpression of XIAP can rescue the apoptotic phenotype caused by PHB1 silencing. We found that overexpression of XIAP in PHB1-silenced cells partially rescued the cell death caused by siPHB1. In this experiment, PHB1 silencing resulted in a significant reduction of His-V5-XIAP protein compared to siControl-treated cells (Figure S5A). The level of His-V5-XIAP was restored in PHB1-silenced cells by

treatment with the proteasome inhibitor MG132 (Figure S5B). Together, these results further indicate that XIAP is protected from proteasomal degradation in the presence of PHB1.

The observation that PHB1 silencing results in increased cell death has potential clinical implications. PHB1 levels correlate with disease progression and chemoresistance in several cancer types, including gastric cancer, colorectal cancer, hepatocellular carcinomas, NSCLC and ovarian cancer (Kapoor, 2013). Interestingly, in ovarian cancer, Gregory-Bass showed a strong positive correlation between the levels of PHB1 and XIAP, suggesting that PHB1 may be coordinately regulated and exert an anti-apoptotic effect in ovarian cancer cells (Gregory-Bass et al., 2008). In this study, we demonstrated an interaction between PHB1 and XIAP and suggest a novel mechanism for the suppression of apoptosis by PHB1. Our findings indicate that the PHB1-XIAP complex promotes an anti-apoptotic response in cancer cells and reinforces PHB1 as a therapeutic target, as silencing of the PHB1 gene expression increases the sensitivity of cancer cells to drug-induced apoptosis. The feasibility of targeting PHB1 as a therapeutic was further demonstrated by our recent finding that the systemic delivery of PHB1-siRNA nanoparticles could increase cisplatin sensitivity in non-small cell lung cancer xenografts in mice (Zhu et al., 2015).

Acknowledgements

We thank Drs. Virginia Guarani and J. Wade Harper for assistance and instruction with mass spectrometry and interactome analysis. We thank Grace Poulin for her technical assistance. We thank Dr. Randolph Watnick for discussion and comments. We thank Dr. Colin Duckett for the gift of pEBB-HA-XIAP plasmids. This work was supported in part by grants from the Lung Cancer Research Foundation (to B.R.Z.) and the National Cancer Institute of the National Institutes of Health (R01CA37393 to B.R.Z.). The content is solely the responsibility of the authors and does not necessarily represent the official views of the National Institutes of Health. This work also was supported by the United States Department of Defense Prostate Cancer Research Program Postdoctoral Training Award (W81XWH-14-1-0268 to Y.X) and the Charles A. King Trust Postdoctoral Research Fellowship Program (to W.Y.).

References

Eckelman, B.P., Salvesen, G.S., and Scott, F.L. (2006). Human inhibitor of apoptosis proteins: why XIAP is the black sheep of the family. EMBO reports *7*, 988-994.

Gregory-Bass, R.C., Olatinwo, M., Xu, W., et al. (2008). Prohibitin silencing reverses stabilization of mitochondrial integrity and chemoresistance in ovarian cancer cells by increasing their sensitivity to apoptosis. International journal of cancer. Journal international du cancer *122*, 1923-1930.

Hornle, M., Peters, N., Thayaparasingham, B., et al. (2011). Caspase-3 cleaves XIAP in a positive feedback loop to sensitize melanoma cells to TRAIL-induced apoptosis. Oncogene *30*, 575-587.

Kapoor, S. (2013). Prohibitin and its rapidly emerging role as a biomarker of systemic malignancies. Human pathology *44*, 678-679.

Lu, M., Lin, S.C., Huang, Y., et al. (2007). XIAP induces NF-kappaB activation via the BIR1/TAB1 interaction and BIR1 dimerization. Molecular cell *26*, 689-702.

Patel, N., Chatterjee, S.K., Vrbanac, V., et al. (2010). Rescue of paclitaxel sensitivity by repression of Prohibitin1 in drug-resistant cancer cells. Proceedings of the National Academy of Sciences of the United States of America *107*, 2503-2508.

Peng, Y.T., Chen, P., Ouyang, R.Y., et al. (2015). Multifaceted role of prohibitin in cell survival and apoptosis. Apoptosis : an international journal on programmed cell death.

Sowa, M.E., Bennett, E.J., Gygi, S.P., et al. (2009). Defining the human deubiquitinating enzyme interaction landscape. Cell *138*, 389-403.

Thuaud, F., Ribeiro, N., Nebigil, C.G., et al. (2013). Prohibitin ligands in cell death and survival: mode of action and therapeutic potential. Chemistry & biology *20*, 316-331.

Zhu, X., Xu, Y., Solis, L.M., et al. (2015). Long-circulating siRNA nanoparticles for validating Prohibitin1-targeted non-small cell lung cancer treatment. Proceedings of the National Academy of Sciences of the United States of America *112*, 7779-7784.

Figure legends

Figure 1: PHB1 binds to XIAP and regulates cell apoptosis

(**A**) Lysates of HEK293 transfected with PHB1-HA were subjected to HA agarose immunoprecipitation followed by Western blotting.

(**B**) Co-immunoprecipitation of endogenous PHB1 and XIAP in Mes-Sa cells. Lysates of Mes-Sa were subjected to anti-PHB1 IP followed by Western blotting.

(**C**) *In vitro* GST-pull down. Direct binding of PHB1 to XIAP is shown in an *in vitro* assay using GST-PHB1 and purified recombinant His-XIAP protein. GST protein served as a negative control.

(**D**) HEK293 cells were transiently transfected with PHB1-HA along with GST-tagged-XIAP-full-length (FL) and XIAP mutation constructs (GST-XIAP-BIR1, GST-XIAP-BIR2 and GST-XIAP-BIR3). IP with anti-HA agarose or anti-GST antibody followed by agarose, followed by Western blotting with anti-HA and anti-GST antibodies. Whole-cell lysates (input) showed that all constructs were expressed in the transfected cells. * heavy chain; ** PHB1-HA.

(**E**) Immunofluorescence of Mes-Sa cells stained with anti-PHB1 (green) and anti-XIAP (red) antibodies. The nucleus is stained with DAPI (blue). Left panel: untreated cells; Right panel: cells treated with 500nM paclitaxel for 16 hrs. Scale bar, 20um.

(**F**) Mes-Sa cells were transfected with siCon or siPHB1 for 2 days, followed by paclitaxel (250nM) treatment for 24 hours. Results of flow cytometry analysis of apoptosis induction are presented in quadrants.

(**G**) Mes-Sa cells were transfected with siCon or siPHB1 for 2 days, followed by paclitaxel treatment for 24 hours. Left panel: Western blotting of Mes-Sa cell lysates

after treatment with 250nM paclitaxel for 24 hours. Right panel: Caspase 3/7 activity after PHB1 silencing in Mes-Sa cells. Background activity values were subtracted from each sample. *p<0.05; ***p<0.001. Error bars are SDs.

(**H**) Mes-Sa cells were transfected with siCon, siPHB1 or siXIAP for 2 days, followed by paclitaxel treatment for 24 hours. Upper panel: Western blotting assessed the efficiency of PHB1 and XIAP knockdown. Lower panel: cell viability of siCon, siPHB1 and siXIAP-transfected cells under paclitaxel treatment was determined by CyQUANT cell viability assay in three independent experiments; *p<0.05; **p<0.01. Error bars are SDs.

Figure 1

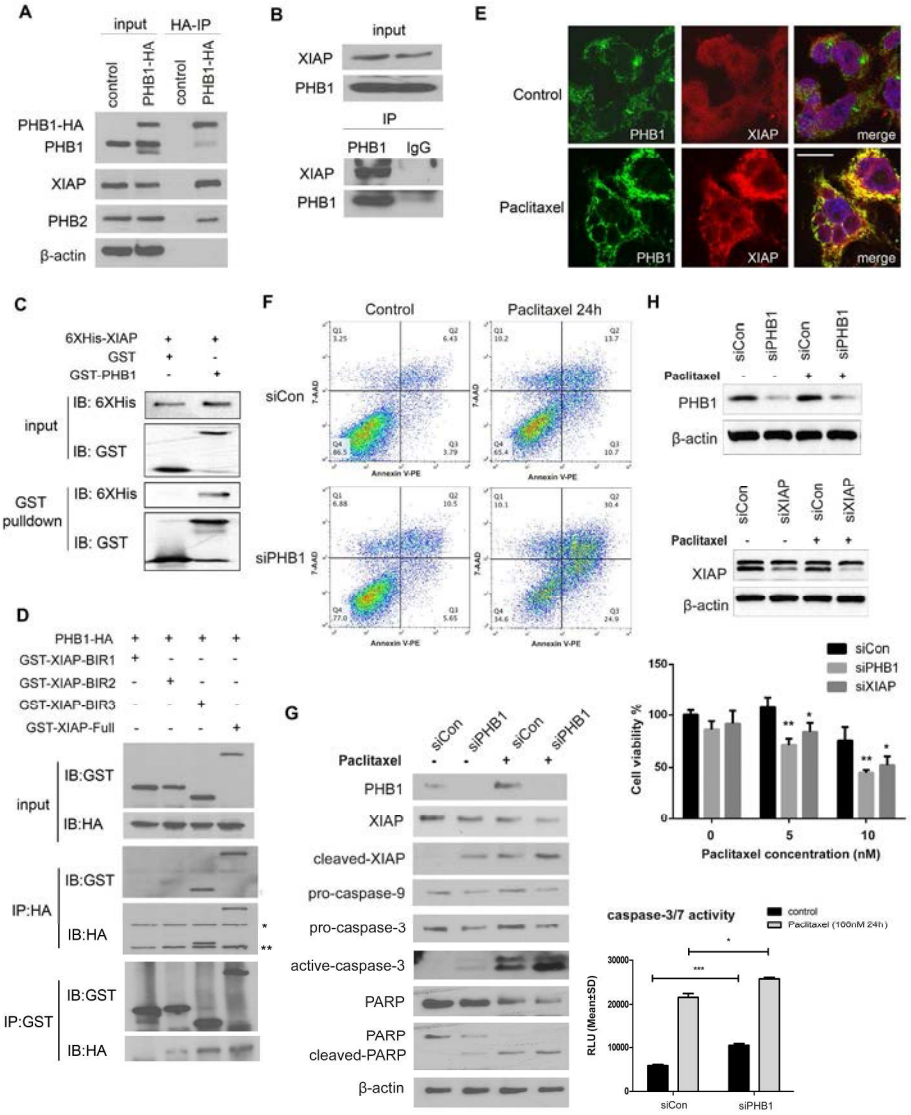

PHB1 binds to XIAP and regulates cell apoptosis
279x361mm (300 x 300 DPI)

SUPPLEMENTAL EXPERIMENTAL PROCEDURES

Cell culture

HEK293 cells were maintained in Dulbecco's modified Eagle's medium (DMEM; Invitrogen) supplemented with 10% fetal bovine serum (FBS; Invitrogen), 1% penicillin-streptomycin (P/S, Invitrogen). Mes-Sa cells were maintained in McCoy's 5A medium (ATCC), 10% FBS, and 1% P/S. Ovarian cancer cell line OVCAR5 were maintained in RPMI-1640, 10% FBS and 1% P/S.

Antibodies and chemicals

Antibodies used in this work included the following: anti-caspase-3, anti-caspase-9, anti-cleaved caspase-3, anti-cleaved caspase-9, anti-DIABLO/Smac, anti-ubiquitin, anti-CoxIV, anti-XIAP (rabbit) and anti-PARP bodies (Cell Signaling); anti-XIAP antibody (mouse, BD Transduction Laboratories); anti-PHB1 (rabbit, Cat# 70672, Abcam), and anti-6XHis antibodies (Abcam); anti-GST antibody (Pierce); Anti-V5 antibody (Life Technologies); anti-PHB1 (mouse, #11-14-10) (Neomarkers); anti-β-actin (Sigma); anti-HA antibody (Santa Cruz Biotechnology).

Plasmids construction and transfection

Sequence-verified human PHB and XIAP open reading frame clones in pENTR223 were recombined into the following Gateway destination vectors: pHAGE (MSCV-N-Flag-HA-IRES-PURO, long terminal repeat [LTR]-driven expression), His-V5-tagged pDEST40 and His-tagged bacteria expression pET59 using λ recombinase.

Plasmids to express HA-tagged XIAP full-length, BIR1-2, BIR2-3 and BIRΔ were gifts from Dr. Colin Duckett (Addgene plasmids: #25674, 25690, 25691, 25686) (Lewis et al., 2004). For BIR GST fusions, the primer pairs used were BIR1-attB1: GGGG-ACA-AGT-TTG-TAC-AAA-AAA-GCA-GGC-TTC-ATG-ACTTTTAACAGTTTTGAAGGATC; BIR1-attB2: GGGG-AC-CAC-TTT-GTA-CAA-GAA-AGC-TGG-GTC-GCTTCCCAGATAGTTTTCAACTTTG; BIR2-attB1: GGGG-ACA-AGT-TTG-TAC-AAA-AAA-GCA-GGC-TTC-ATG-CTGGGAAGCAGAGATCATTTTGC; BIR2-attB2: GGGG-AC-CAC-TTT-GTA-CAA-GAA-AGC-TGG-GTC-GGATGGATTTCTTGGAAGATTTG; BIR3-attB1: GGGG-ACA-AGT-TTG-TAC-AAA-AAA-GCA-GGC-TTC-ATG-TCCATGGCAGATTATGAAGCAC; BIR3-attB2: GGGG-AC-CAC-TTT-GTA-CAA-GAA-AGC-TGG-GTC-ACACTCCTCAAGTGAATGAGTTAAATG; BIR23-attB1: GGGG-ACA-AGT-TTG-TAC-AAA-AAA-GCA-GGC-TTC-ATG-GGTGACCAAGTGCAGTGC; BIR23-attB2: GGGG-AC-CAC-TTT-GTA-CAA-GAA-AGC-TGG-GTC-ATCACCTTCACCTAAAGCATAAAATC. PCR products were subcloned into pENTR233 by BP reaction and then recombined into GST-tagged pDEST27 destination vector using λ recombinase.

For plasmid transfection, the indicated quantity of DNA was transfected using Lipofectamine 2000 (Life Technologies) for HEK293 cells according to the manufacturer's specifications. Transfected cells were harvested 48h post-transfection for further analysis.

siRNA transfection

Synthetic siRNA and control siRNA were purchased from Dharmacon. The target sequences for PHB1 and XIAP were siPHB: 5'-GCG ACG ACC UUA CAG AGC GUU-3' (Patel et al., 2010); siXIAP: GAG UGG UAG UCC UGU UUC AGC UU (Burstein et al., 2004). For small interfering RNA (siRNA) transfection, 50 nM siRNA was transfected using siLentFect (Bio-Rad), according to the manufacturer's specifications. After 24h, the medium was exchanged and, at 72h, the cells were harvested for immunoprecipitation or Western blotting or further treated as indicated for the specific experiments.

Cell viability assay

Cell growth inhibition was determined by CyQUANT assay in 96-well plates. First, 3,000 cells per well per 100 µL were seeded in 96-well plates. On the next day, 100 µL working stock of drug solution of paclitaxel at 2× final concentration was added to the cell suspension. After 72h drug incubation, the culture media were removed and plates were kept at -80°C for more than 24h. Cell numbers were assayed using CyQUANT kit (Life Technologies) as per the manufacturer's instructions. Fluorescence measurements were made using a microplate reader with excitation at 485 nm and emission detection at 530 nm.

Caspase activity assay

To assess caspase-3/7 activity, cells were seeded in 96-well plates at a density of 5,000 cells/well in triplicate and treated for 24h with paclitaxel 48h post-seeding or post-transfection with siRNA. Activity was measured using the Promega assay per the

manufacturer's instructions and presented as fold-increase relative to the respective untreated controls.

Flow cytometry analysis

Cells were seeded in 6-well plates, transfected with siPHB1 or control siRNA, and then treated for 24h with 250 nM paclitaxel 48h post-transfection. The supernatant and the cell monolayer were collected, washed with PBS and processed for detection of apoptotic cells using the Annexin V-PE/7AAD apoptosis detection kit (BD Biosciences), according to the manufacturer's instructions.

Immunoprecipitation and proteomic analysis

HEK293 cells were transfected with a pHAGE lentiviral vector (Murphy et al., 2006), containing open reading frame of PHB1 and a C-terminal HA-Flag tag. After 48h of transfection, 4- by 15-cm plates of approximately 80 to 90% confluent cells were washed once with ice-cold phosphate-buffered saline (PBS) and then harvested in NP-40 lysis buffer (50 mM Tris-HCl [pH 7.5], 0.5% NP-40 substitute, 150 mM NaCl, 12.5 mM NaF) supplemented with Complete Mini EDTA-free protease inhibitor tablets (Roche). Extracts were sonicated at 35% intensity for 8s with a Bronson digital sonifier and were clarified for 20 min at 14,000 rpm, and the soluble fraction was incubated with anti-HA-agarose beads (Sigma) overnight at 4°C. The beads were washed five times with NP-40 lysis buffer and then eluted three times, for 30m each time, at room temperature with 500 µg/ml HA peptide (Sigma). The eluted proteins were concentrated with trichloroacetic acid (TCA; Sigma), trypsinized, loaded onto stage tips and analyzed by liquid chromatography-tandem mass spectrometry (LC-MS/MS) in duplicate runs,

according to previously published protocols (Sowa et al., 2009). Peptides were identified using Sequest and a target-decoy strategy and were subsequently analyzed using *CompPASS* (Behrends et al., 2010; Sowa et al., 2009).

MS data analysis using *CompPASS*

The immunoprecipitation (IP-MS) data from 4 biological repeats were analyzed by *CompPASS* as previously described (Behrends et al., 2010; Sowa et al., 2009). We used a stats table with 172 pulldowns from HEK293T cells generated by the Harper Laboratory (Department of Cell Biology, Harvard Medical School). The total spectral counts (TSC) for each interactor were used to generate raw statistical measures, called Z scores, for each interaction. The weighted D score (WD) score threshold was calculated so that 95% of the data fell below it. The normalized WD (D^N scores) score results from dividing each WD score by the calculated threshold. A D^N score ≥1 and a Z score ≥4 are thresholds above which a protein is considered to be a high-confidence candidate interactor protein (HCIP).

Western blot

Protein extracts were prepared using the lysis buffer described above. Equal amounts of protein, as determined with a bicinchoninic acid (BCA) protein assay kit (Pierce/Thermo Scientific) used according to the manufacturer's instructions, were separated by SDS-PAGE. Immunoprecipitations from HEK293 cells analyzed by Western blotting were prepared using the same protocol used for pulldowns for MS, but the proteins were eluted from the agarose beads by boiling in loading buffer. One-fourth of the immunoprecipitated material was used for each analysis. The proteins were

resolved on SDS-PAGE gels and transferred to nitrocellulose membranes. The blots were blocked with 5% nonfat dry milk in TBST (50 mM Tris-HCl, pH 7.4 and 150 mM NaCl, and 0.1% Tween 20) and then incubated with appropriate primary antibodies. Signals were detected with horseradish peroxidase-conjugated secondary antibodies and enhanced chemiluminescence (ECL) detection system (Amersham/GE Healthcare). When indicated, membranes were subsequently stripped for reprobing. Immunoblots were quantified by using ImageJ software (National Institutes of Health).

In vitro GST pull-down assay

Recombinant 6XHis-XIAP protein was purified using pET59-XIAP from bacteria and incubated overnight at 4°C with 5ug recombinant GST-PHB (Abnova) or GST bound to glutathione-sepharose 4B beads (GE Pharmacia). Samples were centrifuged at 2,000 rpm at 4°C for 5 min and washed 5 times with TEN100 buffer (20mM Tris, PH 7.4, 0.1mM EDTA, 100mM NaCl). SDS-PAGE analysis and Western blotting was performed on the eluted proteins as described above.

Immunofluorescent staining and microscopy

For immunofluorescent staining, cells were plated onto coverslips in 6-well plates and grown overnight. Cells were washed with ice-cold PBS and fixed with 4% paraformaldehyde (PFA, Electron Microscopy Sciences) in PBS for 20 min at room temperature (RT). Cells were then permeabilized by incubation in 0.2% Triton X-100-PBS for 8 min on ice. Next, cells were blocked with PBS blocking buffer containing 2% normal goat serum, 2% BSA and 0.2% gelatin for 1h at RT. Cells were incubated in appropriated diluted primary antibody (1:200 anti-PHB rabbit antibody; 1:100 anti-XIAP

mouse antibody) for 1h at RT, washed with PBS and incubated in goat-anti-mouse-Alexa Fluor 568 and goat-anti-rabbit-Alexa Fluor 488 (Molecular Probes) at 1:500 dilution in blocking buffer for 30 min at RT. Finally, stained cells were washed with PBS, counterstained with 500 nM DAPI and mounted on slides with Prolong Gold antifade mounting media (Life Technologies).

For mitochondrial staining, MitoTracker Green was added 30 min before fixation, according to the manufacturer's instructions (Molecular Probes). All fluorescence images were visualized and captured using an inverted Leica DM-IRE2 microscope (Leica Microsystems). Acquisition parameters were adjusted to exclude saturation of the pixels. For quantification, such parameters were kept constant across the various conditions.

Statistical Analysis

All results in the text and figures are presented as means ± SD. Statistical significance of the results was determined using the Student's *t*-test. $P < 0.05$ is considered significant.

SUPPLEMENTAL FIGURE LEGENDS

Supplemental Figure 1: Identification of XIAP as a novel PHB-interacting protein

A*:* Left panel: Lysates of PHB1-HA-expressing HEK293 cells were subjected to Western blotting using PHB1 antibody. Right panel: Immunofluorescence assay of HEK293T cells with anti-HA (red) and anti-COXIV (green) antibodies. The nucleus is stained with DAPI (blue). Scale bar, 20um.

B*:* IP-MS-Comp*PASS* of PHB1-HA in HEK293 cells. Lysates of PHB-HA-expressing cells were immunoprecipitated with HA resin. Bait complexes were analyzed by LC MS/MS. Analysis was performed in Comp*PASS* against dedicated HEK293 IP-MS databases. High-confidence interacting proteins had normalized weighted D (D^N scores) >1 and Z-scores of >4.

C: Endogenous co-immunoprecipitation of PHB1 and XIAP. Lysates of OVCAR5 were subjected to anti-PHB IP followed by Western blotting.

D: HEK293 cells were transiently transfected with the His-V5-PHB1 construct along with HA-tagged-XIAP-full-length (FL) and XIAP mutation constructs. The following constructs were used: HA-XIAP-FL, HA-XIAP-BIRΔ, HA-XIAP-BIR1-2 and HA-XIAP-BIR2-3. Immunoprecipitation assays with anti-V5 agarose or anti-HA agarose were carried out, followed by Western blotting with anti-HA and anti-V5 antibodies. Whole-cell lysates (input) showed that all constructs were expressed in the transfected cells.

Supplemental Figure 2: Subcellular localization of PHB1 and XIAP

***A**:* Mitochondrial localization of PHB1. Mes-Sa cells were incubated with MitoTracker Green 200nM for 45 min, followed by immunofluorescence assay with anti-PHB1 (red) antibody. Nuclei are stained with DAPI (blue). Scale bar*,* 20um.

***B**:* Immunofluorescence assay of OVCAR5 cells with anti-PHB1 (green) and anti-XIAP (red) antibodies. The nucleus is stained with DAPI (blue). The cells were treated with 250nM of paclitaxel for 16h (right panel) as compared to non-treated cells (left panel). In non-treated cells, PHB1 was primarily localized to mitochondria, whereas XIAP staining was diffused cytoplasmic. After paclitaxel treatment, co-localization of PHB1 and XIAP occurred principally in the cytoplasm, as shown in yellow in the merged image. Scale bar, 20um.

C: Mes-Sa cells were treated with vehicle or with 500nM paclitaxel followed by subcellular fractionation. An antibody against the cytochrome C oxidase subunit IV (COX IV) was used as a mitochondrial marker, and β-actin was used as a cytosolic marker.

Supplemental Figure 3: PHB1 silencing stimulates apoptosis

***A**:* Mes-Sa cells were transfected with siCon or siPHB1 for 2 days followed by staurosporine (STS) treatment for 4h. Results of the apoptosis assay on Mes-Sa are presented in quadrants, as analyzed by flow cytometry. The *x*-axis represents the PE-conjugated Annexin V. The *y*-axis represents 7-AAD. Representative dot plots of siCon untreated cells (top left), siCon STS treated (top right), siPHB1 untreated cells (bottom left) and siPHB STS treated (bottom right). Living cells accumulate in Q4 (PE Annexin V and 7-AAD negative), while cells undergoing apoptosis accumulate in Q3 (PE Annexin

V positive and 7-AAD negative) and cells in end-stage apoptosis or dead cells accumulate in Q2 (PE Annexin V and 7-AAD positive).

***B**:* Mes-Sa cells were transfected with siCon or siPHB1 for 2 days followed by Etoposide treatment for 24h and subjected to Western blotting. Apoptosis was assessed by PARP cleavage. GAPDH was used as a loading control. Right panel shows quantification of cleaved XIAP and cleaved PARP levels.

***C**:* OVCAR5 cells were transfected with siCon or siPHB1 for 2 days followed by paclitaxel treatment for 24h, and subjected to Western blotting. Apoptosis was assessed by activation of caspase 3 and PARP cleavage. β-actin was used as a loading control.

Supplemental Figure 4: Silencing of PHB1 decreases interaction of XIAP with DIABLO

OVCAR5 cells were transfected with siCon or siPHB1 for 2 days followed by paclitaxel treatment for 24h. Immunoprecipitation assays with anti-DIABLO antibody and agarose beads, followed by Western blotting of DIABLO and XIAP antibodies. Whole-cell lysates (input) showed levels of PHB, XIAP and DIABLO.

Supplemental Figure 5: Overexpression of XIAP in PHB1-silenced cells

A: HEK293 cells were transfected with siCon, siCon+His-V5-XIAP, siPHB1, or siPHB1+His-V5-XIAP for 2 days, followed by paclitaxel treatment. Left panel: cell viability was measured 3 days after treatment using CyQUANT assay. *p<0.05; **p<0.01. Error bars are SDs. Right panel: lysates of His-V5-XIAP-transfected cells were subjected to Western blotting.

***B**:* In HEK293 cells, His-V5-XIAP was co-transfected with siCon or siPHB1 for 2 days, followed by MG132 (10uM) treatment for 4 hours or 24 hours. Cell lysates were subjected to Western blotting.

SUPPLEMENTAL REFERENCES

Behrends, C., Sowa, M.E., Gygi, S.P., and Harper, J.W. (2010). Network organization of the human autophagy system. Nature *466*, 68-76.

Burstein, E., Ganesh, L., Dick, R.D., van De Sluis, B., Wilkinson, J.C., Klomp, L.W., Wijmenga, C., Brewer, G.J., Nabel, G.J., and Duckett, C.S. (2004). A novel role for XIAP in copper homeostasis through regulation of MURR1. The EMBO journal *23*, 244-254.

Murphy, G.J., Mostoslavsky, G., Kotton, D.N., and Mulligan, R.C. (2006). Exogenous control of mammalian gene expression via modulation of translational termination. Nature medicine *12*, 1093-1099.

Patel, N., Chatterjee, S.K., Vrbanac, V., Chung, I., Mu, C.J., Olsen, R.R., Waghorne, C., and Zetter, B.R. (2010). Rescue of paclitaxel sensitivity by repression of Prohibitin1 in drug-resistant cancer cells. Proceedings of the National Academy of Sciences of the United States of America *107*, 2503-2508.

Sowa, M.E., Bennett, E.J., Gygi, S.P., and Harper, J.W. (2009). Defining the human deubiquitinating enzyme interaction landscape. Cell *138*, 389-403.

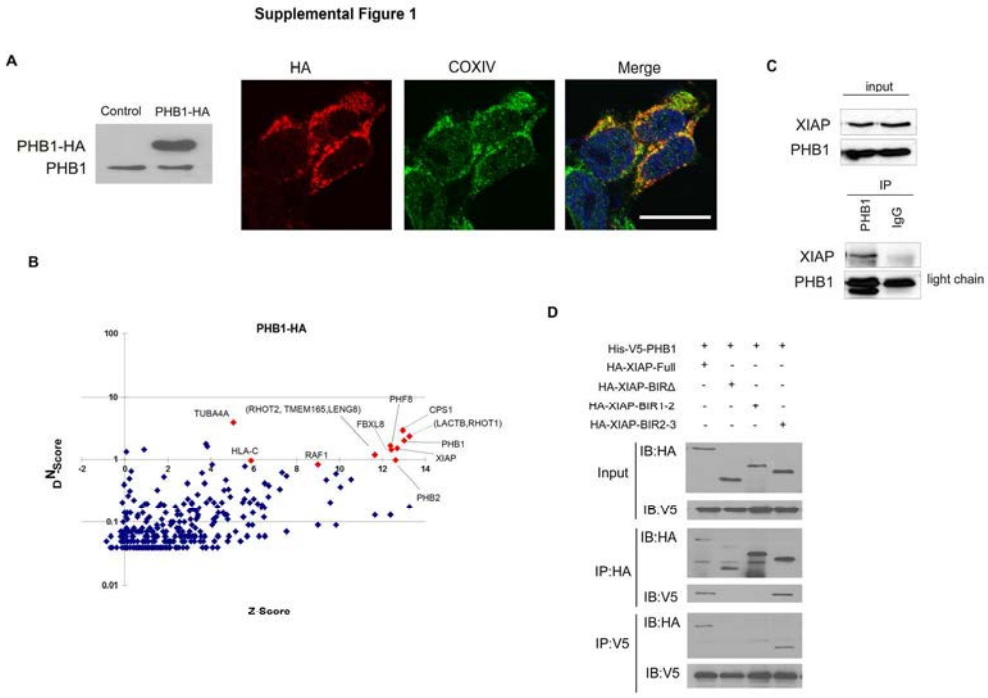

203x147mm (300 x 300 DPI)

Supplemental Figure 2

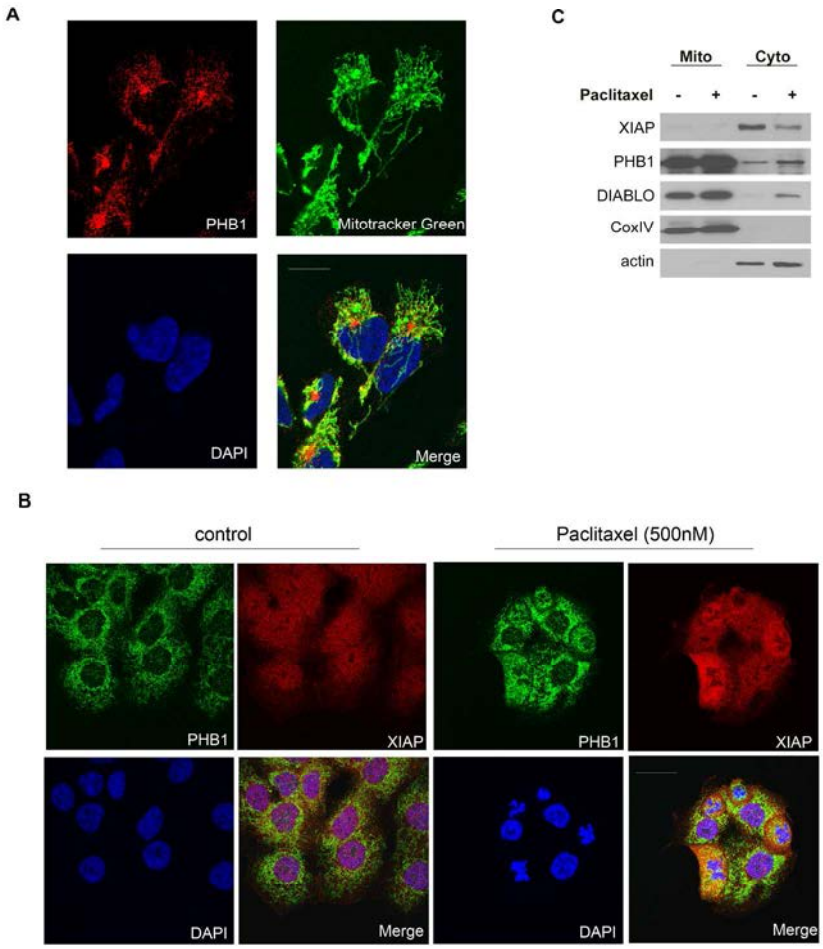

Subcellular localization of PHB1 and XIAP
266x350mm (300 x 300 DPI)

Supplemental Figure 3

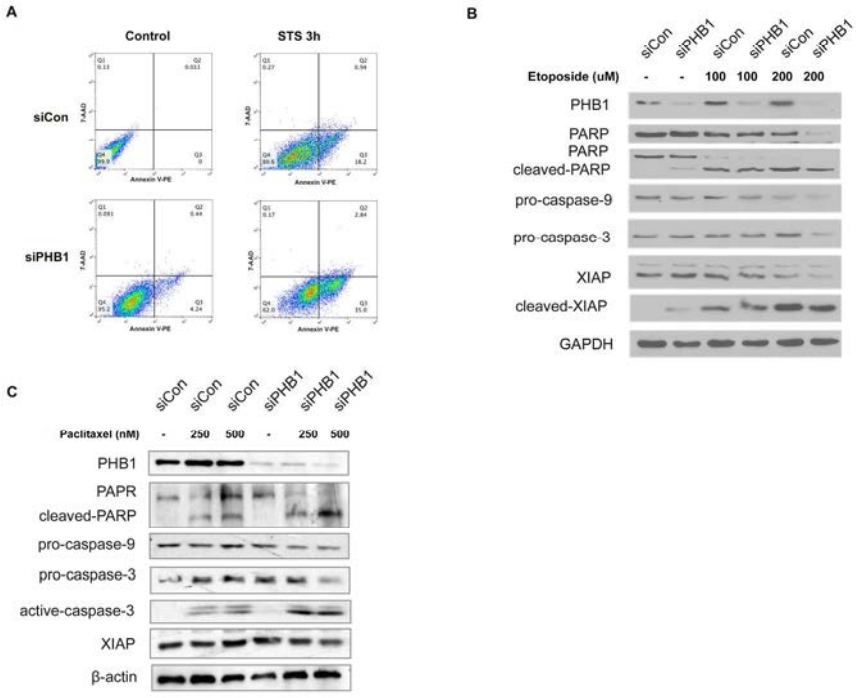

215x166mm (300 x 300 DPI)

Supplemental Figure 4

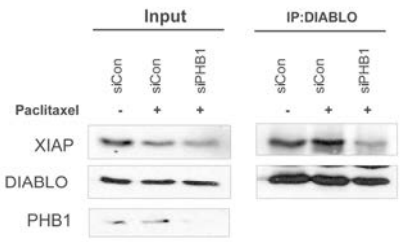

138x93mm (300 x 300 DPI)

Supplemental Figure 5

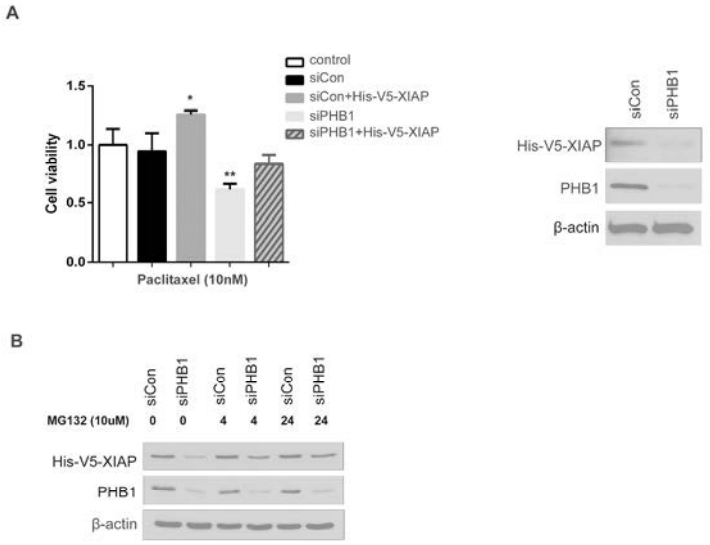

279x361mm (300 x 300 DPI)